This is to certify that the
thesis entitled

NUMERICAL STUDIES ON THE STRESS-WAVE
PROPAGATION IN SOLID AND FOAM MATERIALS

presented by

Zhen Zheng

has been accepted towards fulfillment
of the requirements for the

M.S. degree in Civil Engineering

Major Professor's Signature

8/26/2010

Date

NUMERICAL STUDIES ON THE STRESS-WAVE PROPAGATION IN SOLID AND FOAM MATERIALS

By

Zhen Zheng

A THESIS

Submitted to
Michigan State University
in partial fulfillment of the requirements
for the degree of

MASTER OF SCIENCE

Civil Engineering

2010

ABSTRACT

NUMERICAL STUDIES ON THE STRESS-WAVE PROPAGATION IN SOLID AND FOAM MATERIALS

By

Zhen Zheng

Improved understanding on the propagation of stress waves and means of controlling them could lead to techniques that minimize the damage resulting from blast and impact loads. This research was aimed at investigating the propagation of stress waves in homogeneous and non-homogeneous solid and open-cell foam materials in one and two dimensions through numerical simulations. One-dimensional wave propagation studies considered cantilever bar models to verify the theory related to stress wave propagation and energy dissipation. Two-dimensional wave propagation used simply supported sandwich plates, composed from aluminum face sheets and specially designed foam core, to examine stress wave management. Results from the bar simulations were consistent with theoretical solutions. Numerical simulations in the sandwich plates showed that stress waves can be attenuated and redirected, and that energy dissipation is observable, especially when using tailored, or functionally graded, foam cores. It is concluded that "engineered" cellular solids can not only absorb energy to protect against blast and impact loads but that they may be used in strategic, or tailored, forms to manage the propagation of damaging stress waves, the energy dissipation and the kinetic energy that imparted to a protected structure of the structure's occupants.

Dedicated to my father, mother and younger sister

ACKNOWLEDGEMENTS

I wish to express my sincere appreciation to my advisor Dr. Rigoberto Burgueño, although I know these words cannot state all my gratitude to him. I am grateful for his invaluable guidance during the whole course of this investigation, and his excellent advice on my future career. Many thanks are given on his patience and efforts on this thesis as well. He is a remarkable researcher and has a talent on explaining concepts and ideas in a clear and simple yet thoughtful way based on his broad knowledge. I have always learnt a lot after each meeting with him, for example his creative thinking, and this has helped me with a new insight into many problems. I believe all the skills that I have learned from him will benefit my future life.

Sincere thanks are also given to my other committee members, Dr. Jung-Wuk Hong and Dr. Nizar Lajnef, for being part of my committee and providing feedback on the work.

It is also a pleasure to thank those graduate students who discussed with me and gave me suggestions during my study. Here I want to thank one of my best friends Jian Rui. He is smart, knowledgeable and always shows up if I need help. He helped me to revise my thesis draft even when he was on vacation in China and rehearsed my presentation online when in Buffalo. His suggestions and encouragement helped me to overcome difficulty I faced and finally made it. This thesis has consolidated the friendship between us.

Finally and most importantly, I would like to thank my family for their love, patience, endless support and understanding, which has encouraged me to accomplish my research. They are always there for me.

TABLE OF CONTENTS

LIST OF TABLES

LIST OF FIGURES

CHAPTER 1. INTRODUCTION

1.1 Motivation

Wave propagation is an important phenomenon in engineering. All structures that are subjected to an impact or dynamic loading, such as blast loading due to an explosion, or impact loading from a moving object at high speed, experience the propagation of stress waves within the material. If the magnitude of stress wave varies within the elastic limit, the structures will have an elastic deformation and recover their original configuration (neglecting second-order effects). However, if the magnitude of the stress wave exceeds the material elastic limit, then the structure will suffer permanent plastic deformation, and could potentially fail. It is thus important to study the mechanism of stress wave propagation and the way in which they may be controlled so as to minimize damage.

Stress wave propagation management is an important area in engineering practice. It includes military applications, automotive crashworthiness design and aerospace research. In the military, research in stress wave propagation is conducted to design protective devices such as warheads and body armor with material that can maintain its integrity and attenuate the magnitude of stress wave under a high speed impact or blast loading. In civil engineering, more and more significant structures need to be protected to mitigate strong stress waves from accidental or malicious impact or blast events. In the automotive industry, crashworthiness is an essential design aspect of the automotive product. Research in impact stress wave propagation helps researchers understand crash behavior of structures and materials, and develop energy-absorbing systems that can handle the potential dynamic impact loads. In aerospace applications, engineers investigate the propagation of the dynamic stress in aircraft frames by using supercomputers to simulate non-linear numerical models.

1.2 Concept of Stress Wave Propagation

Stress wave propagation is a common but complicated phenomenon in the world. In an isotropic elastic medium, stresses propagating inside can be divided into waves of dilatation and waves of distortion(Kolsky 1963). In a plane dilatational wave the direction of particle velocity is parallel to the direction of wave propagation; in a plane distortional wave those two directions are perpendicular to each other. Only these two waves propagate in an extended solid if it is unbounded. In addition, Rayleigh surface waves propagate in a free surface of the solid or in a surface boundary between two solids.

Among the waves produced by shock loading in two dimensions, the dilatational wave is of prime interest since it induces large deformations and damages in the solid. When a load reaches the structure, a large amount of kinetic energy will be imparted. From a microstructural perspective, particles will start to move quickly once they gain kinetic energy. They hit other conjoint particles thus stress magnitude starts to rise and energy is transmitted to other particles. After the energy transmission, stress magnitude begins to decay and the particles will slow down. This transit stress travels through the material in the form of a compressive stress wave(Smith and Hetherington 1994). As shown in Figure 1, a simply-supported beam is under a pressure loading in the middle of top side. Once the pressure is applied on the top surface of the beam, the stress starts to propagate inside of the beam in all the directions (denoted in dashed arrows) in the form of a compressive stress wave.

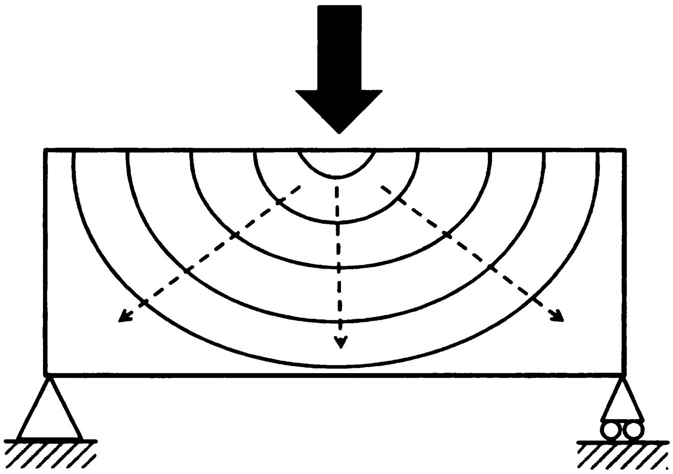

Figure 1. Schematic of Stress Wave Propagation in 2D

Stress wave propagation occurs in different mediums. If the stress wave travels in a model with single material, it can be specified as stress wave propagation in a homogeneous material. If it travels in a medium consisting of two or more materials, it may be referred to as stress wave propagation in a non-homogeneous material. Two types of materials are widely used in analysis and experiments: solid materials such as steel and aluminum, and foam materials which are porous solids.

Stress wave propagation has been investigated extensively during the past decades. Researchers studied stress wave propagation in homogeneous solid materials such as steel and aluminum, in homogeneous foam materials such as aluminum foam, in non-homogeneous solid materials such as graded metal-ceramic composites, and in non-homogeneous foam materials that can be layered or functional graded foam. It has been found that the efficiency of energy dissipation and stress mitigation in foam materials is much higher than in solid materials.

However, the concept of guiding or controlling the propagation of stress waves in two dimensions has not been explored. To the author's knowledge there are no experimental, theoretical or numerical studies available to date on this concept. Therefore, in the studies carried out in this thesis, a tailored foam structure was employed to demonstrate that the path of the stress wave propagation could be controlled. In the structure, stress waves may not propagate in a straight or linear way due to modified foam material. This idea is illustrated in Figure 2, which shows a simply-supported foam beam with reinforced arch foam (zone in grey color) surrounded by a weaker foam and subjected to a pressure load at the middle of the top surface. This study is aimed at demonstrating that after the impact load is applied on the structure, most of the stress wave (denoted in solid lines) will propagate very fast in the reinforced zone and will be directed to the supported region, and that stress waves of reduced intensity (shown in dashed lines) will travel in the weaker foam regions. As a result, the magnitude of the stress in the middle of the bottom facesheet decreases while the stresses in the simply-supported region increase when compared with a model with a homogeneous foam core. During the process of the stress wave propagation, the kinetic energy imparted by the exterior force is dissipated and stored as internal energy in the form of plastic deformation in the strong and weak foam.

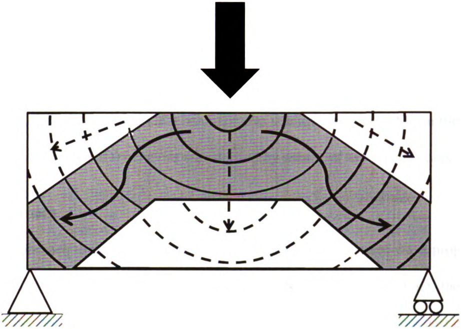

Figure 2. Schematic of stress wave propagation in tailored foam structure

1.3 Hypothesis

The hypothesis behind this study is that the stress waves created from blast and impact loads can be managed, or directed, by using open-cell foam materials with engineered constitutive behavior. Such behavior could lead to the development of new materials and structures with enhanced resiliency to impact and blast loads for use in stand-alone structures or as protection devices.

1.4 Scope of the Study

This study is to provide first-level validation of the hypothesis that the stress-waves from blast and impact loads can be managed (i.e., directed, attenuated, and controlled) through design of high performance cellular materials. The results will be used to establish the design criteria for the fabrication of the nano-reinforced cellular structures. The study was undertaken to numerically evaluate the propagation of the stress waves in homogeneous and non-homogeneous materials in one and two dimensions. One-dimensional (1D) behavior was studied by means of a cantilever bar, and two-dimensional (2D) behavior was studied by means of sandwich beams.

1.5 Approach

The approach to this study is the numerical simulation of stress-wave propagation using the nonlinear finite element program LS-DYNA (LS-DYNA). First, theoretical solutions for one-dimension, which have been extensively studied during past decades, were used to validate the numerical results from 1D models. Upon validation of 1D models with theoretical solutions, the model was used to evaluate other one-dimensional problems. The validated approach in one-dimension was then assumed to be appropriate to study two-dimensional response. Further, the features of stress wave propagation gained from the 1D studies were used as criteria to evaluate results from the 2D analyses. Results for the 2D models are considered to provide a level-1 validation of the mentioned research hypothesis and provide guidance for future experimental studies.

1.6 Organization

The remainder of this thesis is organized as follows. Chapter 2 provides a summary on the theory of elastic and plastic wave propagation in homogeneous and non-homogeneous solid material. Elastic and plastic wave energy distribution in bi-material is presented. Details on the modification of foam materials are presented as well. In addition, a review is given on the studies and works done in the past decades on stress wave propagation in homogeneous and non-homogeneous solid and foam materials. Chapter 3 deals with the study of stress wave propagation in solid material in one dimension. A cantilever bar model was employed. Steel was used for the homogeneous model, while a steel/aluminum hybrid bar was used for the non-homogenous model. Results from numerical simulations were discussed and compared with theories. Chapter 4 deals with the stress wave propagation in foam material in one dimension. Two kinds of foam materials were used, and results from homogeneous and non-homogeneous models highlight the features of stress wave propagation in foam materials. In Chapter 5, studies on the stress wave propagation in foam material in two dimension are presented. Analyses were conducted on four aluminum foam sandwich plates with varied configurations. Results derived from the numerical studies in this thesis confirm the postulated research hypothesis. Finally in Chapter 6, conclusions are provided and future research needs are identified.

CHAPTER 2. THEORETICAL BACKGROUND AND LITERATURE REVIEW

2.1 General

This chapter presents the concept of stress wave propagation, theoretical background on stress wave propagation in solid materials, introduction to foam materials, and developments of research on stress wave propagation.

Sections 2.2 and 2.3 provide well-established and widely accepted knowledge on the mechanism of stress wave propagation in solid materials, and the properties of foam materials with a concept of energy dissipation to help comprehend the complex behavior of stress waves from sophisticated studies and experiments. Meanwhile, it is important to know that all the theories provided here will be used to examine and validate the accuracy of numerical models conducted in this study, as no experimental data or theoretical solutions are available at present for models employed in this study.

Section 2.4 shows research that has been done before on four fields based on the classification of material.

2.2 Stress Wave Propagation in Solid Material

More than one century ago, researchers started to study elastic stress wave propagation in solid materials (Lamb 1904), where deformations occurred in the material while it was still in its elastic region. In 1930 Donnell extended the work for materials behaving in under plastic deformations (Donnell 1930). Stress wave propagation in solid material such as steel has been studied extensively and documented very well (Smith and Hetherington 1994). Therefore, it constitutes important and fundamental knowledge to understand more complex phenomena of stress wave propagation in homogeneous and non-homogeneous materials.

2.2.1 Elastic Stress Wave Propagation in Solid Material

This section deals with two important concepts of velocity related to the phenomenon of stress wave propagation, stress wave reflection and transmission in homogeneous and non-homogeneous models.

At the beginning of this section, the elastic wave speed relation in homogeneous material is presented. The concept of particle velocity is then introduced. After introducing the two velocities, mechanism of stress wave reflection and transmission in homogeneous material explains how those two velocities determine if a propagating stress wave is compressive or tensile based on a certain boundary condition. One example on homogeneous cantilever bar is added to illustrate how to apply this mechanism in different models. In addition, energy transmission of elastic stress wave in non-homogeneous (bi-material) model is explained.

2.2.1.1 Elastic Wave Speed

All materials propagates the effects of external loads by means of elastic wave propagation. In a one-dimensional homogeneous structure, the elastic wave speed depends on the homogeneous material's mass density and Young's modulus (Achenbach 1973), that is:

$$c = \sqrt{\frac{E}{\rho}} \tag{1}$$

This is a widely used equation and has been validated by many experimental data. It indicates that elastic stress wave propagates at a constant speed in a homogeneous material. A theoretical proof of Equation (1) is available (Davis 2000). Figure 3 shows a homogeneous bar with forces applied on the left surface. During the propagation time t, the distance of a propagation of particle velocity is vt in the positive x direction. Since the area of the cross-section is A, a volume (zone in black) formed by the particle velocity is calculated as $V = Avt$. At the same time, stress wave has propagated from 0 to a distance ct in the positive x direction, the volume formed by the propagation of wave velocity (denoted in black box and white box) is calculated as $V = Act$, where v is the particle velocity, c is the wave velocity, and A is the area of cross-section. According to Figure 3, strain is computed as $\varepsilon = \frac{v}{c}$. Given Hooke's law and Newton's equation of motion $F = m(v/t)$, the following equation is derived:

$$F = A\sigma = AE\varepsilon = AE(v/c) = m(v/t) = \rho ctA(v/t) \tag{2}$$

From the Equation (2) above, $c = \sqrt{E/\rho}$ is obtained.

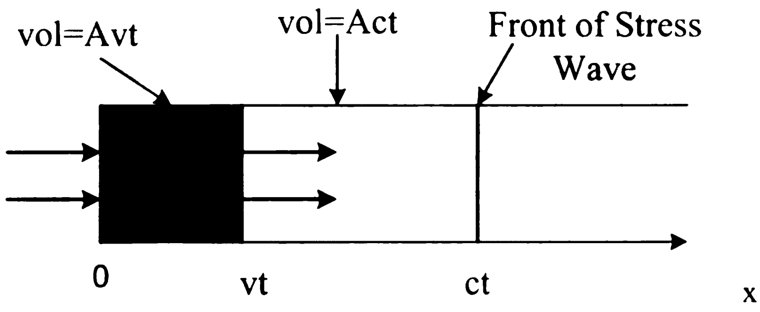

Figure 3. Constant Velocity at Front End of Bar Due to Compressive Stress

When propagating in two and three dimensions, an elastic wave speed depends on a mass density, Young's modulus and Poisson's ratio as shown in Equation (3), where c_l is speed of longitudinal wave, E is Young's Modulus, ρ is density, v is Poisson's ratio. This equation also shows that wave velocity is a constant value when it propagates in a homogeneous material.

$$c_l = \sqrt{\frac{E}{3\rho(1-2v)}} \tag{3}$$

Another equation to calculate wave velocity at a specific location was proposed by Paulino and Zhang (Paulino and Zhang 2005):

$$C_d(x) = \sqrt{\frac{E(x)(1-\upsilon(x))}{(1+\upsilon(x))(1-2\upsilon(x))\rho(x)}} \tag{4}$$

where $C_d(x)$ is speed of longitudinal wave, $E(x)$ is Young's Modulus, $\rho(x)$ is density, $v(x)$ is Poisson's ratio, x indicates the specified location.

The three equations presented above give similar results under the same conditions. Equation (3) and (4) were derived from different experimental data. Equation (1) is widely accepted and offers reasonable results, thus it would also be used in following studies.

2.2.1.2 Particle Velocity

When an exterior load is applied on a structure, the imparted kinetic energy makes particles move. In Figure 4, a pressure load with magnitude σ is applied on the free surface of a bar. The black box represents an area formed by the propagation of stress waves at a time internal δt .Because of the conservation of momentum, particle velocity v can be calculated through Equation (5):

$$v = \frac{\sigma}{\sqrt{\mathrm{E} \cdot \rho}} \tag{5}$$

where σ is stress applied on the structure, E is Young's Modulus, ρ is density. Equation (5) indicates that particle velocity is constant if the material and loading are determined.

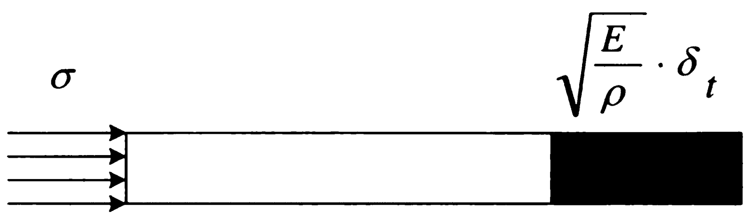

Figure 4. Wave Propagation in δt Time

2.2.1.3 Elastic Wave Reflection and Transmission in Homogeneous Material

In general, two kinds of velocities appear in the defining the phenomena of wave propagation: particle velocity and wave velocity. Particle velocity is used to describe the velocity of a particle (real or imaginary) in a medium as it transmits a wave. Wave velocity represents how fast the message of movement is transmitted from one group of particles to others. They are different in that particle velocity is much slower than the wave velocity in a single material.

Figure 5 offers a model to describe mechanism of elastic stress wave propagation in homogeneous material(Smith and Hetherington 1994). Particle velocity and stress wave velocity, as discussed above play important roles in this model. The mechanism derived from this model is significant for studies conducted in the following chapter, as it is one important criterion to evaluate and comprehend results from numerical models.

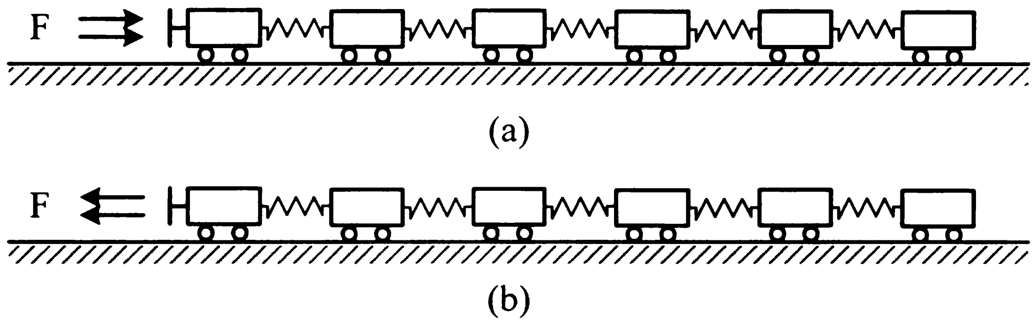

Figure 5. (a) Transmission of a Compressive Wave Front; (B) Transmission of a Tensile Wave Front

In Figure 5, each small truck represents a particle while the springs between each truck represent the intermolecular force. The truck velocity is a particle velocity, and the velocity that the movement transmits from one truck to another is the wave velocity. When the direction of the particle velocity is parallel to the direction of the wave velocity, this wave will be a compressive wave. When the particle velocity and the wave velocity move in opposite directions, this wave will be a tensile wave. For example, Figure 5(a) shows that particle velocity is directed to the right due to a force in the same direction. The wave velocity will also be directed to the right. Therefore, this wave is a compressive wave. Figure 5(b) shows that the particle velocity is directed to the left due to a force applied to the left, but the movement is transmitting from left to right, meaning the wave velocity is in the right direction. Hence, this wave is a tensile wave.

The mechanism from Figure 5 can be applied to other elastic homogeneous models that have dissimilar configurations and boundary conditions. Figure 6 presents an analysis on elastic wave propagation in a homogeneous cantilever bar modeled by using the concepts state above. A pressure load is applied at the free end of the cantilever bar. Particle and stress wave velocities are generated simultaneously. In Figure 6, the big arrow represents wave velocity and the small arrow represents particle velocity.

In Figure 6(a), the wave and particle velocities are in the same direction. Thus this wave is a compressive wave.

In Figure 6 (b), because no displacement and velocity is allowed at the fixed end, a compressive wave reflects back with the same velocity magnitude but in the opposite direction. According to the conservation of momentum, a particle also rebounds back with the opposite velocity. Thus, again, the wave and particle velocities are in the same direction. This wave is also a compressive wave. However, the stress intensity at the fixed end will double because of the overlap of two compressive waves.

In Figure 6 (c), displacement and velocity is allowed at the free end. Thus, the wave reflects back at the free end, but particles continue to move because of their inertia. At that time the bar experiences stretching. Wave velocity and particle velocity act in the opposite directions, so this wave is a tension wave. Stress intensity is zero at the free end because of an overlap of compressive and tensile waves with the same magnitude.

In Figure 6 (d), because no displacement and velocity is allowed at the fixed end, the tension wave reflects back with the same velocity magnitude but in an opposite direction. Because of the intermolecular force, the particles are also being pulled back with the opposite velocity. As a result, the wave and particle velocities propagate in opposite directions. This wave is a tensile wave.

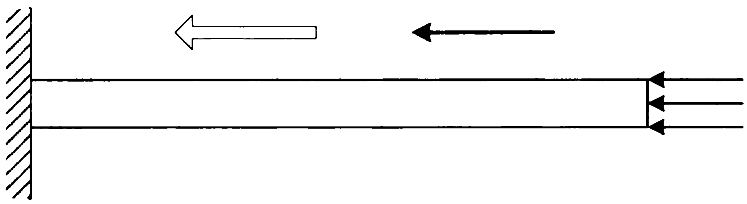

(a) Velocity directions when the wave travel from the right side to the left side

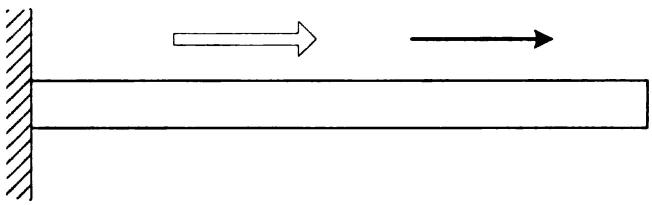

(b) Velocity directions when the wave rebounds at left fixed end and travels from the left side to the right side

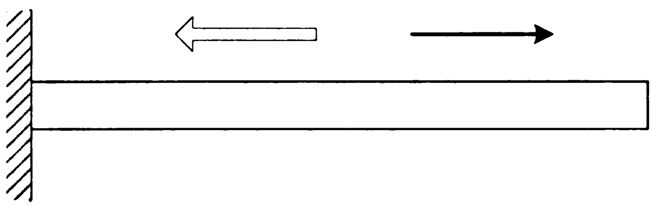

(c) Velocity directions when the wave rebounds at the right free end and travels from the right side to the left side

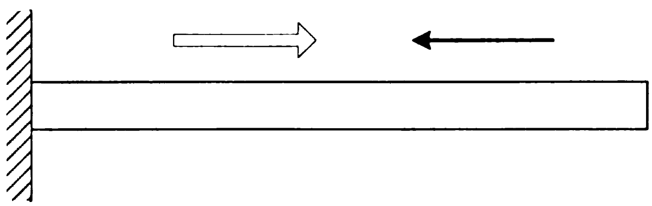

(d) Velocity directions when the wave rebounds at the left fixed end and travels from the left side to the right side

Figure 6. History of Wave Velocities

2.2.1.4 Elastic Stress Wave Reflection and Transmission in Non-homogeneous Material

Figure 7 below shows a non-homogeneous model (bi-material) to illustrate the concept of stress wave reflection and transmission at the interface of two dissimilar materials(Smith and Hetherington 1994). When a stress wave travels from material 1 to material 2, it breaks into two parts: in one part the wave reflects back into material 1 and in the other part wave transmits into material 2. The magnitude of reflected and transmitted waves can be calculated with Equations (6) and (7). From these equations, stresses can be calculated once two materials' mass densities, Young's modulus and original stress are known.

$$\sigma_b = 2\left(\frac{\sqrt{E_2\rho_2}}{\sqrt{E_1\rho_1}+\sqrt{E_2\rho_2}}\right)\sigma_a \tag{6}$$

$$\sigma_c = \left(\frac{\sqrt{E_2\rho_2}-\sqrt{E_1\rho_1}}{\sqrt{E_1\rho_1}+\sqrt{E_2\rho_2}}\right)\sigma_a \tag{7}$$

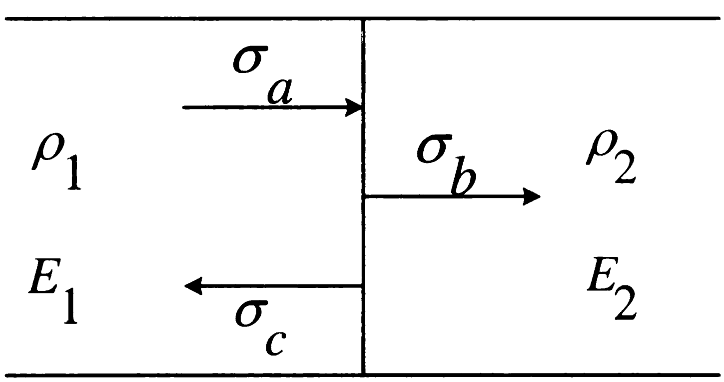

Figure 7. Reflection and Transmission at an Interface between Dissimilar Materials

2.2.2 Plastic Stress Wave Propagation in Solid Material

Plastic stress wave refers to a stress wave propagating inside a plasticized material. It is much more complicated than elastic wave since the material is in a non-linear situation. Once a plastic wave is generated within a material, the speed of wave propagation slows down and the kinetic energy is dissipated (explained in section 2.42) due to permanent plastic deformations in the material.

2.2.2.1 Plastic Wave Speed

Equation (8) below is used to compute the velocity of plastic wave propagation (Donnell 1930). where C_p is velocity of plastic stress wave, ρ is mass density, σ is stress and ε is strain. This equation indicates that the speed of plastic wave varies if the stress-strain curve of a material is non-linear beyond elastic limits. In general, the speed of plastic wave is smaller than the speed of elastic wave, since the tangent modulus of the non-linear region in the stress-strain curve is smaller than elastic modulus.

$$C_p = \sqrt{\frac{1}{\rho}\frac{d\sigma}{d\varepsilon}} \tag{8}$$

Because plastic waves shows different features in dissimilar materials, researchers developed other models to deal with such situations. Equation (9) offers another model to explain the speed of plastic stress waves (G.Vaughn et al. 2005), where $E_t = \frac{d\sigma}{d\varepsilon}$, ρ is mass density, σ is stress, e is mathematical constant and ε is strain. However, this equation has three limitations:

1) If yielding happens with small strains and $E_t << |\sigma|$, $c = \sqrt{E_t/\rho}$ that is identical to the equation proposed by Donnell.
2) If a plastic compression wave propagates along an elastic-perfectly plastic rod ($E_t = 0$), the speed of plastic wave $c = \sqrt{\sigma_Y/\rho}$ where σ_Y is the yield stress.
3) If $E_t = \sigma$, the wave speed of a tensile wave is close to zero.

$$c_l = \sqrt{\frac{E_t - \sigma}{\rho} e^{-\varepsilon}} \qquad (9)$$

2.3 Introduction on Foam Materials

A foam material is a porous material commonly existing in nature and people's life. It is widely used in architectural, industrial, medical and consumer applications primarily due to its light weight compared to its strength/stiffness and the many functions that can be given to the open cavities of the material..

Foam materials are generally divided into two groups: open-cell and closed-cell foams. The mechanical behavior of open-cell foam materials is easier to predict since the gas inside closed-cell foams increases stiffness under compressive loading.

Foam materials are available in a variety of forms. They can be made of metal, metal alloys or ceramic materials. Foam materials made of aluminum have been often used in research related to understanding the mechanical properties of foams as well as their design features.

Studies in this thesis are based on open-cell aluminum foams due to the large amount of research has been done on this material, and the availability of well-developed models to simulate their constitutive behavior. Further, the research being considered as an extension to the presented study is to be conducted on open-cell aluminum foams. It was thus meaningful to simulate this material in the numerical simulation in the current research.

Since one objective of these studies is to demonstrate that a modified, or "engineered," foam material may allow control over the propagation of stress waves, it is helpful to know the properties of foam material and the means of modifying them. Considerable research evidence exists to prove that foam materials are good at protecting structures by means of mitigating stress and dissipating kinetic energy. It is then also important to learn the mechanisms of stress mitigation and energy dissipation in foam materials.

2.3.1 Properties of Open-cell Foams

Gibson and Ashby have summarized an extensive treatise on the behavior and modeling of foam materials (Gibson and Ashby 1988). Their work has shown that open-cell foams may be adequately modeled based on the behavior of simple unit cells. One of the simplest three-dimensional cells that can be used to simulate the behavior of open-cell foams is shown in Figure 8 (Gibson and Ashby 1988).. This cellular solid is a cubic cell whose edges are made up of solids struts at a microstructural level. At each face, two half-length struts are assumed to connect with other cells with identical configuration. The collection of many cells forms a foam block commonly used in experiments.

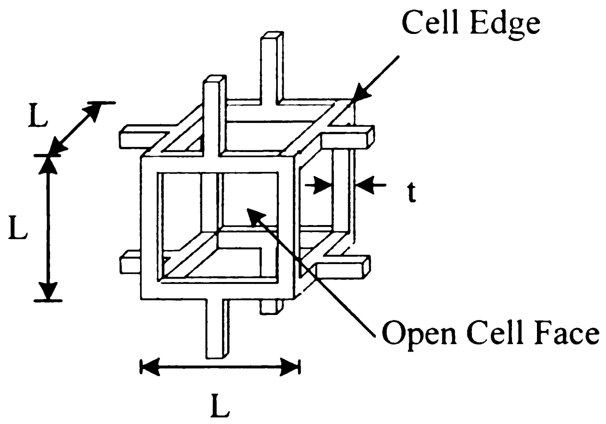

Figure 8. Cubic Model for Open-cell Solid [From (Gibson and Ashby 1988)]

Generally, the tensile modulus E_t of a metal foam is greater than its compressive one, E_c. It has been observed that open-cell foams experience three stages while loaded in compression. The first stage consists of deformations of the cell edges while the solid material is in its linear elastic range. Once the compressive load goes beyond the yield stress of the solid material, the foam enters the plastic collapse region and its macroscopic response features a plateau region in its stress strain response. As the cells collapse completely, the edges and faces of cells touch each other and the foam material enters the densification region at the macro scale, which leads to a rapid increase in the resisted stresses while the strains do not change significantly.

Results from experiments show that the relative density, ρ^* / ρ_s (i.e., the mass density of the foam divided by the mass density of solid material) and the properties of the material of which the foam is made from determine the crushing behavior of open-cell foams. Table 1 lists the equations proposed by Gibson and Ashby (Gibson and Ashby 1988) to calculate the mechanical properties of open-cell foams based on the simple unit cell in Figure 8.

In Table 1, ρ^* is the mass density of the foam material; ρ_s refers to the mass density of the solid material from which the foam is made of; E_s is the Young's modulus of solid material; σ_{ys} refers to the yield strength of the solid material; σ_{fs} is the fracture strength of the solid material.

Table 1. Mechanical Properties of Open-cell Foam Material [From (Gibson and Ashby 1988)]

Property	Open-cell foam material
Relative Density	$\dfrac{\rho^*}{\rho_s}$
Modulus of Elasticity, E [GN/m^2]	$E^* \approx E_s\left(\dfrac{\rho^*}{\rho_s}\right)^2$
Shear Modulus, G [GN/m^2]	$G^* \approx 0.375E_s\left(\dfrac{\rho^*}{\rho_s}\right)^2$
Poisson's Ratio	$\upsilon^* = \dfrac{E^*}{2G^*} - 1$
Compressive Elastic Strength [MN/m^2]	$\sigma^*_{el} = 0.03E_s\left(\dfrac{\rho^*}{\rho_s}\right)^2\left(1+\left(\dfrac{\rho^*}{\rho_s}\right)^{1/2}\right)^2$

Table 1(cont'd)

Compressive Plastic Strength $[MN/m^2]$	$\sigma^*_{pl} = 0.3\sigma_{ys}\left(\frac{\rho^*}{\rho_s}\right)^{3/2}$
	$\sigma^*_{pl} = 0.23\sigma_{ys}\left(\frac{\rho^*}{\rho_s}\right)^{3/2}\left(1+\left(\frac{\rho^*}{\rho_s}\right)^{1/2}\right)$ (including density correction)
Compressive Crushing Strength $[MN/m^2]$	$\sigma^*_{cr} = 0.65\sigma_{fs}\left(\frac{\rho^*}{\rho_s}\right)^{3/2}$
Densification strain	$\varepsilon_D = 1-1.4\left(\frac{\rho^*}{\rho_s}\right)$
Tensile Plastic Stiffness $[GN/m^2]$	$E^*_A = E_s\left(\frac{\rho^*}{\rho_s}\right)$
Tensile Plastic Collapse $[MN/m^2]$	$\sigma^*_a = \sigma_{ys}\left(\frac{\rho^*}{\rho_s}\right)$
Tensile Brittle Strength $[MN/m^{3/2}]$	$K^*_{IC} = 0.65\sigma_{fs}\sqrt{\pi l}\left(\frac{\rho^*}{\rho_s}\right)^{3/2}$

In addition, Table 2 lists formulas to predict the behavior of open-cell metal foams derived from experimental data (Ashby et al. 2000).

Table 2. Mechanical Properties of Open-cell Metal Foam [From (Ashby et al. 2000)]

Mechanical properties	Open-cell metal foam
Young's modulus (GPa), E	$E = (0.1-4)E_s\left(\frac{\rho}{\rho_s}\right)^2$
Shear modulus (GPa), G	$G \approx \frac{3}{8}E$
Bulk modulus (GPa)	$K \approx 1.1E$
Flexural modulus (GPa)	$E_f \approx E$
Poisson's ratio	0.32-0.34
Compressive strength (MPa)	$\sigma_c = (0.1-1.0)\sigma_{c,s}\left(\frac{\rho}{\rho_s}\right)^{3/2}$
Tensile strength (MPa)	$\sigma_t \approx (1.1-1.4)\sigma_c$
Endurance limit (MPa)	$\sigma_e \approx (0.5-0.75)\sigma_c$
Densification strain	$\varepsilon_D = (0.9-1.0)\times\left(1-1.4\left(\frac{\rho}{\rho_s}\right)+0.4\left(\frac{\rho}{\rho_s}\right)^3\right)$
Loss coefficient	$\eta \approx (0.95-1.05)\times\frac{\eta_s}{(\rho/\rho_s)}$
Hardness (MPa)	$H = \sigma_c\left(1+2\frac{\rho}{\rho_s}\right)$
Initiation toughness (J/m^2)	$J^*_{IC} \approx \beta\sigma_{y,s}l\left(\frac{\rho}{\rho_s}\right)^p$

Comparing Table 1 and Table 2 it can be seen that the formulae are similar. The parameters in Table 2 were chosen based on experimental data and empirical experience. Formulas in Table 1 are more specific and can be plotted easily. Thus the stress-strain curves used for the analyses in this thesis are based on these formulas presented in Table 1.

As previously noted, the compressive stress-strain curve for open-cell foam has three regions: linear elasticity, plastic collapse and densification. In experiments, the dramatic increase of the stress-strain curve happens after the foam has been compressed to a relative density of about 0.5.

Based on the formulas offered in Table 1, a new set that describes the macro-scale compression behavior of open-cell metal foams is deduced and provided in Table 3. The equations can be used to define the complete compressive stress-strain model for an open cell foam of given relative density and known base solid material. Two parameters D and m that are derived from experimental data are used to calculate strain in plastic and densified regions, and stresses in densification region. In the current thesis, D=2.3 and m=1.

Table 3. Parameters of Theoretical Stress-Strain Curve of Open-Cell Foam

	Strain	Stress
Elastic region $0<\varepsilon<\varepsilon_e$	$\varepsilon_e = 0.3\dfrac{\sigma_{ys}}{E_s}\left(\dfrac{\rho}{\rho_s}\right)^{-\frac{1}{2}}$	$\sigma^* = E_s\varepsilon\left(\dfrac{\rho}{\rho_s}\right)^2$
Plateau region $\varepsilon_e<\varepsilon<\varepsilon_d$	$\varepsilon_d = \varepsilon_D\left(1-\dfrac{1}{D}\right)$ $\varepsilon_D = 1-1.4\dfrac{\rho}{\rho_s}$	$\sigma^* = \sigma^*_{pl}$ $\sigma^*_{pl} = \sigma_{ys}\times 0.3\times\left(\dfrac{\rho}{\rho_s}\right)^{\frac{3}{2}}$
Densification region $\varepsilon_d<\varepsilon<\varepsilon_D$	$\varepsilon_d = \varepsilon_D\left(1-\dfrac{1}{D}\right)$ $\varepsilon_D = 1-1.4\dfrac{\rho}{\rho_s}$	$\sigma^* = \sigma^*_{pl}\dfrac{1}{D}\left(\dfrac{\varepsilon_D}{\varepsilon_D-\varepsilon}\right)^m$ $\sigma^*_{pl} = \sigma_{ys}\times 0.3\times\left(\dfrac{\rho}{\rho_s}\right)^{\frac{3}{2}}$

By using relative density 0.3 and $\sigma_{ys}/E_s = 1/30$ the compressive stress-strain response for an open-cell foam was calculated and the complete trace is shown in Figure 9. The values and plot are in agreement with the results provided by Gibson and Ashby (Gibson and Ashby 1988). Normalized stress-strain curves with different relative densities are also plotted.

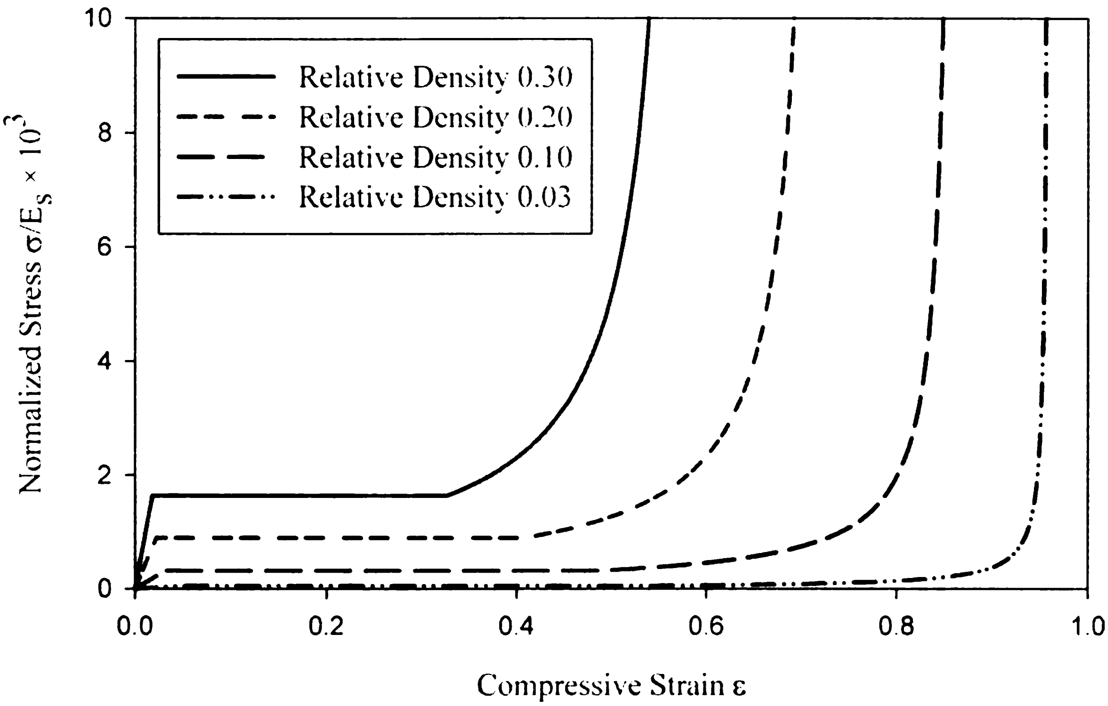

Figure 9. Normalized Theoretical Stress Strain Curves of Rigid Plastic Foams

Since these formulas can predict the identical curves from (Gibson and Ashby 1988), they can also offer a stress-strain curve of plastic foam by using real material properties. By using a relative density of 0.3, a yield stress for aluminum of 80MPa, and a Young's modulus 80 GPa, a normalized compressive stress-strain curve of open-cell aluminum foam is shown in Figure 10, in which the onset of plastic strain is 0.55×10^{-4}, the onset of densification strain is 0.327 and the limit densification strain is 0.580. These values are identical to data from (Gibson and Ashby 1988). The plastic stress is calculated to be 3.9 MPa can be obtained as well from Figure 10.

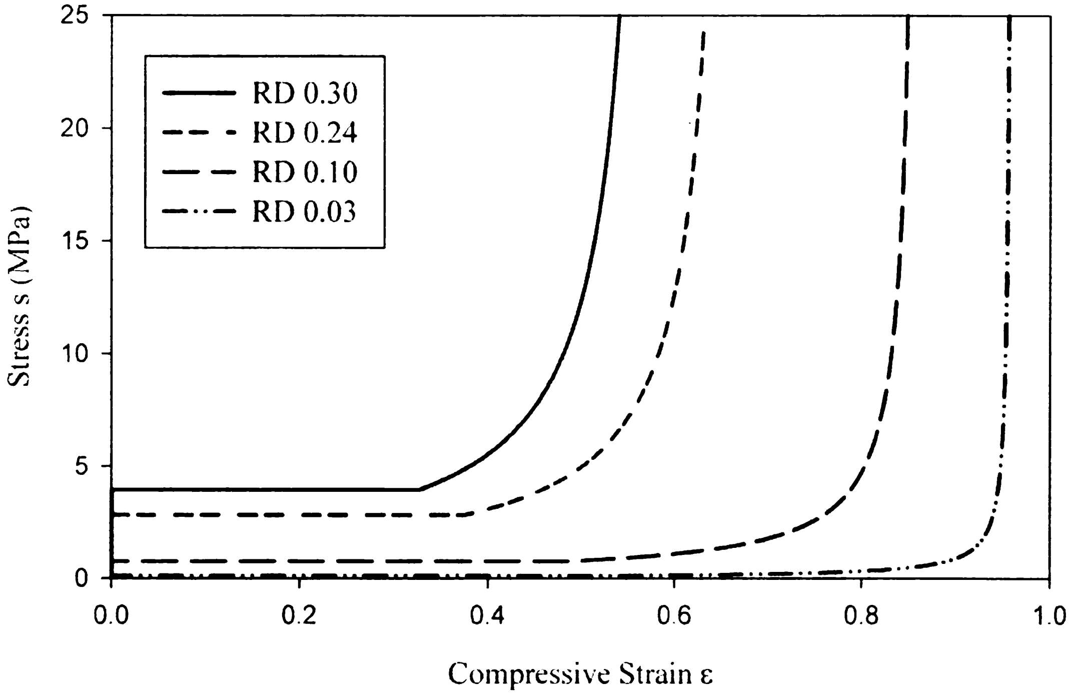

Figure 10. Plastic Foam Theoretical Stress-Strain Curves with Different Relative Density

By decreasing the relative density of the foam the plastic plateau region extends, the plastic, or yield, stress drops, and the onset of densification strain moves toward higher values. For example, for a foam with a relative density of 0.1, the stress-strain curve is shown in Figure 10. The onset of plastic strain is 0.0316, the onset of densification strain is 0.486, the limit end of densification strain is 0.860, and the plastic stress is 0.75 MPa.

2.3.2 Energy Dissipation in Foam Materials

The macro-scale compressive stress-strain response of a typical metal foam is composed of three regions: linear elasticity region, plastic collapse plateau region and densification region. The kinetic energy produced by impact and blast loading is mainly dissipated under the plateau region. In this region, the kinetic energy is transferred into strain energy and fracture energy due to permanent deformation. A schematic of this compressive stress strain behavior is shown in Figure 11.

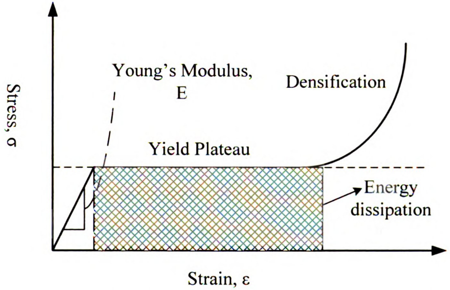

Figure 11. Schematic of Compression Stress Strain Curve of Plastic Foam

Tests on aluminum-based foams show that the dependence of the plastification stress, or plateau stress, on strain rate is not strong. Nonetheless, it is important to separate the effect of strain rate and impact velocity on the dynamic response of metallic foam. The negligible effect of stain rate is associated with the fact that aluminum displays only minor strain rate sensitivity. In contrast, material inertia leads to enhanced stresses at high impact velocities.

Homogeneous foam is most efficient for absorbing energy when the demand strain just reaches to onset of densification. This is because most energy is absorbed under the plastic plateau region (denoted in shadow area in Figure 11) without a significant increase in stress.

In order to maximize the energy dissipation area shown in Figure 11, one approach is to modify the relative density of the foam, and/or the Young's modulus and yield strength of solid material. As these three parameters increase, the yield stresses of the foam material increase but the densification strain decreases.

2.4 Developments of Research on Stress Wave Propagation

The following sections provide an overview of the research that has been done in the past decades related to stress wave propagation, which may be categoraized the medium of propagation: stress wave propagation in homogeneous solid materials, in non-homogeneous materials, in homogeneous foam materials and in non-homogeneous foam materials.

2.4.1 Stress Wave Propagation in Homogeneous Solid Material

The problem of stress wave propagation has been studied extensively over the past century. Analytical solutions to elastic wave propagation in homogenous material were among the first and most significant contributions to the topic. An analytical solution for one dimensional (1D) stress wave propagation in a homogeneous material (Meirovitch 1967) was given as follows:

$$\sigma(x,t) = \sigma^0 f(t + \frac{x}{C_d}) + \hat{\sigma}^0 f(t - \frac{x}{C_d}) \tag{10}$$

where C_d is the speed of waves, σ^0 is initial stress, $\hat{\sigma}^0$ is dynamic stress, t is time and x is a location.

Equation (9) was validated by (Paulino and Zhang 2007) through numerical studies on a slender bar model subjected to a half-sine impulsive tension load. In a 1D homogeneous bar, the half-sine stress wave travels in the slender bar at constant speed and maintains its half-sine shape in spite of experiencing reflection at the boundaries. Comparisons between the numerical and analytical solutions showed that these two results agreed with each other very well.

However, no widely accepted theoretical solutions are available for stress wave propagation in 2 dimensions (2D) so far. Some researchers have implemented theoretical and numerical studies(Li et al. 2001; Berezovski et al. 2003). But the solutions were not considered suitable for the models studied in this thesis. Although (Dizaji and Jafari 2009) provided a three-dimensional (3D) fundamental solution of wave propagation, it is still not widely accepted and too complicated for direct application.

Therefore, validating numerical models in one dimension with analytical solutions and theoretical principles will provide confidence on the framework of numerical simulations on two-dimensional models, under the condition that no experimental data and analytical solution is available for the validation of the numerical simulations.

2.4.2 Stress Wave Propagation in Non-Homogeneous Solid Material

Research on stress wave propagation in non-homogeneous solid material includes studies on layered solid material and functionally graded metal (FGM) materials.

The transmission and reflection of stress wave and energy at the interface between dissimilar materials in layered solid material is a unique feature when compared with homogeneous materials. Thus, studies in this field originated when the attention shifted from homogeneous models to layered solid materials.

Much of the work on understanding wave propagation in layered non-homogeneous solid materials was focused on the geometric dispersion of elastic waves. As the interest on the influence of scattering effects induced by internal interfaces on shock wave propagation in a layered non-homogeneous model emerged, a series of experimental studies were conducted on this topic(Zhuang et al. 2003). Results showed that the interface scattering in periodically layered composite affected bulk response of the composites to shock compression loading. The effect was to slow down the propagating speed of shock wave.

Further, shock energy was dissipated and dispersed by the impendence mismatch at the interface during propagation. This is because the planar interfaces interacted with the incident shock wave, and the transmitted and reflected waves, whose amplitudes were determined by impedance factors (Chen et al. 2004). The discontinuities are not only due to the dissimilarity of materials, but also the non-linear reactions from these materials. An application of nonlinear stress–strain relation for materials in numerical simulations of the plate impact problem of a layered non-homogeneous medium was developed to capture the effects form material's nonlinearity (Berezovski et al. 2006). This introduced a modified nonlinear stress–strain relation $\sigma = \rho c^2 \varepsilon(1 + A\varepsilon)$, and a modified sound velocity $\hat{c} = c\sqrt{1+2A\varepsilon}$, in which ρ is the density, c is conventional longitudinal wave speed, A is a parameter of nonlinearity.

As stated above, dispersion and attenuation were observed in experiments on layered solid models. This indicates that this kind of structures can be one option for energy dissipation, and scattering effects occurring at the interface, and which need to be considered during numerical analyses and experiments.

As a new kind of material, functionally graded materials (FGM), attracted researchers' attentions since its properties can be changed according to a linear or non-linear function as specified by designers (Erdogan 1995). This feature of high customization minimizes the limitation on the material and gives researchers more opportunities to optimize a structure to meet its demands.

From experiments and numerical simulations, results have shown that layered materials and FGM material with different functions of gradation have have an influence not only on the dynamic behavior of these structures but also on the probability and locations of failures (Li et al. 2001). A metal-ceramic composite material was used, and the volume fractions of the reinforcement were varied for different cases. Different volume fractions of reinforcement were assigned for the individual layer in a layered model, and smooth gradations of ceramic volume fractions across the thickness of the plate were assigned to the functionally graded model. These numerical models were verified by experiments. Results shows the dispersion of waves as a result of the gradation of the material and the gradation of material properties, can affect the dissipate energy and strain energy in the model. Meanwhile, in order to improve the accuracy of the numerical simulation on FGM materials, new kinds of finite elements with graded properties to simulate stress wave propagation were developed (Santare et al. 2003). Researchers have not developed an analytical solution to the two-dimensional problem, so they compared results between graded and ordinary elements. Results show that conventional elements offer a discontinuous stress field in the direction perpendicular to the material property gradient while the graded elements give a continuous distribution. An eight-noded isoparametric formulation was used to solve one-dimensional examples. Results were compared with the analytical solution provided by (Chiu and Erdogan 1999).

2.4.3 Stress Wave Propagation in Homogeneous Foam Material

Porous materials or foams have unique characteristics such as light weight, low yield stress, easy to reach large deformation due to its microstructure. There exists a large amount of research that has showed that the way of absorbing energy or attenuating stress is through plastic deformation (see 2.3.2). Thus, foam materials have been the subject of study in many research projects related to energy dissipation and stress mitigation.

Considerable research on stress wave propagation in homogeneous cellular material was conducted during recent years. The compressive properties and energy dissipation of aluminum alloy foam and aluminum foam under dynamic loading was recently studied by (Wang et al. 2001). Results show that energy absorption efficiency peaks at a compressive strain of 0.2-0.3, and it decreases when porosity increases at a fixed value of strain. The efficiency of energy absorption in aluminum alloy foam was found to be greater than the one in pure aluminum foam.

Meanwhile, validation studies of the material constitutive foam model in LS-DYNA were conducted (Hanssen et al. 2001). Results show that constitutive model 63 is closed to the deformed shape of an experimentally-crushed cube. Therefore, this constitutive model was employed in the current studies.

Research on the dynamic testing and modeling of soft structural material made of metals such as aluminum honeycombs and foams (Zhao 2001) found an enhancement of the crushing strength under high speed impact loading in foam materials. The inertia effects associated with the localization of crushing contributed to this phenomenon. The experimental data also showed the existence of a shock front in cellular structure under impact load, especially at low critical velocities around 50 m/s (Zhao et al. 2007). A high speed camera was used to capture the strain field image in the cellular material, and this image was used to measure the shock front velocity and analyze shock enhancement (Pattofatto et al. 2009). The image analysis showed that the shock wave propagates at a constant velocity through the foam.

Research on elastic waves propagating through an ideal cellular structure with a closely packed array of thin-walled rings was carried out by Shim et al. (Shim et al. 2008). Results showed that the dominant mode of elastic energy propagation in a thin-walled ring arrays is flexural instead of extensional and shear waves. Three kinds of ring packing arrangements, as shown in Figure 12, were employed in experiments: square-packed, transverse close-packed and vertical close-packed arrangement. An impact force was applied on the ring arrays. Results showed that a higher bar velocity c_0 and a thicker ring wall h lead to higher wave propagation speeds through the ring array.

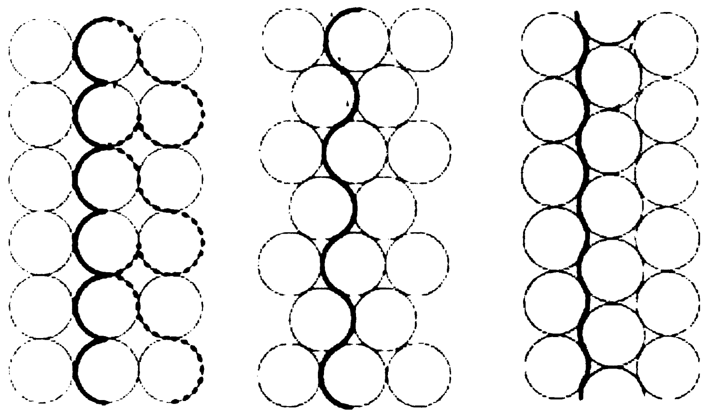

Figure 12. Ring Packing Arrangements in Experiments: (a) Square-packed, (b) Transverse Close-packed and (c) Vertical Close-packed Arrangement[From Shim et al (2008)]

2.4.4 Stress Wave Propagation in Non-Homogeneous Foam Material

Research has shown that foam materials have a better performance than solid materials in terms of energy dissipation and stress mitigation. In addition, scattering effects at the interface of two dissimilar materials reduces the stress wave energy and disperses the stress wave. Therefore, it is natural to combine these two advantages to maximize the capacity of energy dissipation and stress mitigation of foam material.

During recent studies, five novel layered material models for impact application have been assessed by experiments and numerical simulation (Tasdemirci and Hall 2009). Results showed that geometrically tailoring a multilayered material system to minimize stress propagating into the backing plate is possible for any specified impact velo

con

a ni

con

exp

red

C

ma

ide

sin

lo

AE

velocity. In other words, stress waves or impact loading energy could be mitigated and controlled in an appropriate design by using dissimilar solid materials. In the designs, a rubber or Teflon foam was used as an interlayer to separate a ceramic faceplate and a composite backing plate (Figure 13). Four FEM models were validated by experiments and the results showed that use of multiple Teflon foam interlayers could reduce average stresses in the layered material.

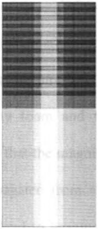

Figure 13. Baseline Configuration and Different Cases of Interlayer Configurations Used in the Finite Element Study. [From Tasdemirci and Hall (2009)]

With the development of modern materials engineering knowledge and manufacture techniques, functionally graded foam material (FGFM) appear to be an ideal candidate to maximize the energy absorbing capacity of a material or structure, since its properties can be customized based on required functions.

During recent studies, functionally graded foam model perform perfectly under low energy impact loads (Cui et al. 2009). One model established by ABAQUS(ABAQUS) was used to develop the material's characteristics of energy dissipation. Besides the results that FGFM performed perfectly under low energy impacts, the model showed that when the impact energy was high, the low-density region of the graded foam absorbed only a small fraction of the total energy since it densified very soon after plastic collapse. For foam materials with a given density, it was determined that at a certain critical stress the efficiency of foam is maximized. Meanwhile the duration of a high acceleration due to an impact can be reduced.

The propagation of stress waves through functionally graded foam material has been studied as well. In the study by Kiernan et al. (Kiernan et al. 2009), a finite element model of a Split Hopkinson Pressure Bar (SHPB) test was developed to carry out simulations on uniform density foam and the results were validated against laboratory SHPB tests. It was found that the magnitude of transmitted stress wave was smaller when the stress wave propagated from a stiff material into a soft one. An increasing density gradient would lead to an amplified transmitted stress. Once the finite element model was validated by experimental data, the optimization work was conducted by the combination of yield stress and density range of foam materials through numerical models.

2.5 Summary

The foregoing review shows that the phenomenon of stress wave propagation has been investigated extensively during the past decades. Researchers have identified the fundamental mechanisms of stress wave propagation in solid materials, discovering that plastic deformation causes energy dissipation. In addition, the scattering effect in layered materials has been shown to play an important role in reducing induced kinetic energy. An increasing or decreasing gradation of stiffness in a non-homogenous material leads to an increasing or decreasing transmitted stress wave, respectively, when compared with the propagation of a stress wave in a homogeneous material. As researchers' attention shifted from solid to foam materials, it has been found that the efficiency of energy dissipation and stress mitigation in foam materials is much higher than in solid materials. Similar conclusions were derived from research on non-homogeneous materials as well. The dispersion of stress wave at the interface between two dissimilar materials has been shown to reduce stress magnitude and propagated kinetic energy. When stress waves travel from stiff material to soft material, the magnitude of the stress reduces.

Based on an extensive review, the research done to date has focused on the concept of energy dissipation and stress mitigation. However, another concept, the direction of stress wave propagation in two dimensions remains undeveloped. By conducting studies on the concept of guiding the stress wave propagation in this thesis, the complete thought of stress wave management, which includes control on the energy dissipation and control of the speed, magnitude and direction of the stress wave, will be fully extended.

CHAPTER 3. ONE-DIMENSIONAL STRESS WAVE PROPAGATION IN SOLID MATERIALS

3.1 General

This chapter presents numerical studies on stress wave propagation in solid materials in one dimension. The study is based on the response of a cantilever slender bar subjected to a compressive impulsive load at its free end. Studies were performed on a homogeneous model, consisting of a single material bar, and a non-homogeneous model, consisting of a bi-material bar.

The speed of stress wave propagation and the energy transfer between kinetic energy and internal energy were the responses of interest for the homogeneous model. The energy transfer between distinct materials (i.e., different stiffness) was the response of main interest for the non-homogeneous model.

The homogeneous model employed steel as the material, while the non-homogeneous model featured steel and aluminum segments (half each). A mesh sensitivity study was carried out to determine an appropriate size of mesh element.

Results showed that stress wave propagated in a homogeneous material at a constant speed. Part of the kinetic energy is stored as internal energy due to permanent plastic deformation. At the interface of distinct materials (different stiffnesses), one part of the stress is reflected and the other part is transmitted to other material in proportion to the mass density and Young's modulus of the materials.

Although stress wave propagation in 1D has been extensively studied during past decades and it is well documented in papers and books, numerical simulations of this behavior were performed to validate the numerical approach. The results showed that the numerical models in this chapter offered reasonable results and the conclusions drawn from them was consistent with theoretical solutions.

3.2 Model Definition

In this section, information of homogeneous model would be offered. A study on mesh sensitivity would be presented as well. And this study was used to determine an appropriate size of a mesh element.

3.2.1 Model Description in 1D Cases

A cantilever bar with a length 0.9m and a height 0.045m (Figure 14) was used to investigate elastic and plastic stress wave propagation in a homogeneous material. In this model, the right surface, the top and the bottom of the bar are free of tractions and the left surface is fixed to a rigid boundary.

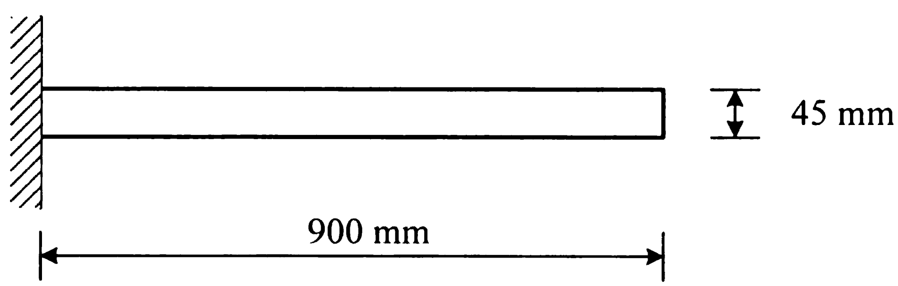

Figure 14. Homogeneous Slender Bar Model for Solid Material in 1D Cases

After a mesh sensitivity study, an appropriate mesh discretization was determined to be 300 × 15 squares, each was divided into 2 triangular elements (Figure 15). The 3-node element type was a shell element with linear shape functions and a single integration point. Since this plane strain element can capture the deformation of the model, and it reflects the behavior of dilatational wave from the impacted load.

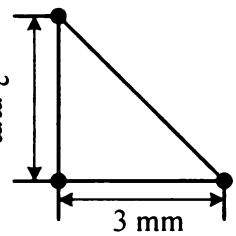

Figure 15. Right-triangle Shape Shell Element

3.2.2 Mesh Sensitivity Study

The mesh sensitivity study was performed for the homogeneous elastic model. The material was steel (Figure 20) and a unit impulsive tension force was applied (Figure 22). Three different meshes were evaluated. To compare the performance of the different models, three locations were chosen to extract stress histories, as shown in Figure 16. All of 3 points were at mid-height of the bar.

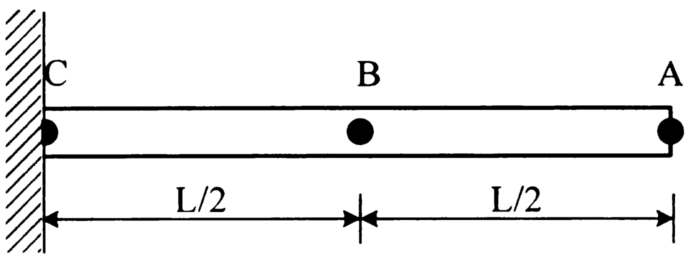

Figure 16. The Locations of Chosen Elements in 1D Models

3.2.2.1 Mesh Case 1

The bar was discretized into 300 × 15 quads, each divided into two T3 elements (3-node element with linear shape functions and has a right-triangle shape as shown in Figure 15). This led to a mesh with 4,816 nodes and 9,000 T3 elements.

Figure 17 shows the stress history of mesh case 1. A solid line shows the stress history at point A; the dash-double-dot line represents stress from point B, and the dashed line indicates the stress at point C. As shown in the graph, the triangular stress wave travels in the slender bar at a constant speed and maintains its triangular shape wave in spite of reflections at the boundaries. The stress magnitude at point A is 0.323 MPa. Stress wave reaches point C at 0.15 ms and the magnitude of stress wave doubles to 0.667 MPa. When the rebound stress wave comes back to point A at 0.30 ms, the magnitude of stress wave is zero. This agrees with the theory provided in the Chapter two.

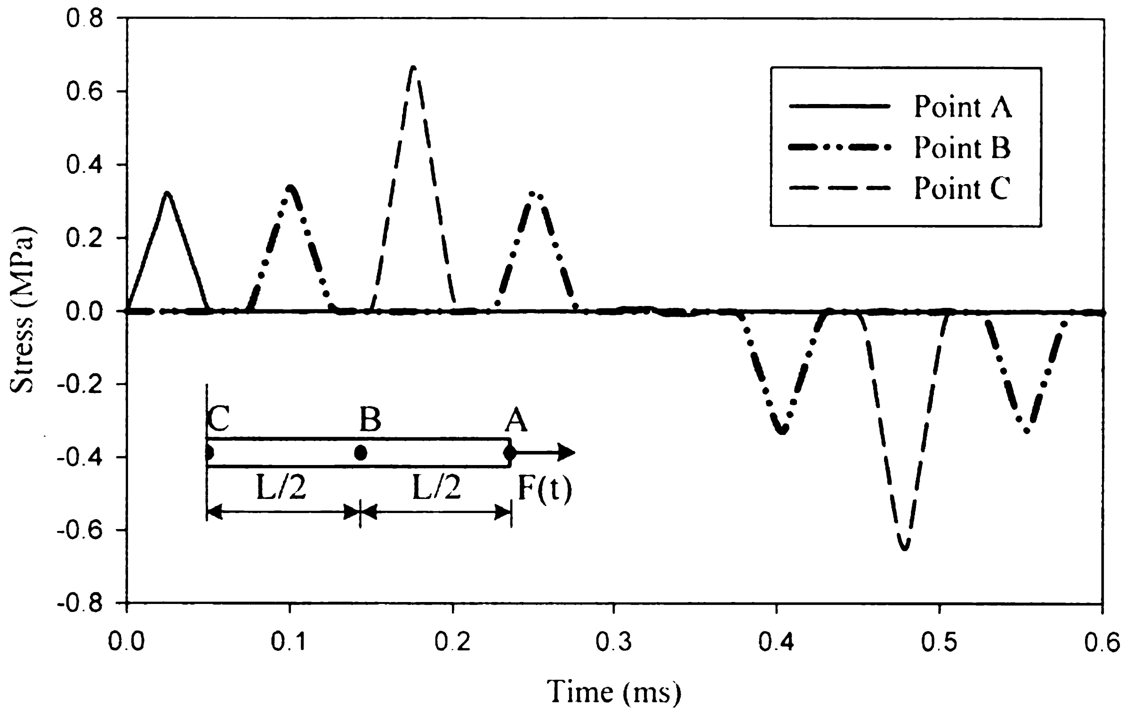

Figure 17. Stress History of T3 Element with Length 3 mm

3.2.2.2 Mesh Case 2

The bar was discretized into 150 × 8 quads, each divided into two T3 elements (3-node element with linear shape function and has a right-triangle shape). This led to a mesh with 1359 nodes and 2,400 T3 elements.

Figure 18 shows the stress history of mesh case 2. Stress histories from the three points follow the same plotting convention as presented in mesh case 1. In this case, the stress magnitude at point A is 0.188 MPa and it doubles to 0.372 MPa at point C. The difference in the stress magnitude is only due to the different mesh size.

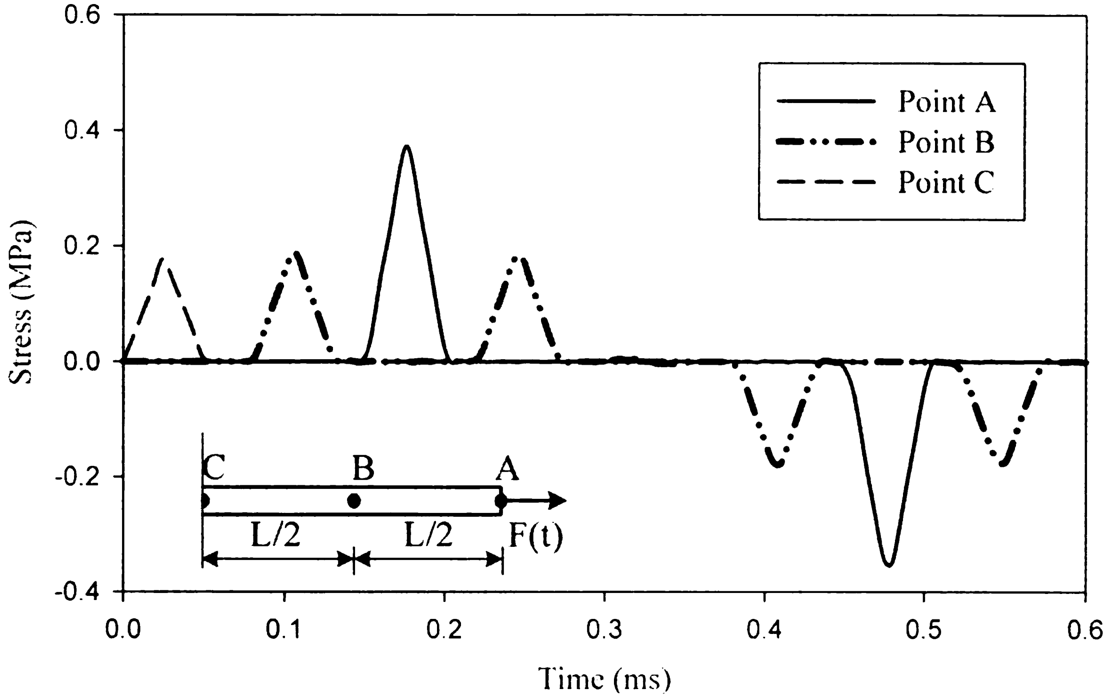

Figure 18. Stress History of T3 Element with Length 6 mm

3.2.2.3 Mesh Case 3

The bar was discretized into 300 × 15 quads. This led to a mesh with 4,816 nodes and 4,500 elements. Figure 19 shows the stress history in mesh case 3. Stress histories from the three points follow the same plotting convention as presented in mesh case 1. At 0.025 ms the stress magnitude at point A is 0.327 MPa and it doubles to 0.670 MPa at point C (at 0.175 ms). Comparing Figure 19 with Figure 17, it can be seen that stress histories from both cases are very close.

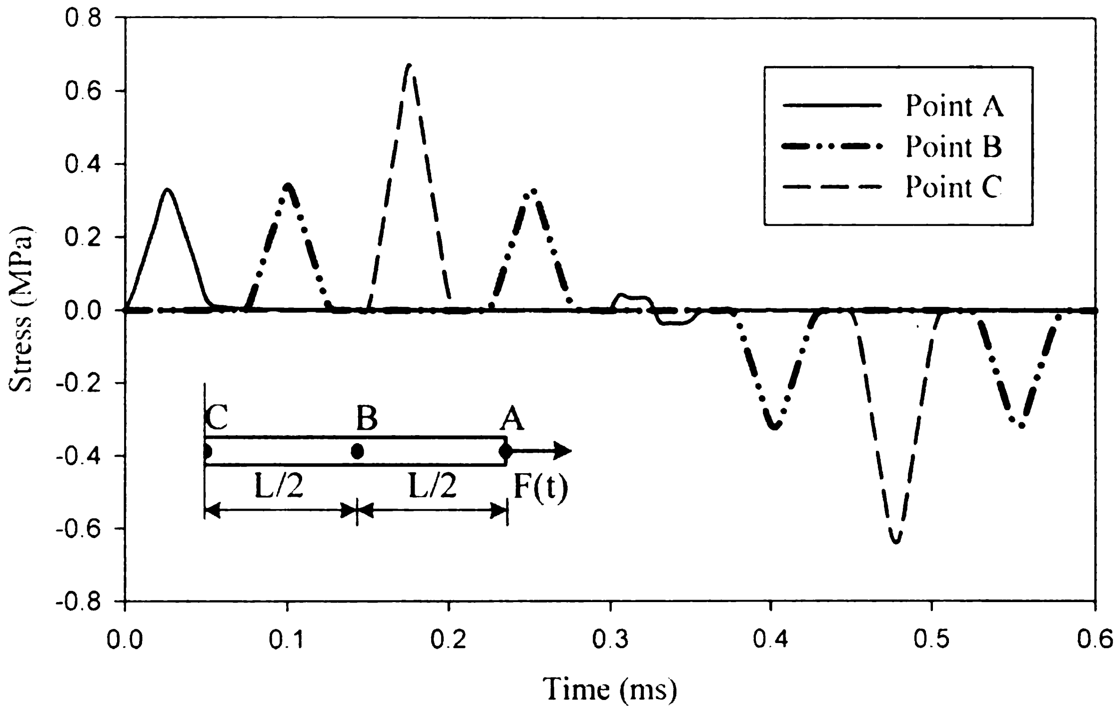

Figure 19. Square Element with Length 3 mm

3.2.2.4 Conclusion

In mesh case 1, the maximum stress is around 0.64 MPa and the minimum stress is around -0.63 MPa when the element is a T3 with 3mm length. In mesh case 2, the maximum stress is around 0.37 MPa and the minimum stress is around -0.37 MPa when the element is a T3 with 6 mm length. In mesh case 3, the maximum stress is around 0.65 MPa and the minimum stress is around -0.67 MPa when element is a square with length 3mm.

From these results, it can be seen that minimum element size should be set in order to capture accurate wave propagation behavior. Elastic wave velocity is the same in each case since wave velocity is a material's property that is determined by Young's modulus and mass density. However, stresses vary with element size. It was also seen that stresses did not change much when different element types were employed. Mesh case 1 was thus chosen for the numerical models.

3.3 Material Modeling

Two different materials were used in the numerical simulations: steel and aluminum.

The materials properties for Steel were: Young's modulus: 200 GPa, mass density: 7800kg/m^3, Poisson's ratio: 0.3, yield stress: 200MPa; plastic tangent modulus: 50MPa, and ultimate tension strength: 400MPa. A stress-strain curve for the steel material is shown in Figure 20. The MAT_001 material model in LS-DYNA was used as the elastic steel constitutive model. The MAT_024 material model in LS-DYNA was used as the elastic-plastic steel constitutive model.

The properties of Aluminum were: Young's modulus: 80 GPa, mass density: 2800kg/m^3, Poisson's ratio: 0.33, yield stress: 80MPa, plastic tangent modulus: 10MPa, and ultimate tension strength: 110MPa. A stress-strain curve for aluminum is shown in Figure 21. The MAT_001 material model in LS-DYNA was used as the elastic aluminum constitutive model. The MAT_024 material model in LS-DYNA was used as the elastic-plastic steel constitutive model.

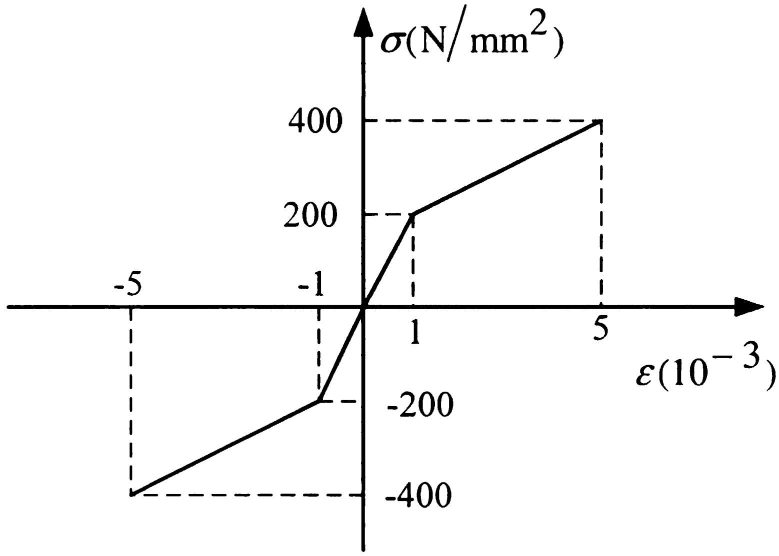

Figure 20. Stress Strain Curve for Steel

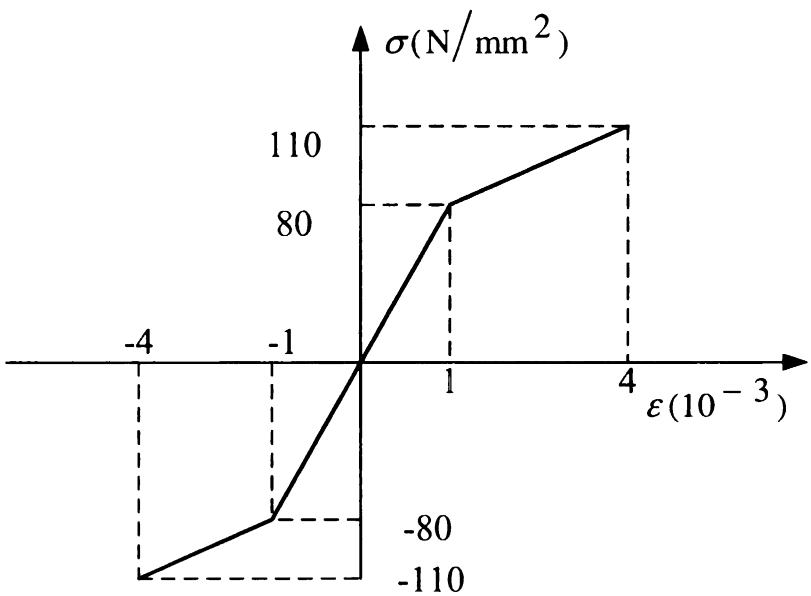

Figure 21. Stress Strain Curve for Aluminum

3.4 Stress Wave Propagation in Homogeneous Solid Materials

In this section, results from the simulation of homogeneous solid models are presented and discussed. The aim of these studies is to develop and validate the framework for the finite element models within which the remainder of the analyses will be conducted. Numerical models, corresponding loading histories and materials are presented. Simulation results, namely particle velocities, stresses, and energy distributions are compared with values from elastic and plastic wave propagation theory. The locations chosen to extract the response measures are those shown in Figure 16.

3.4.1 Case Studies

This section presents three case studies on the stress wave propagation in homogeneous materials. Case 1 deals with the elastic wave propagation in a homogeneous material under a unit tensile force. Results from this case are compared with results from (Paulino and Zhang 2007) and comparison with close-form solutions validated the accuracy of the results from the numerical model. Case 2 deals with the elastic wave propagation in a homogeneous material under a unit compression force. Case 3 studies the phenomena of plastic wave propagation in a homogeneous material under a 1kN compressive force. Results were be verified by comparing it to existing knowledge on 1D stress wave propagation in homogeneous materials.

3.4.1.1 Case 1

Case study 1 was defined for the study on elastic wave propagation in homogeneous material under a unit tension force. The model used material model MAT001 in LS-DYNA with steel properties. The loading condition was a 1N tensile pulse load as shown in Figure 22.

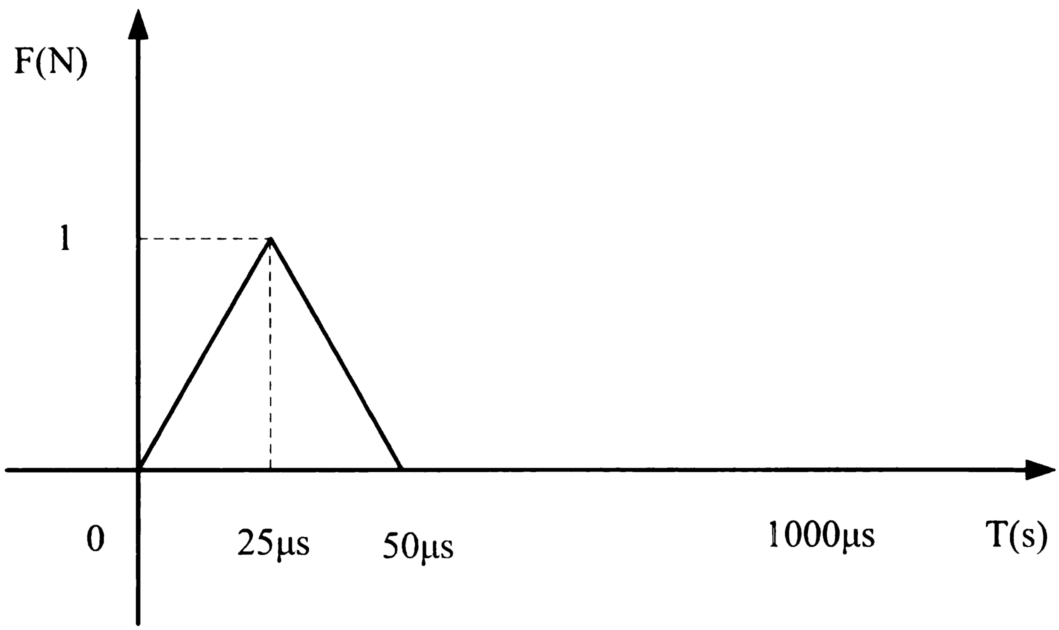

Figure 22. Unit Tension Pulse Force Loading History

3.4.1.2 Case 2

Case study 2 was defined to study elastic stress wave propagation in a homogeneous material under a unit compression force. The model used material model MAT001 in LS-DYNA with steel properties. The loading condition was a 1N compressive pulse load as shown in Figure 23.

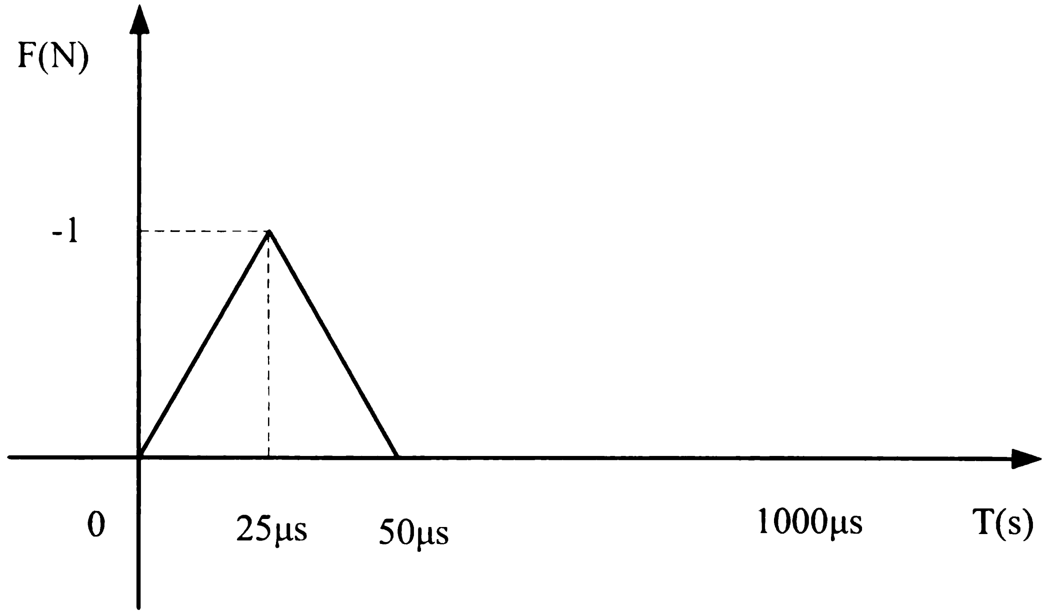

Figure 23. Unit Compression Pulse Force Loading History

3.4.1.3 Case 3

Case study 3 was defined to study the propagation of plastic stress waves in a homogeneous material. The loading condition was a compression force of 1kN at cantilever end (Figure 24). The material model used was MAT024 in LS-DYNA with elastic-plastic steel properties. A study using the MAT024 material model in LS-DYNA was also carried out. The purpose of this study was to determine whether MAT024 was an appropriate constitutive model to simulate elastic-plastic behavior. The load used in this case study was 100 MPa (see Figure 25).

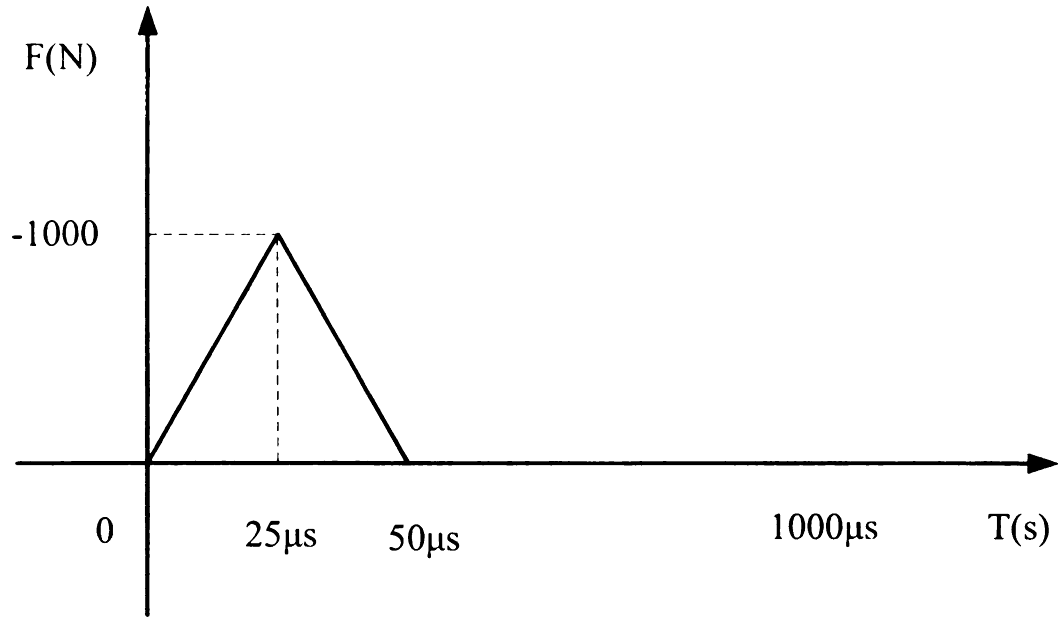

Figure 24. Compression Loading Pulse Force with 1kN Force

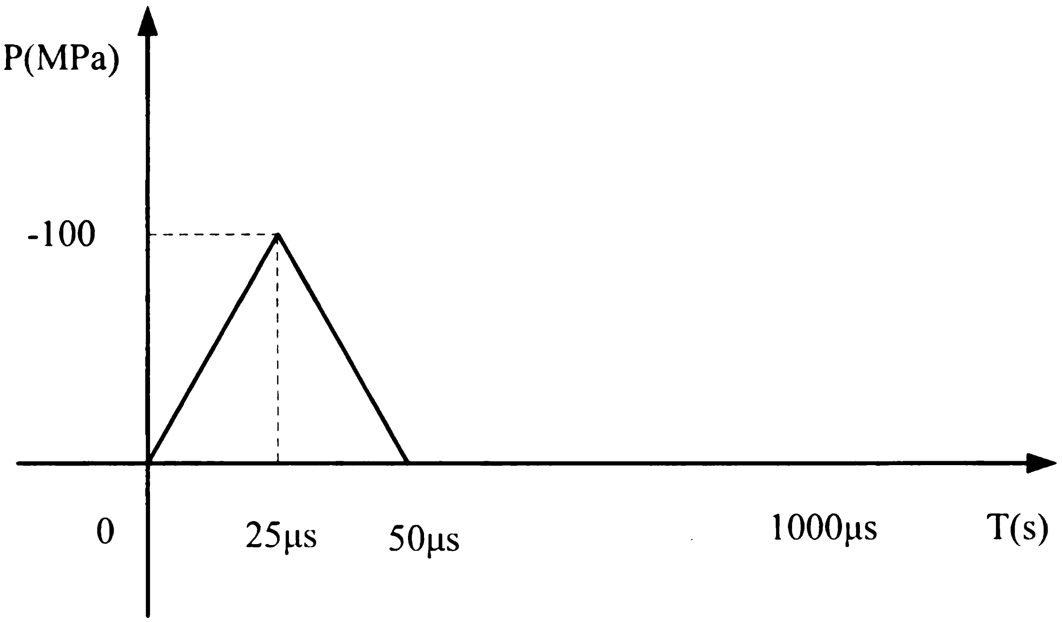

Figure 25. Compression Pressure Pulse with Magnitude 100 MPa

3.4.2 Results

3.4.2.1 Case 1: Validation of 2D Homogeneous Model under Tension Loading

Figure 26 shows results from the homogeneous numerical model. As shown in the graph, the triangular stress wave travels in the slender bar constantly (in this case, the speed of stress wave propagation is 5064 m/s) and maintains its triangular shape despite of reflection at the boundaries. The stress magnitude at point A is 0.323 MPa. The stress wave reaches point C at 0.15 ms and the magnitude of the stress wave doubles to 0.667 MPa. When the rebounded stress wave comes back to point A at 0.30 ms, the magnitude of stress wave is zero. This is response is consistent with the theory of stress wave propagation in solids as presented in Chapter two.

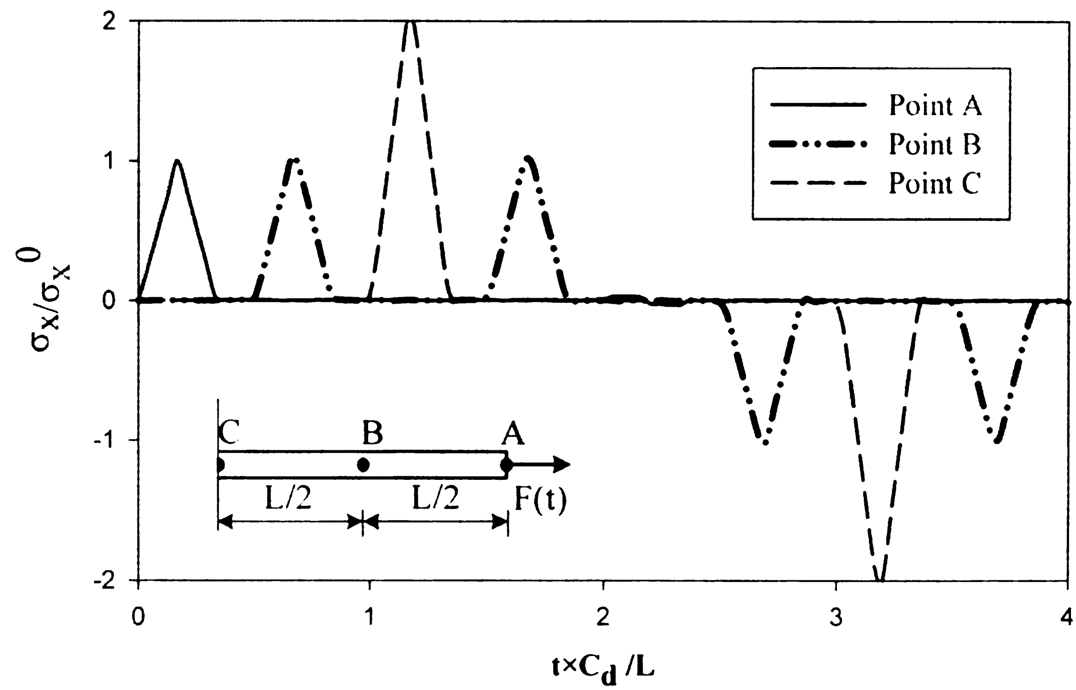

Figure 26. Stress History of Homogeneous Bar in Case 1 in 1D

Figure 27 shows the result from (Paulino and Zhang 2007) who provided a numerical solution to the same problem. In Figure 27, numerical results obtained at location x = L are denoted by a dark solid line, those at location x = 0.5L are shown by the dashed line and those at location x = 0 are shown by the dash-dot line. Analytical results are shown by a thin solid line. It can be seen magnitude of stress wave doubles at the fixed boundary and becomes zero at the free surface end. Thus, the results obtained by (Paulino and Zhang 2007) (Figure 27) agree with the ones obtained from the finite element simulation shown in Figure 26.

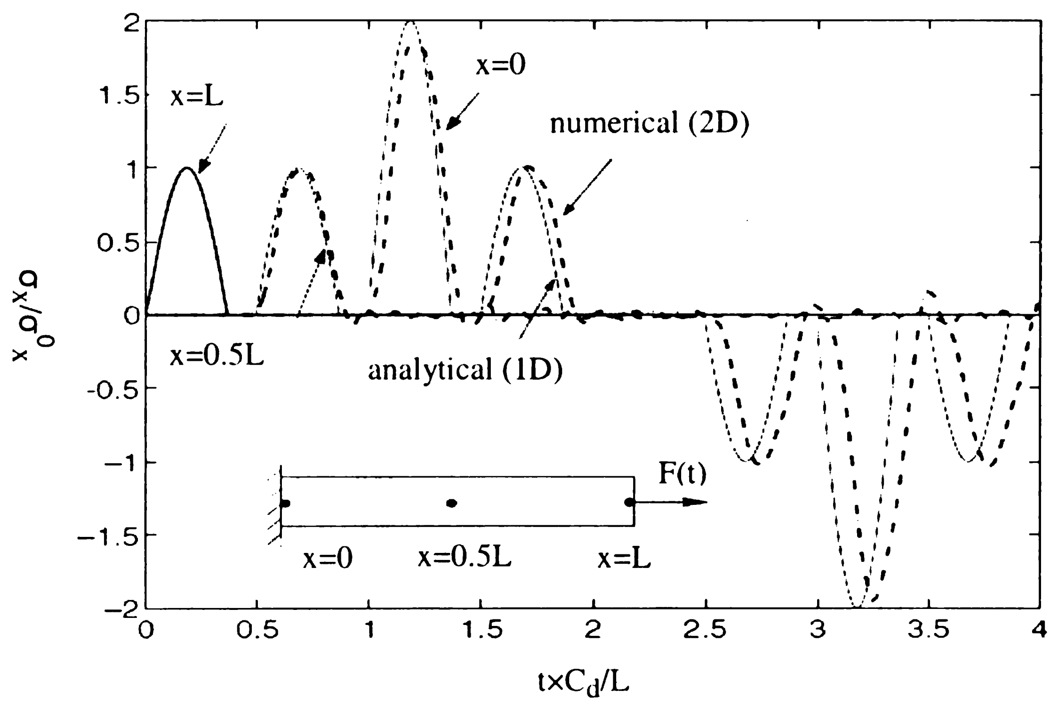

Figure 27. Stress History for Homogeneous Bar (2D Simulation) Subjected to Transient Loading and Its Comparison with 1D Analytical Solution [From Paulino and Zhang (2007)]

3.4.2.2 Case 2: Elastic Wave Propagation in Homogeneous Material

3.4.2.2.1 Particle Velocity of 2D Homogeneous Model under Compression Loading

Figure 28 shows the particle velocities in the elastic steel models under a 1N impulsive compressive load. The results in Figure 28 show how the wave traveled from the right free end towards the fix support and then and back during the first period. It can be seen that the velocity changes sign (i.e., from a compression wave to a tension wave) at approximately 0.19ms (most easily seen in dashed line), as it rebounds at the fixed end. It can be seen that particle velocity at the fixed end is almost zero and that the velocity at the free end doubles from the initial particle velocity upon completing a full period.

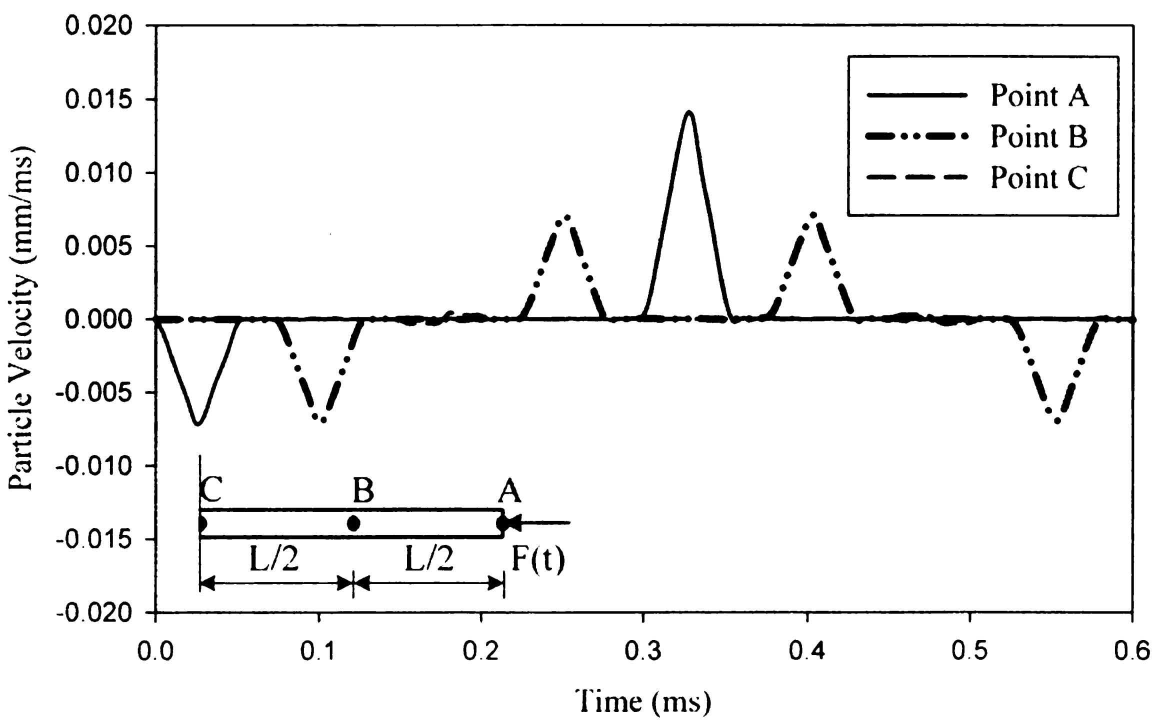

Figure 28. Particle Velocity in Elastic Steel Model under 1N Compression Force

3.4.2.2.2 Homogeneous 2D Model under Compression Loading

In this model, a compression impulse force was added on the free end of the bar. Figure 29 shows the stress history extracted from the model in Case 2. It can be seen that at the beginning the bar was subjected to a compression wave and later subjected to a tension wave. The absolute values of magnitude and rising times are the same as the ones in the tension model; the only difference is the signs.

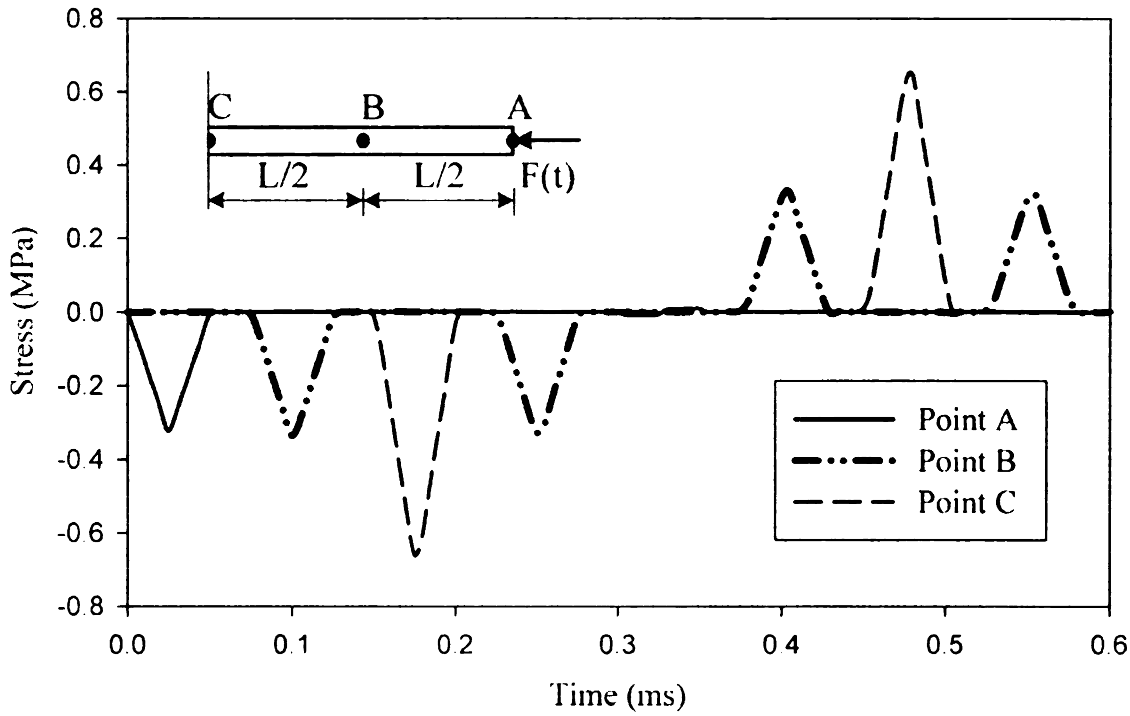

Figure 29. Stress History of Homogeneous Bar in Case 2 in 1D

The internal energy, kinetic energy and total energy distributions in the elastic steel model are shown in Figure 30. Internal energy and kinetic energy transfer to each other completely without any residual energy. Meanwhile, the total energy, which is 2.1×10^{-6} J, stays constant after the impulse load fades away.

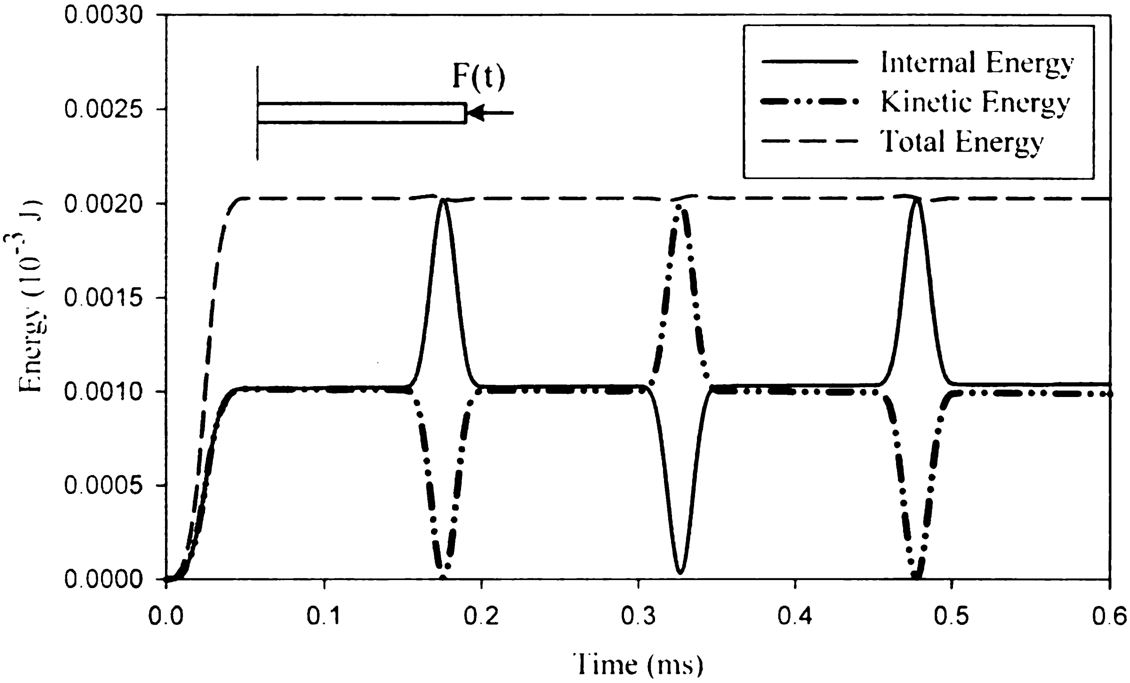

Figure 30. Energy Distribution in Case 2 in 1D

3.4.2.3 Case 3: Plastic Wave Propagation in Homogeneous Material

The aim of this case study was to evaluate the characteristics plastic stress wave propagation. A 1 kN impulsive compression force was again applied at the free end of the bar. Material model MAT 024 in LS-DYNA was used to simulate elastic-plastic behavior of steel with properties as presented in Section 3.3.

Figure 31 shows the stress history in a slender bar with a plastic tangent modulus of 50GPa. It can be seen that the slope of stress history curve changes due to decreased tangent modulus after yielding at a time of approximately 0.19 ms. Yielding of the bar causes a sudden drop in stress which is then recovered by the traveling stress wave. Nonetheless, the speed of the loading stress wave, seem by the front end of the stress history trace slope is reduced.

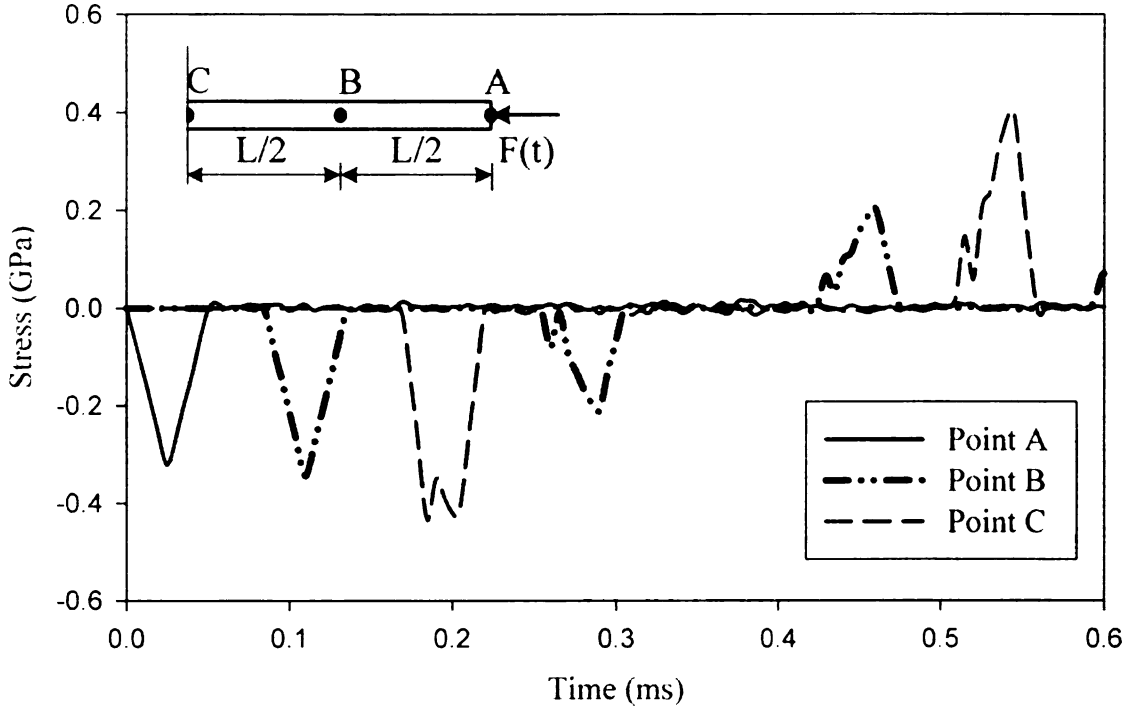

Figure 31. Stress History in Case 3 in 1D

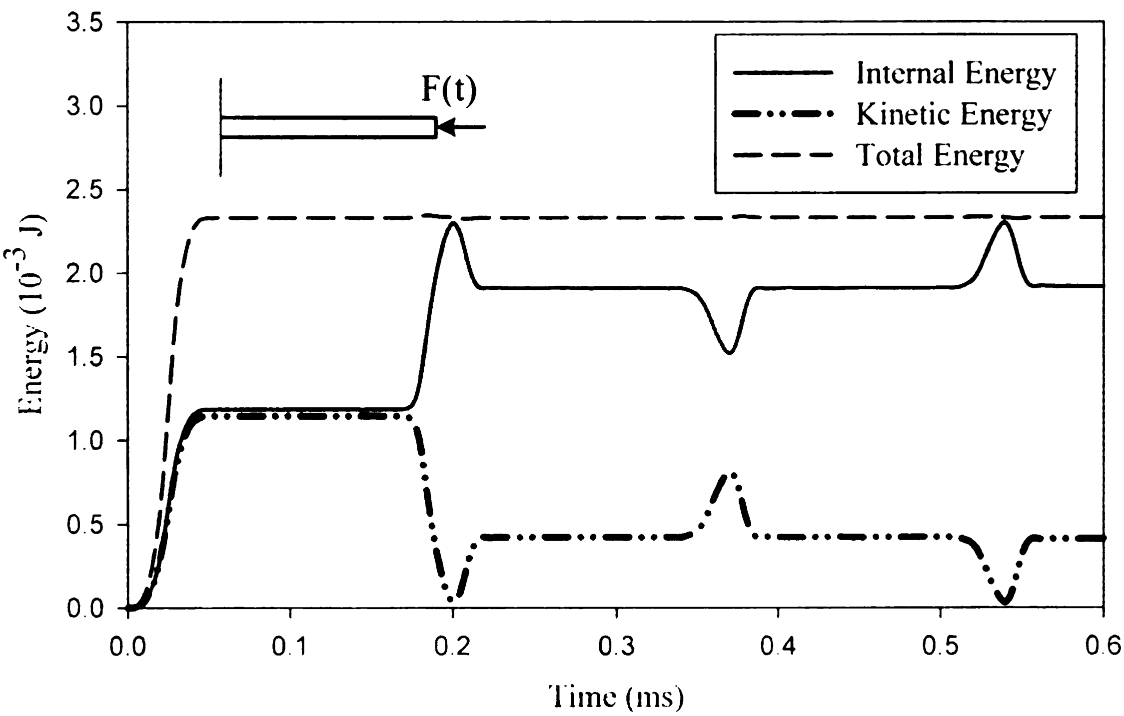

Figure 32. Energy Distribution in Case3 in 1D

Figure 32 shows the internal energy, kinetic energy and total energy distributions in a steel material that suffers plastic deformations during the transmission of the stress wave. The total energy is 2.3×10^{-3}J; about 1.5×10^{-3}J of energy are stored as internal energy due to plastic deformation and about 0.8×10^{-3}J of elastic strain energy is transferred between kinetic energy and internal energy.

In this model, MAT 024 was used to simulate an elastic-plastic behavior for steel. To verify the constitutive model the first step was to apply a pressure load below the yield stress of material and thus obtain a stress history equal to that of the elastic model. The magnitude of the compressive impulse pressure was 100MPa. The load history employed in this model is shown in Figure 25. Figure 33 and Figure 34 show the stress histories in the elastic model. Figure 35 and Figure 36 show the stress histories in the elastic-plastic model.

Comparing Figure 35 and Figure 36 with Figure 33 and Figure 34, it can be seen that those stress histories in elastic-plastic model were almost the same as the ones extracted from elastic materials, when the load pressure was less than yield stress in elastic-plastic model. As a result, MAT 024 in LS-DYNA was considered appropriate to simulate elastic-plastic behavior.

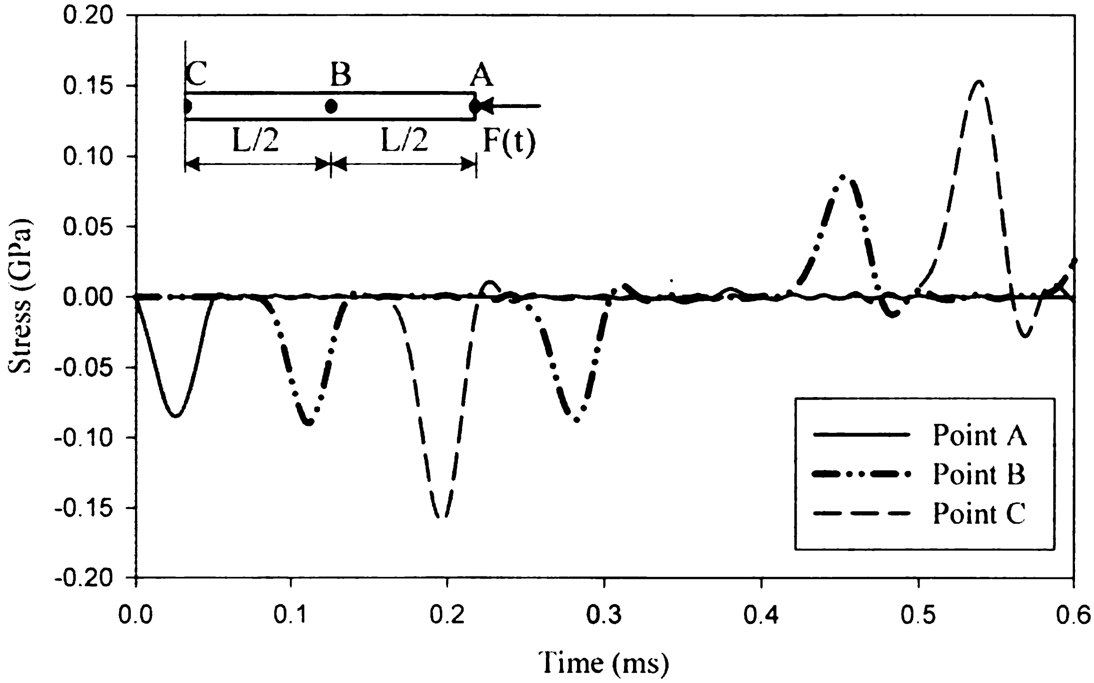

Figure 33. Stress History at Chosen Locations in Steel Elastic Model under 100Mpa within 0.6ms

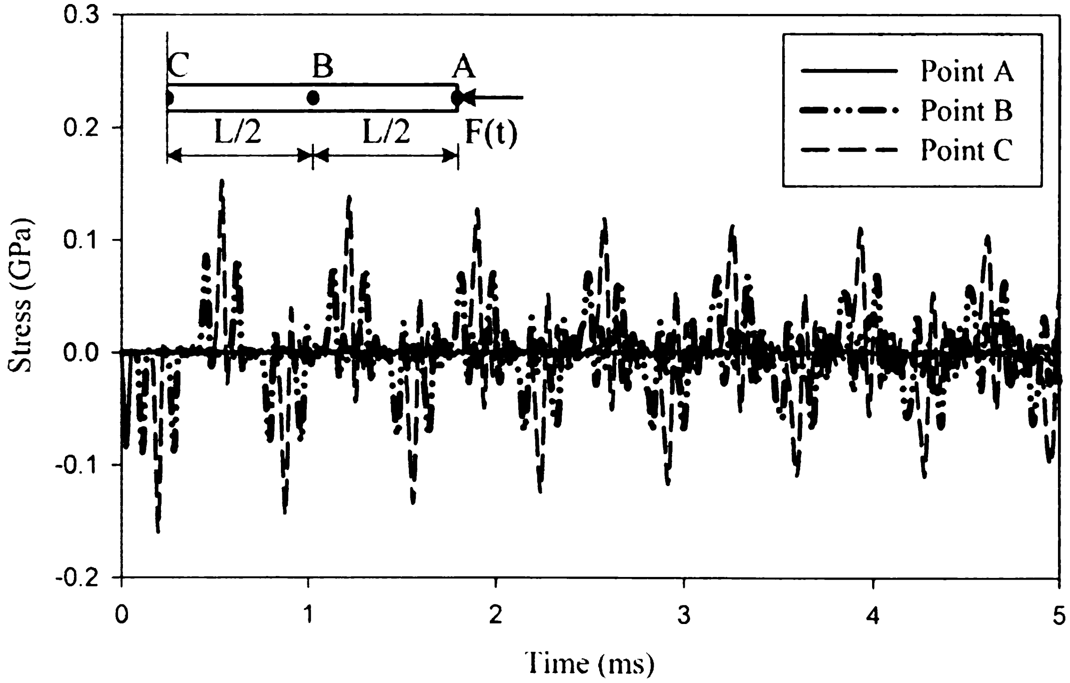

Figure 34. Stress History at Chosen Locations in Steel Elastic Model under 100Mpa within 5 ms

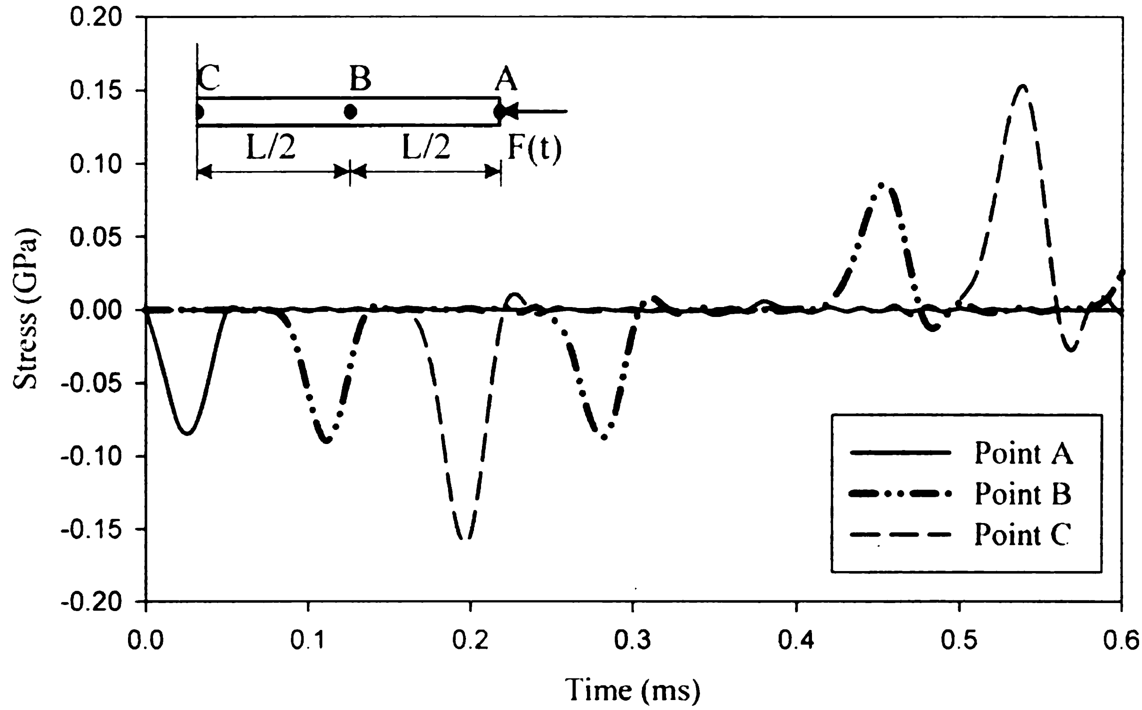

Figure 35. Stress History at Chosen Locations in Steel Plastic Model under 100Mpa within 0.6ms

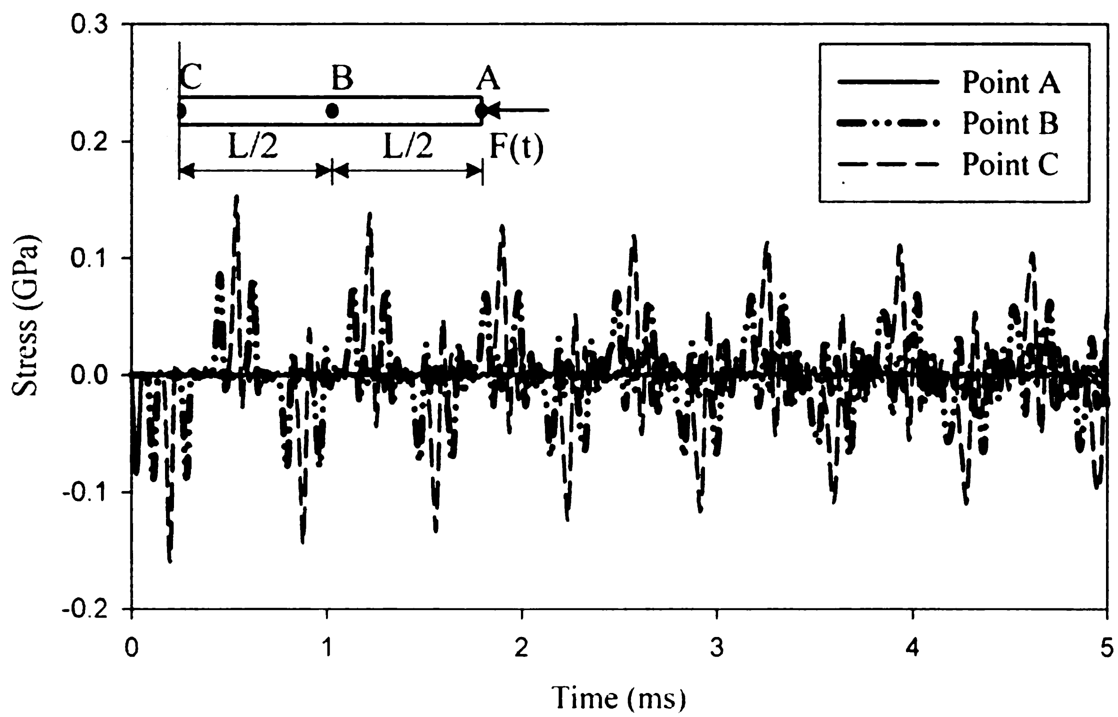

Figure 36. Stress History at Chosen Locations in Steel Plastic Model under 100Mpa within 5ms

3.4.3 Discussion

The presented results have shown that the simulation of elastic wave propagation by means of finite element analysis in LS-DYNA led to results that were consistent with theoretical solutions. The behavior of a slender bar under impulsive tensile load was first modeled and compared with the results by (Paulino and Zhang 2007). The models correctly capture the amplification (double) of the stress wave at the fixed boundary and the dissipation of the wave at the free end. The model also correctly computes zero particle velocity at the fixed end while that at the free end doubles. The element type and the mesh geometry were selected based on a sensitivity study.

With such evaluation, the model was considered appropriate for use in the study of stress wave propagation under compressive impulse loads and elastic-plastic materials. As expected, the studies of stress wave propagation under compressive loads showed that the behavior is the same as for the case of a tensile load, except for the obvious change in sign and the direction of the stress wave propagation.

With respect to the propagation of plastic stress waves in homogeneous materials, the models seem to have correctly captured the reduction in transferred kinetic energy due to the energy that is dissipated in the plastic deformations. The reduction of the stress wave velocity was also apparent by observing the reduced slope of the leading edge of the stress wave from the stress history traces.

3.5 Stress Wave Propagation in Non-Homogeneous Solid Materials

In this section, results from the simulation of non-homogeneous solid models are presented and discussed. Non-homogeneity in the current context refers to the presence of two materials with distinct elastic modulus (i.e., stiffness). The aim of the analyses presented in this section was to evaluate the characteristics of stress-wave propagation at the interfaces of dissimilar materials. Numerical models, corresponding loading histories and materials are presented. Simulation results, namely particle velocities, stresses, and energy distributions are compared with values from elastic and plastic wave propagation theory. The locations chosen to extract the response measures are those shown in Figure 16.

3.5.1 Model Particulars

The model used to evaluate the characteristics of elastic and plastic wave propagation in bi-material (or non-homogeneous) bars is shown in Figure 37. The model consists of a slender cantilevered bar of 0.9m in length and a height of 0.045m. The bar geometry was divided into two equal parts such that the material in Part 1 was defined to be steel and the material for Part 2 was defined with the properties of aluminum. The model was loaded with an impulsive compressive pressure load of 1MPa at the bar free end (Figure 38).

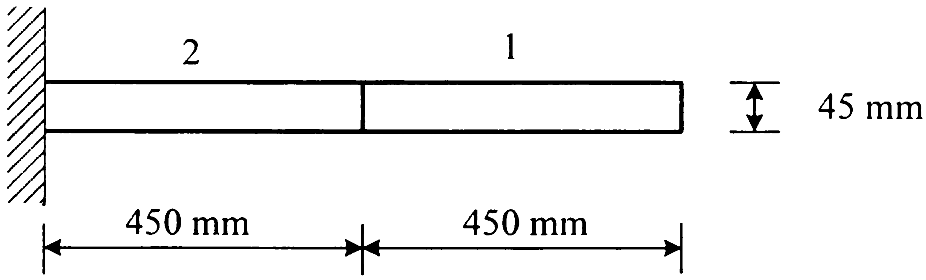

Figure 37. Bi-Material Bar Model in 1D

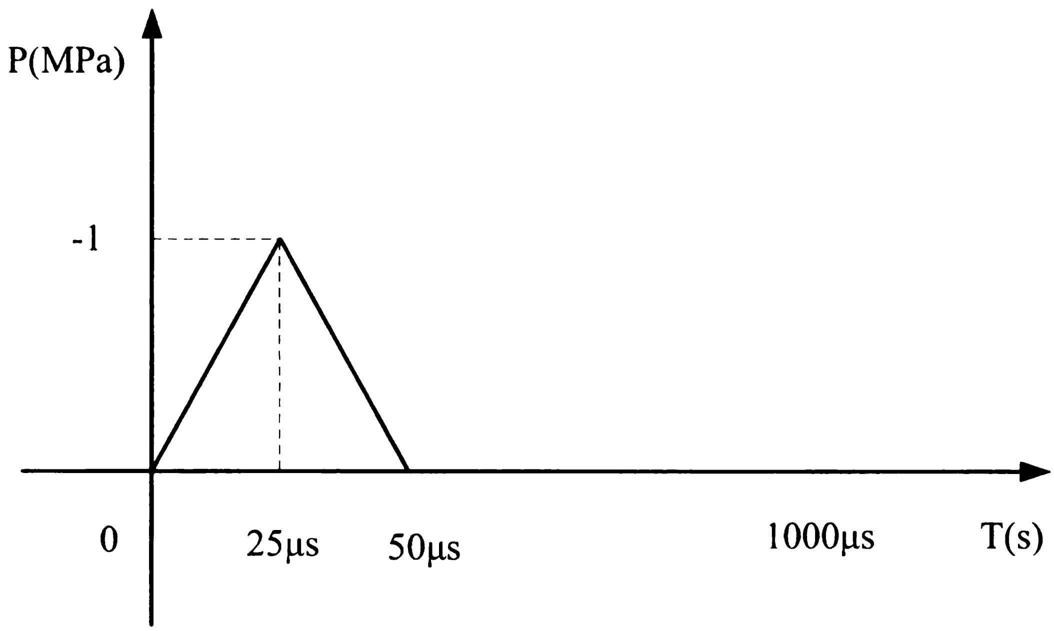

Figure 38. 1MPa Compression Pressure Load

3.5.2 Results

In a non-homogeneous model it is important to notice that when stress wave travels across two dissimilar materials (different stiffness) it will separate into two parts at the material interface. One part wave would reflects back to the material in which the wave was initially traveling while the other part is propagated or transmitted to the neighboring material.

In this model the elastic wave travel from Part 1 (steel) to Part 2 (aluminum). According to the equations (6) and (7), 55% of the original stress magnitude propagates, or travels, into the aluminum part of the bar, and 45% of the stress reflects back. Results from the model are shown next to match this theory very well. Two points were chosen to obtain the stress history response as shown in Figure 39. The stress history at points A and B are shown in Figure 40.

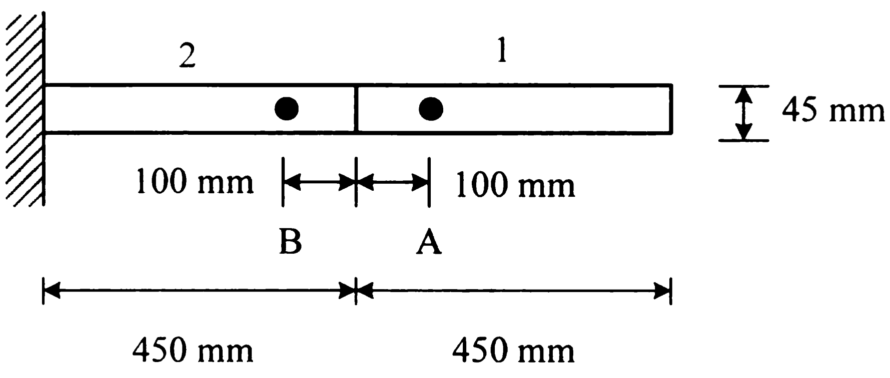

Figure 39. Points Locations in Bi-material Model

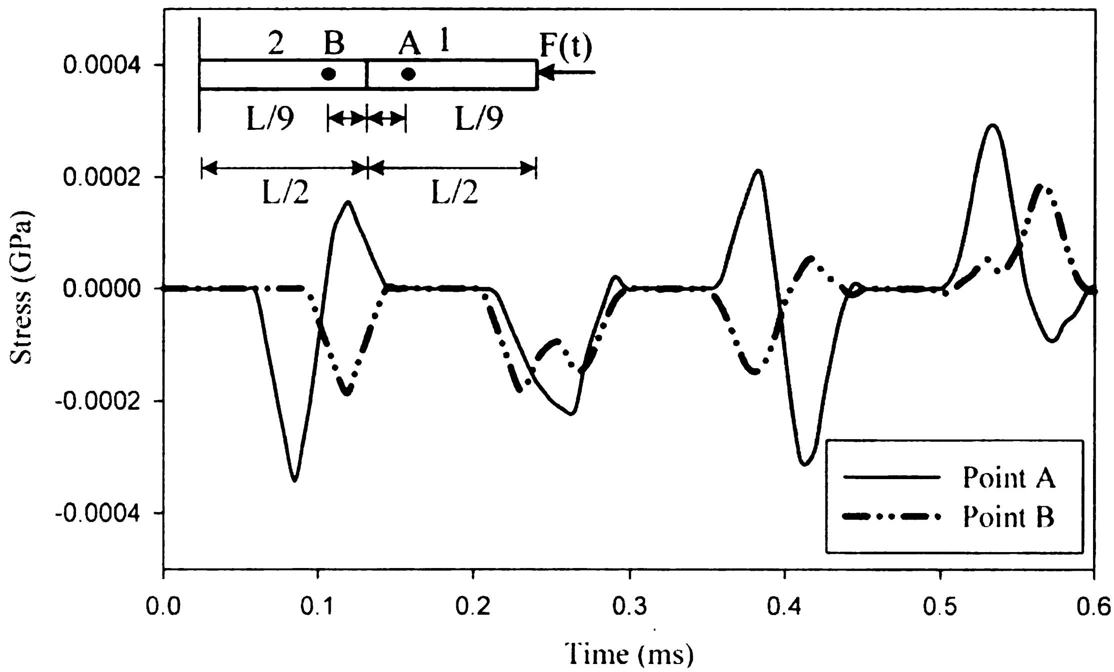

Figure 40. Stress History at Given Locations in Bi-Material Model

From Figure 40 it can be seen that the magnitude of the stress in location A at 0.08 ms is -0.33 MPa. According to the presented theory, the compressive stress that would be transmitted into aluminum should be -0.1815 MPa. It can be observed in Figure 40 that the numerically computed value at location B is approximately -0.18 MPa at 0.12 ms. Similarly, the theoretical magnitude of the reflected tension stress wave is 0.1485 MPa, while from Figure 40 the value is about 0.15 MPa at 0.12 ms.

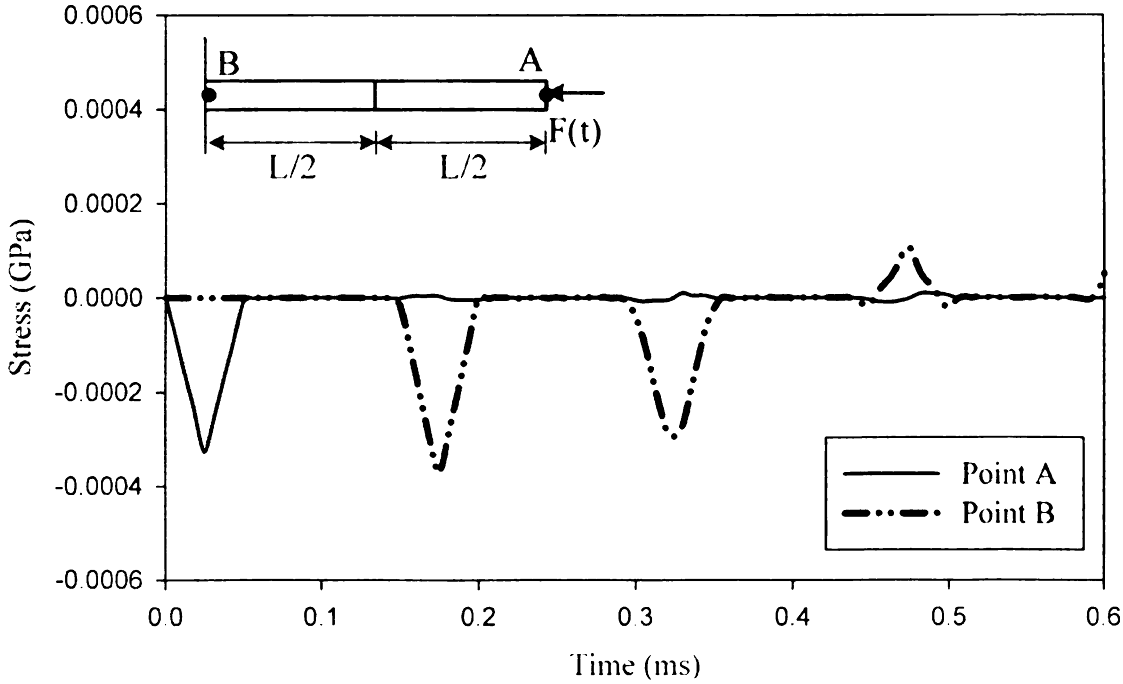

Figure 41. Stress History of Two End Points in Bi-Material Model

Figure 41 shows the stress history at locations near the boundaries of the bar. It can be seen that at the free end (Point A) the maximum stress was about 0.33 MPa at 0.025 ms, while the peak stress at the fixed end (Point B) was 0.38 MPa at 0.175 ms, less than what can be observed from the results for the homogeneous model. This results are consistent with the refraction of stresses that takes place at the material interface and indicates that the stress transferred at a material interface is reduced since part of it reflects back to the source material.

Figure 42, Figure 43 and Figure 44 show energy distributions for the non-homogeneous model. It can be seen that total energy was 2.25 $\times 10^{-6}$ J. About 78% of the total energy (1.75 $\times 10^{-6}$ J) was transmitted into the aluminum part while the other 22% (0.5 $\times 10^{-6}$ J) reflected back into the steel part when the stress wave reaches the material interface at 0.12 ms.

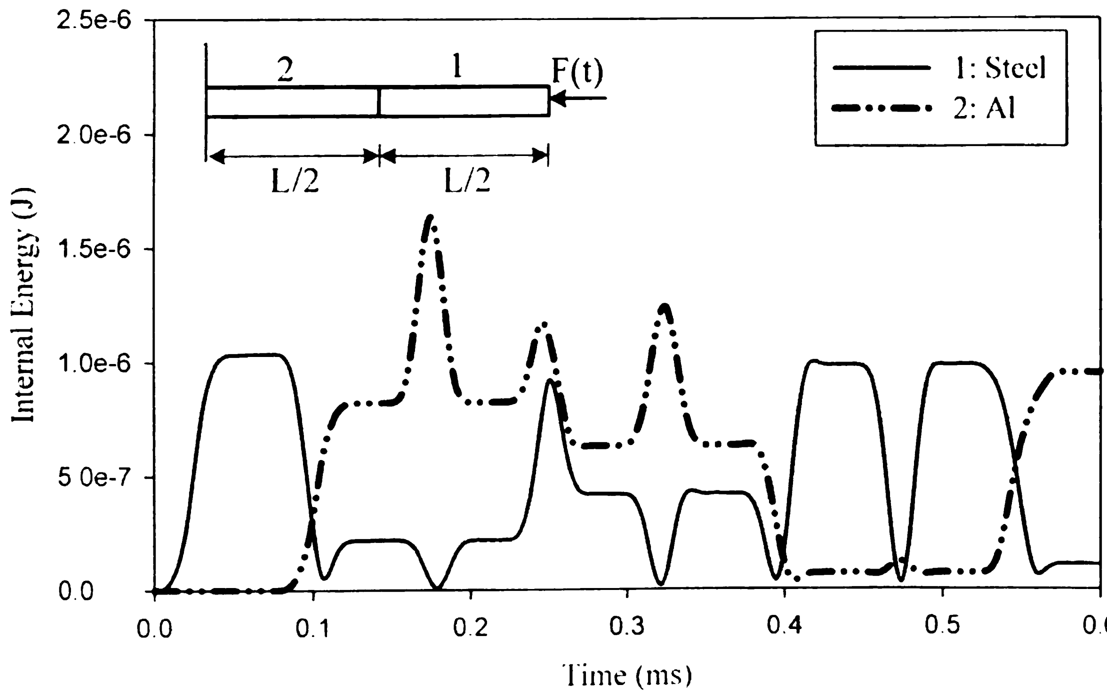

Figure 42. Internal Energy Distribution in Bi-Material Model

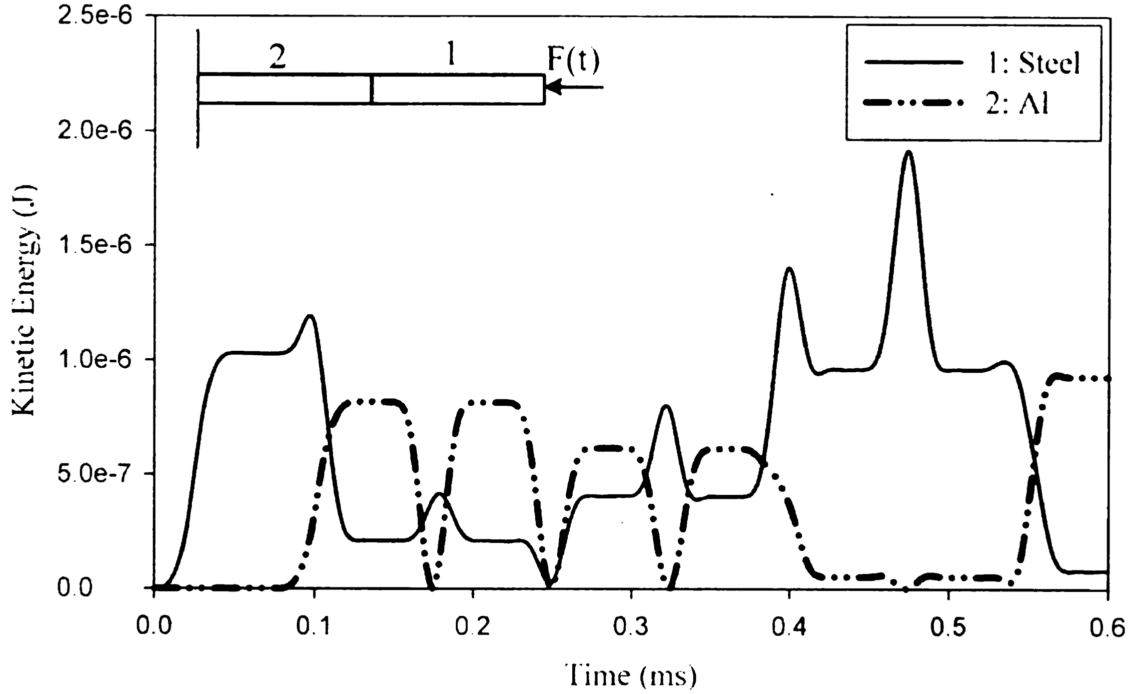

Figure 43. Kinetic Energy Distribution in Bi-Material Model

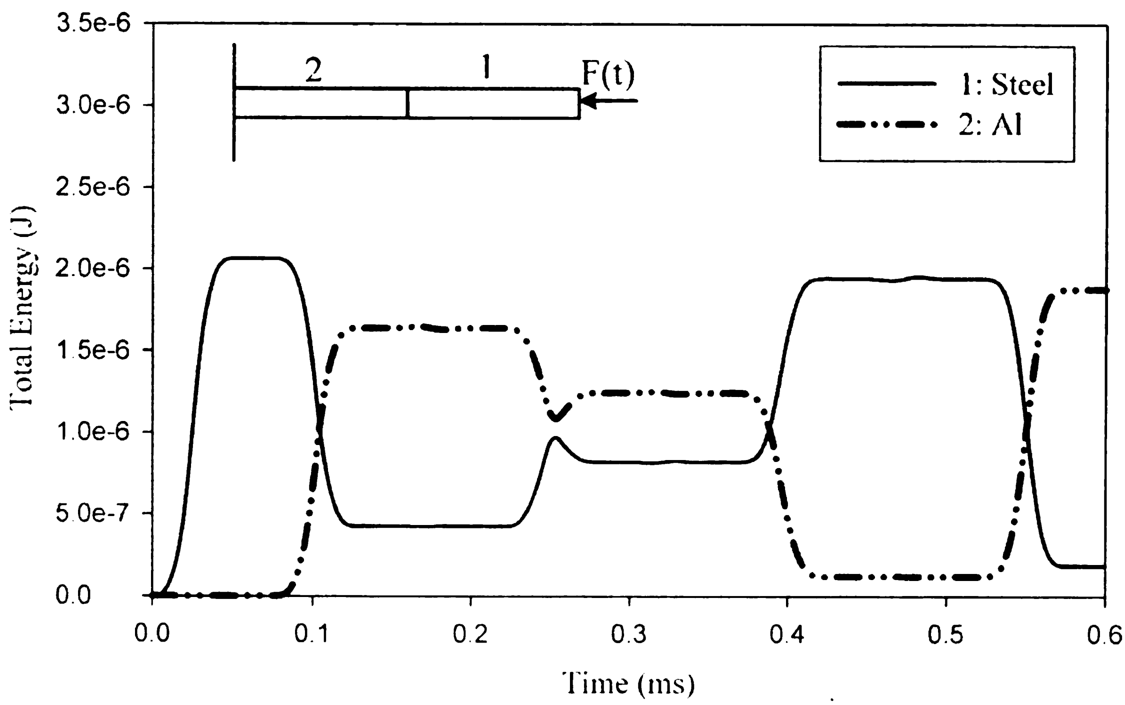

Figure 44. Energy distribution in Elastic Bi-material Model

3.5.3 Discussion

The results provided above show that the propagation of stress waves across materials with different stiffness brings about important features. As shown in Figure 40, stresses reflect and transmit at the interface of dissimilar materials in proportion to their properties, namely, mass density and Young's modulus. An important effect of the wave refraction at the material's interface is that the propagated stress is reduced since part of it is reflected (see Figure 41). Finally, the way in which the energy is shared by the two materials becomes more complex, but clearly complimentary. The results from the finite element simulation were found to be in agreement with theoretical models, thus providing confidence on the approach.

3.6 Summary

This chapter presented a series of numerical studies aimed at evaluating the characteristics of stress wave propagations in homogeneous and non-homogeneous (bi-material) solid materials. The goal of studying one-dimensional behavior was to validate the framework of using finite element simulations to study the propagation of stress waves in foams and two-dimensional domains (Chapters 4 and 5). Compliance between the numerical (finite element) models and theoretical principles was confirmed thus giving confidence to the use of the approach for further studies. The following summarizes important features learned from the presented studies.

Stress waves in elastic homogeneous models propagate at a constant speed that is controlled by the material's mass density and elastic stiffness (Young's modulus).For the cantilever bar studied here, the magnitude of the stress doubles upon being fully reflected at the fixed boundary and reduces to zero at the free boundary. When the stress magnitude exceeds the proportionality limit of the material, the speed of the stress wave reduces since it then depends on the instantaneous plastic elastic modulus of the material. In addition, there is a transfer from kinetic energy to permanent strain energy due to plastic deformations. Such behavior leads to the reduction of the propagated stresses, which is consistent with the concept of using plastic deformation as an effective means for stress mitigation of impulsive loads.

Stress wave propagation across dissimilar materials (non-homogeneous) leads to the decomposition of the stress wave into transmitted and reflected components whose magnitude depends on the relative material properties (mass density and elastic stiffness) of the materials meeting at the interface. The interface of dissimilar materials will clearly affect the magnitude of the stress waves that travel inside the structure, leading to a more complex distribution of energy participation than what occurs in a homogeneous material.

CHAPTER 4. ONE-DIMENSIONAL STRESS WAVE PROPAGATION IN FOAM MATERIALS

4.1 General

This chapter presents numerical studies on stress wave propagation in foam materials in one dimension. The studies were carried out on a cantilever foam bar subjected to a compressive impulsive load at its free end. A homogeneous model including a single foam material bar and two non-homogeneous models consisting of two kinds of foam materials were used. The responses of interest were the capacities of energy dissipation, stress mitigation and large deformation.

The homogeneous model used an aluminum foam with a relative density (ρ^*/ρ_S) of 0.06 while the non-homogeneous models used considered a bar made of an aluminum foam with two relative densities (half each) of 0.06 and 0.24. The only difference between the two non-homogeneous models was the sequence of the foam segments with different relative density. Non-homogeneous model 1 had the foam with 0.06 relative density in the first half part of the bar (attached to the fixed boundary condition) and the foam with 0.24 relative density in the second half part (at the free end). In the non-homogeneous model two, the sequence was opposite.

Results indicate that stress magnitude decreases dramatically in the process of plastification and that the dissipated kinetic energy is stored as internal energy in the foam materials. This is due to the large deformations that occurred in a crushable foam. Thus, foam materials are highly effective in mitigating stress and reducing kinetic energy. The sequence of foam material in a non-homogeneous model has been shown to effect stress wave propagation, where stiffer foam near the load application will lead to smaller deformations, with the opposite design having an inverse consequence.

The findings from these studies can be used as criteria to understand the behaviors of stress wave propagation in two dimensional foam structures such as those presented in Chapter 5.

4.2 Model Definition

The previously used cantilever bar is used again in this chapter to evaluate the performance of foam materials under impact loads. One difference to the models presented in Chapter 3 is that the bar was modeled with two metal plates added on its two ends (Figure 45). The reason is that foams are much weaker than a solid material, thus the two thin plates were added to avoid local deformations and allow a more even distribution of stress demands at the reaction and load application locations. The height of foam and metal plate is 45mm. The length of the foam bar is 900 mm and the thickness of metal plate is 3 mm. In this model, the foam part was divided into two equal parts (Parts 1 and 2). This configuration was helpful to detect the locations of large deformation and to compare results between homogeneous and non-homogeneous designs, where in the later the foam materials for each part were different. The interaction between two foam parts and between foam and metal plate were assumed to be a perfect bond.

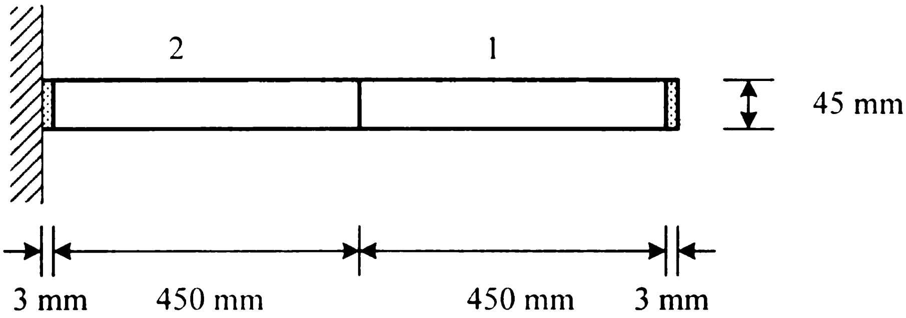

Figure 45. Cantilever Bar Model for Foam Material in 1D Cases

4.3 Material Modeling

The materials used in this chapter were aluminum and aluminum foam. The properties of aluminum are listed in Table 4. The properties of aluminum foam are presented in Table 5 as well. The constitutive model used to simulate aluminum was the MAT_001 material model from LS-DYNA. Considering that aluminum foam has the capability of withstanding large deformations, MAT_063 crushable foam material model was used to simulate open-cell foam material. As mentioned in Chapter 2, stress-strain curves of open-cell foam material can be defined based on the relative density of the foam and the properties of the material of which the foam is made of. The relative densities of aluminum foam used here are 0.06 and 0.24. The compressive stress-strain curves are shown in Figure 46.

Table 4. Properties of Aluminum Plate in 1D Foam Bar

	Al Plate
E (GPa)	80
ν	0.3
ρ (kg/m^3)	2800
σ (MPa)	80

Table 5. Material Properties of Foams in 1D Foam Bar

Property	Foam	
Relative density	0.06	0.08
E (GPa)	0.29	0.51
ν	0.33	0.33
ρ (kg/m^3)	168	224
σ (MPa)	0.35	0.54

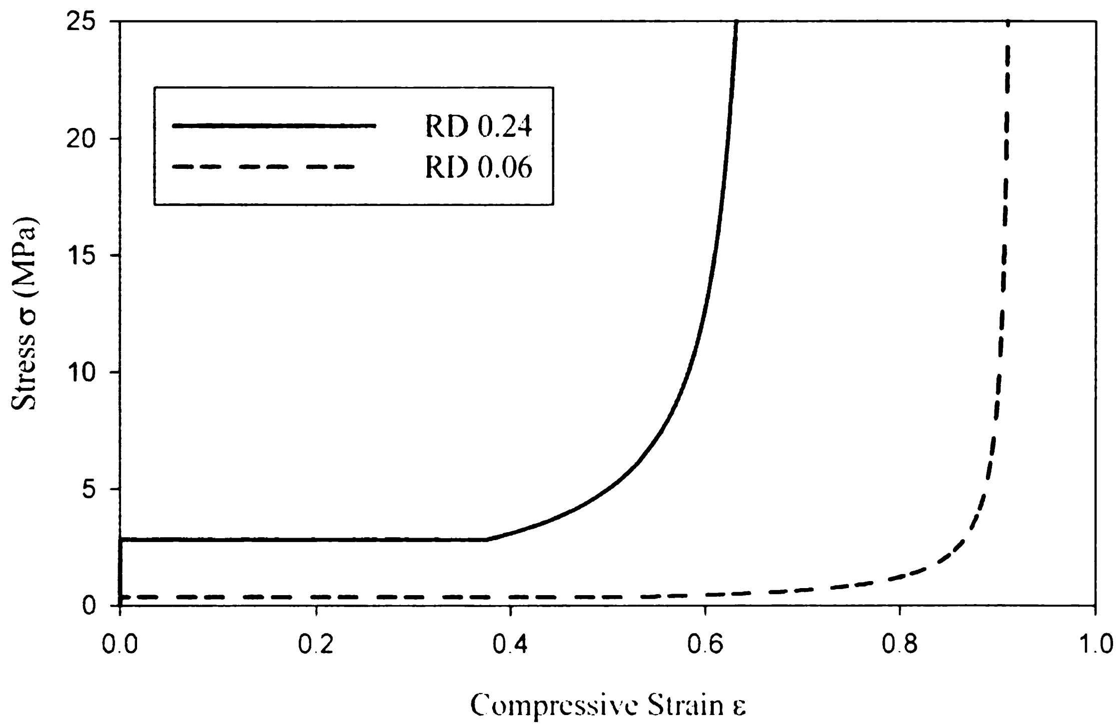

Figure 46. Stress Strain Curves of Foam Materials in 1D Cases

4.4 Stress Wave Propagation in Homogeneous Foam Materials

This section presents results from the simulation of a homogeneous foam model. The purpose of this study is to show features of stress wave propagation in a homogeneous cantilever bar made of open-cell foam material. Meanwhile, comparisons between homogeneous and non-homogeneous models can show the influence of changing materials on stress wave propagation. The locations chosen to extract the response measures are those shown in Figure 47.

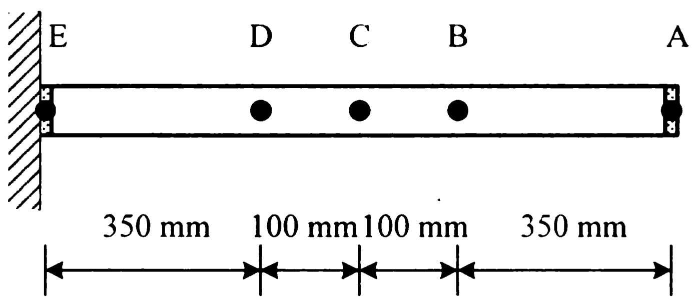

Figure 47. Specified Locations on the Homogeneous Foam Model in 1D Case

4.4.1 Case Study

This case was defined for the study on plastic wave propagation in a homogeneous foam model under an impulse compressive pressure with a magnitude of 100 MPa. The model used material model MAT_063 in LS-DYNA with the properties of foam with 0.06 relative density. The loading condition is shown in Figure 25.

4.4.2 Results

Due to the low speed of stress wave propagation in a foam, all the information shown here is within time domain from 0 to 5 ms. Figure 48 shows the internal energy in the homogeneous model. Almost all the internal energy is stored in the Part 1 of foam core. The energy in Part 1 increases dramatically before 1.0 ms, and then tends to stabilize at 14.7 J at 5 ms. The internal energy in Part 2 has a very small value 0.252 J at 5 ms.

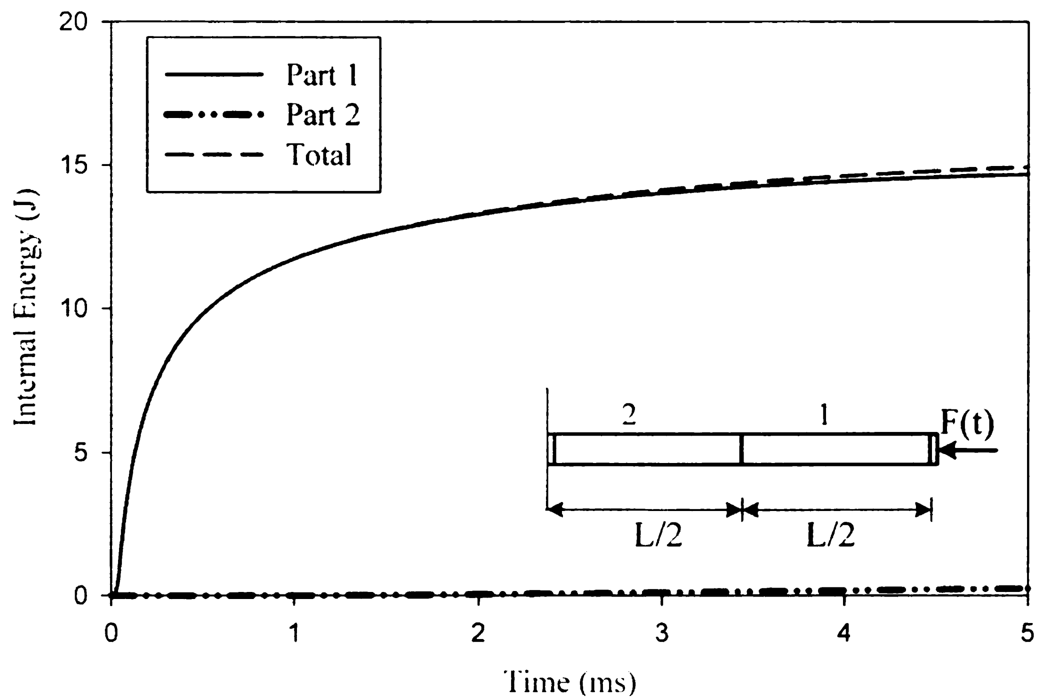

Figure 48. Internal Energy History for Homogeneous Foam Model in 1D

Figure 49 presents the kinetic energy history in the homogeneous foam bar model. It shows that kinetic energy in Part 1 increases rapidly upon the load application, peaks at 3.9 J at 0.24 ms and then goes down. The kinetic energy in Part 2 is 0.0293J, indicating that this part almost remained static during the first 5 ms. Finally, a curve of the overall kinetic energy can be seen to overlap the one of Part 1 and is only marginally higher after 1.4 ms.

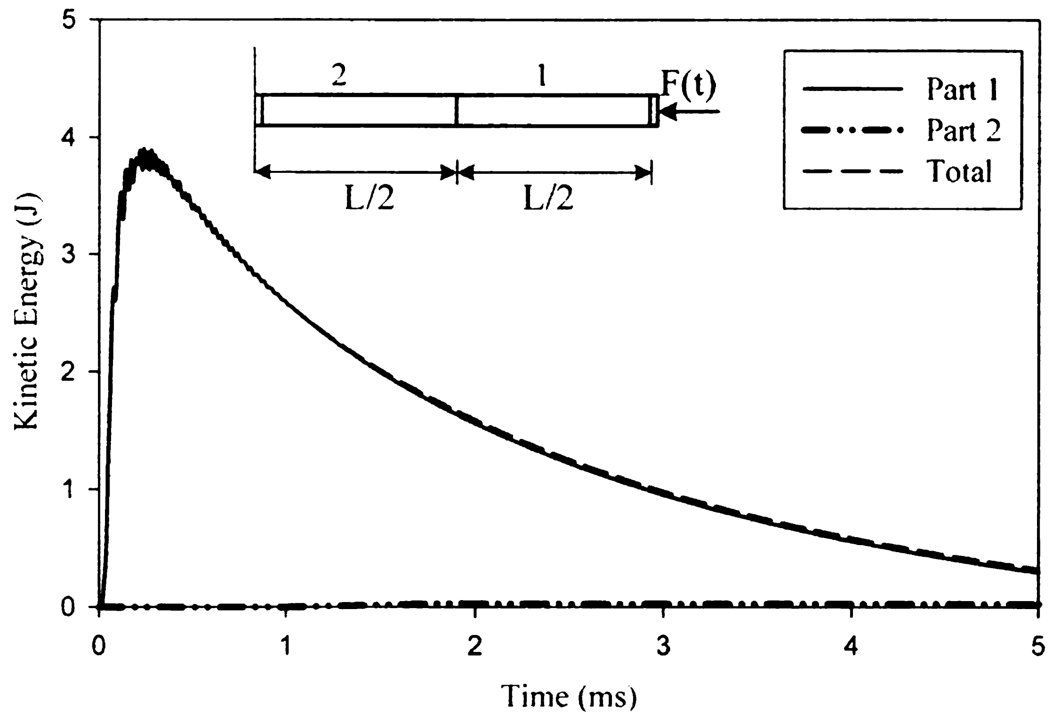

Figure 49. Kinetic Energy History for Homogeneous Foam Model in 1D

4.4.3 Discussion

The results listed in Table 6 below show that the stress wave propagation in homogeneous foam material has great features. Table 6 shows that the peak stress decreased dramatically in the foam material during the process of propagation. In Part 1, the stress magnitude decreased from 42.6 MPa at point A to 0.35 MPa at point C due to the large plastic deformations that took place in this part. Thus, most of the foam in Part 1 crushed, which causes a great amount of kinetic energy to be dissipated in the part as internal energy. The foam in Part 2 suffered a much smaller deformation during the wave propagation because the magnitude of the stress wave in it was lower than the yield stress of foam material.

In addition, the speed of stress wave propagation in the foam material was much slower than that in a solid material. It took 0.15 ms for the stress wave to propagate from one end of the bar to the other in the solid bar. However, the same stress propagation in the foam took 1.4 ms.

Table 6. Results from Homogeneous Foam Model in 1D Case

	Homogeneous Model
Stress at point A (MPa)	42.6
Stress at point B (MPa)	0.36
Stress at point C (MPa)	0.35
Stress at point D (MPa)	0.35
Stress at point E (MPa)	0.36
Kinetic energy of Part 1 foam (J)	3.9
Kinetic energy of Part 2 foam (J)	0.0293
Internal energy of Part 1 foam (J)	14.7
Internal energy of Part 2 foam (J)	0.252
Deformation of Part 1 in x direction (mm)	238.699
Deformation of Part 2 in x direction (mm)	17.7953

4.5 Stress Wave Propagation in Non-Homogeneous Foam Materials

In this section, results from the simulation of non-homogeneous foam models are presented. The aim of the analyses shown in this section was to observe the features of stress-wave propagation in multiple foam materials. Numerical models, corresponding loading histories and materials properties are presented. Simulation results, namely stress and energy history are shown as well. The locations chosen to extract the response measures are shown in Figure 47.

4.5.1 Case Study

The bi-material (or non-homogeneous) model used to capture the characteristics of plastic wave propagation is shown in Figure 45. The configuration of this model is identical to the homogeneous model. However, dissimilar materials were assigned to two parts. In Model 1, a foam material with a relative density 0.06 was assigned for Part 1 and a foam material with a relative density 0.24 for Part 2. Model 2 followed an opposite sequence. The models were loaded with an impulsive compressive pressure load of 100MPa at the free end of the bar.

4.5.2 Results

Figure 50 and Figure 51 show results from Model 1, where Part 1 is a foam with a relative density of 0.06 and Part 2 is a foam with a relative density of 0.24. Figure 50 shows the internal energy (consisting of elastic and plastic strain energy) stored in the foam parts. The energy in Part 1 increases rapidly before 1.0 ms, then tends to stabilize at 14.9 J at 5 ms. The energy in Part 2 has a very small value 0.0182 J at 5 ms.

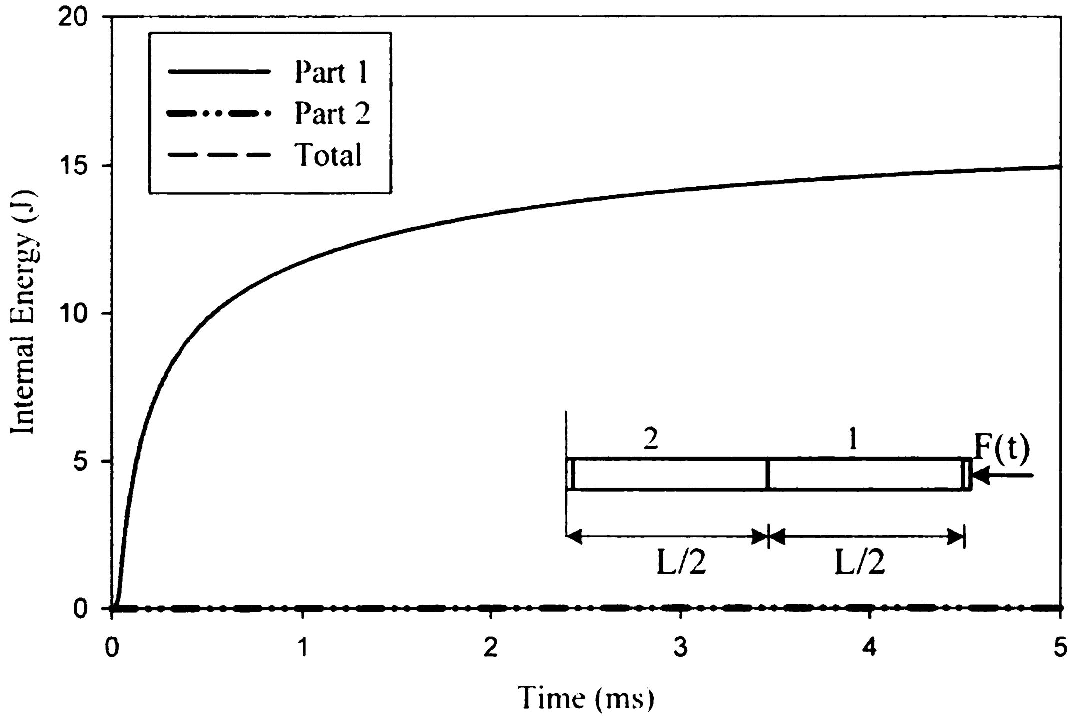

Figure 50. Internal Energy History for Non-homogeneous Foam Model 1 in 1D

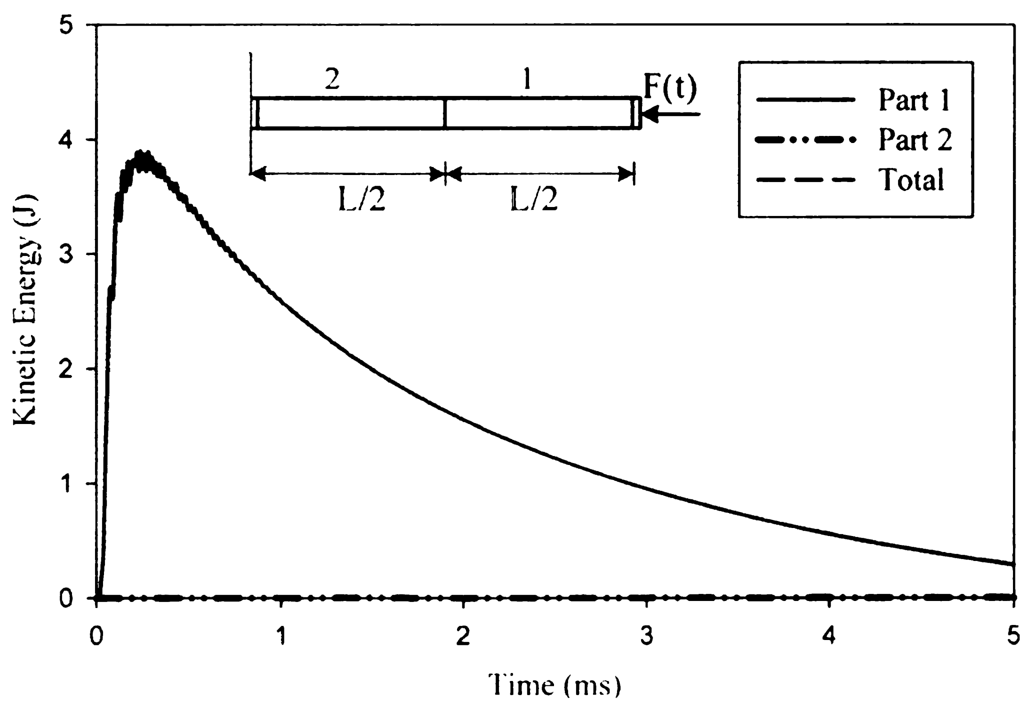

Figure 51. Kinetic Energy History of Non-homogeneous Foam Model 1 in 1D

Figure 51 shows the kinetic energy history for Model 1. The kinetic energy in Part 1 increases rapidly, it peaks at 3.9 J in 0.24 ms and then decays. The kinetic energy in Part 2 is only 0.00294J, indicating that this part remained essentially static during the first 5 ms of response.

Figure 53 is results from Model 2, where Part 1 is a foam with a relative density of 0.24 and Part 2 is a foam with a relative density of 0.06, Figure 52 shows the internal energy stored in the foam parts. The internal energy in Part 1 increases rapidly before 0.8 ms and then tends to stabilize at 12.0 J at 5 ms. The energy in Part 2 has a very small value 0.357 J at 5 ms.

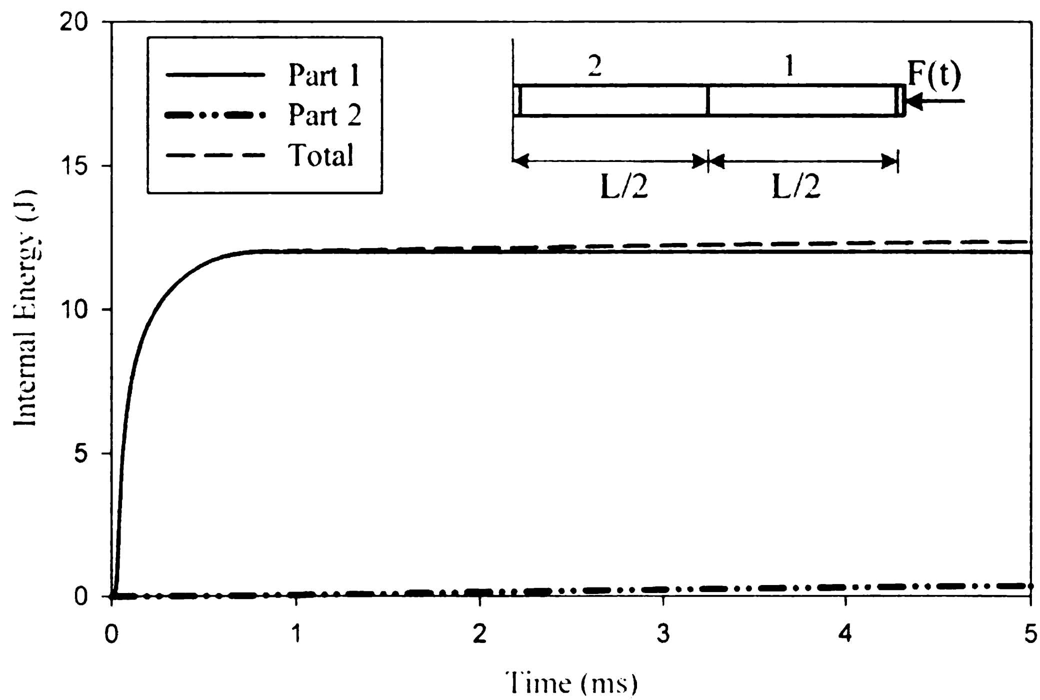

Figure 52. Internal Energy History of Non-homogeneous Foam Model 2 in 1D

Figure 53 shows the kinetic energy history in for Model 2. As the load is applied on the bar the kinetic energy in Part 1 quickly increases, peaking at 3.44 J in 0.07 ms, and then decreased rapidly after 0.07 ms. The kinetic energy in Part 2 was 0.0342 J, which means that it almost remained static during the first 5 ms of response.

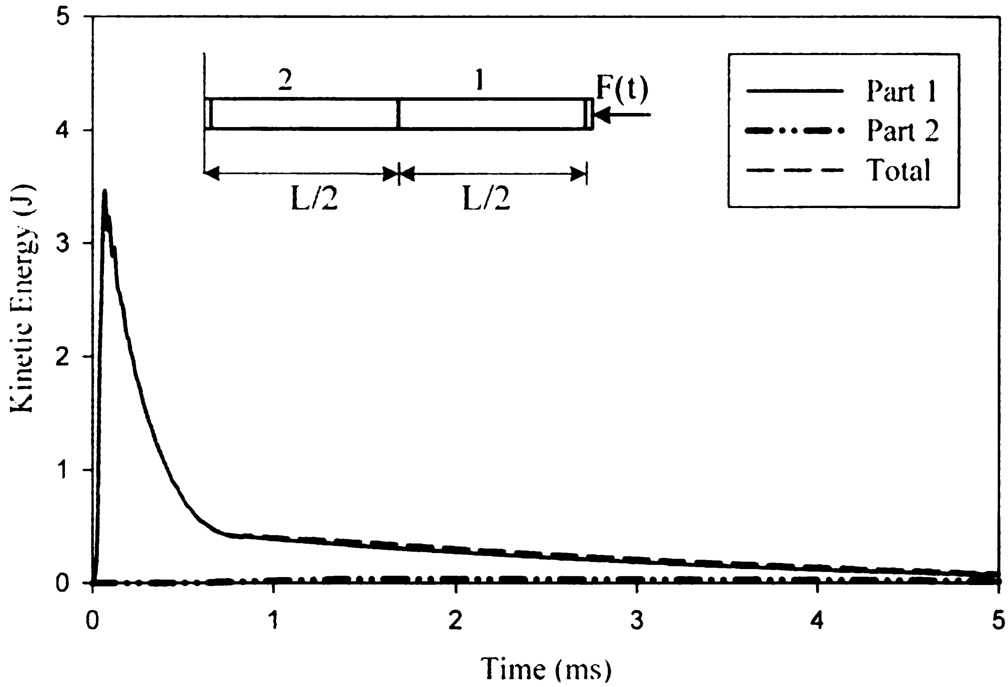

Figure 53. Kinetic Energy History of Non-homogeneous Foam Model 2 in 1D

4.5.3 Discussion

The results listed in Table 7 show that the stress wave propagation in non-homogeneous foam models has interesting characteristics. As shown in Figure 50, the internal energy is mainly stored in the weaker material in Part 1. Given that large deformations (see Table 7) happen in the same part, Model 1 confirms the conclusion from the solid models in Chapter 3 that larger plastic deformation will contribute to larger internal energy dissipation. When comparing deformations between the two models, Model 2 had much smaller values for both parts, while the energy dissipation in Model 2 was slightly lower than that of Model 1. This indicates that adding stiffer material to locations close to loads can prevent severe damage. Considering the trend of stress from the free end (Point A) to the fixed end (Point E), the magnitude of stress is affected by the stiffness of material. In a non-homogeneous model, an increasing stiffness of the material in the direction of the stress wave propagation will lead to higher transferred stresses, compared with a model with a deceasing material stiffness. This is consistent with the results from (Cui et al. 2009).

Table 7. Results from Non-homogeneous Foam Model in 1D Case

	Non-Homogeneous Model	
	Model 1	Model 2
Stress at point A (MPa)	42.6	54.9
Stress at point B (MPa)	0.366	2.82
Stress at point C (MPa)	0.395	0.443
Stress at point D (MPa)	0.734	0.351
Stress at point E (MPa)	0.968	0.369
Kinetic energy of the part 1 foam (J)	3.9	3.44
Kinetic energy of the part 2 foam (J)	0.00294	0.0342
Internal energy of the part 1 foam (J)	14.9	12.0
Internal energy of the part 2 foam (J)	0.0182	0.357
Deformation of part 1 in x direction (mm)	255.377	36.0426
Deformation of part 2 in x direction (mm)	1.149	24.1994

4.6 Summary

This chapter showed numerical studies aimed at evaluating the characteristics of stress wave propagation in homogeneous and non-homogeneous (bi-material) foam materials. The goal of studying one-dimensional models was to understand the behavior of stress wave propagation in foams and thus evaluate the performance of two-dimensional foam models (Chapter 5). The results were reasonable and confirmed findings by other researchers. The following summarizes important features learned from the presented studies.

Stress waves in homogeneous foam models propagate at a lower speed compared with homogeneous solid models. The stress magnitude deceases dramatically because most of the kinetic energy transfers to internal energy by means of large plastic deformations in the foam material. This is consistent with the conclusion from Chapter 3. It is clear that foams are suitable to be used as a buffer material for energy dissipation and stress mitigation.

The propagation of stress waves across dissimilar foam materials (non-homogeneous) highlighted that arranging material's stiffness and strength sequence can lead to a better performance on stress mitigation and energy dissipation. A stiffer material near the load application will reduce the overall deformation in the model dramatically without losing much kinetic energy dissipation. A layered non-homogeneous with an increasing sequence of stiffness of material in the direction propagation will lead to a higher stresses at the end of the bar, while an opposite will lead to a lower stresses.

CHAPTER 5. TWO-DIMENSIONAL STRESS WAVE PROPAGATION IN FOAM MATERIALS

5.1 General

This chapter presents studies on the two-dimensional stress wave propagation in foam materials. Deformations, stress mitigation and energy dissipation are of prime concern. The aim is to evaluate the performance of using homogeneous and non-homogeneous open-cell foam cores in a sandwich beam subjected to an impulsive pressure load.

Four types of sandwich aluminum foam beams, with a length of 72 mm and height of 27 mm, were evaluated. The sandwich foam panels featured an open-cell aluminum foam core and two outer face sheets assumed to be of solid aluminum material. The model differences were in the open cell foam core. The foam core in the first design consisted of a homogeneous foam material with a low relative density and thus a relatively low strength. The second design features a foam core with a strategically reinforced region in which the reinforcement effect was implemented by considering a foam with a lower relative density. The third design features a core with layers of foams made of different relative densities, with lower relative density at the top and a higher relative density at the bottom. The fourth design also features a layered foam core but in this case the relative stiffness decreases from top to bottom. The panels were modeled as two-dimensional simply-supported beams and constrained from horizontal deformations to represent testing of a circular (or disk) panel inside a shock tube chamber. Three levels of impulse pressure loads, 1MPa, 2MPa and 3MPa, were applied on the full span of the top facesheet.

Results from the numerical simulations indicate sandwich beams with strategically reinforced non-homogeneous cores performed best in terms of deformations, stress mitigation and energy dissipation. The results further show that the findings from Chapter 4 on 1D stress wave propagation in foam materials can be used to predict the behavior of foam sandwich plates in 2D. Finally, the studies in this chapter indicate that strategically reinforced (or tailored) foam structures can be used for stress wave management.

5.2 Model Definition

Four models were used in this study. Following conventional sandwich plate designs, each model is made up of 3 parts: top facesheet, foam core and bottom facesheet. Differences exist on the design of the foam cores. The top and bottom facesheets have a length of 72 mm and height of 1.5 mm. The overall length of the foam core is 72 mm and height is 24 mm. In order to detect the stress redirection, simple supports are modeled as a vertical restraint along a 6 mm region at the ends of the lower facesheet. The facesheets and foam core are assumed to be perfectly bonded and so are the interfaces between foam regions with different relative densities. The material in the facesheet is aluminum. The sandwich beam cores are assumed to be made from open-cell aluminum foams with varied relative densities. The facesheet was simulated with the elastic material model MAT001 in LS-DYNA, and the crushable foam material model MAT063 was used to simulate the foam material.

Details for the mesh were the same as the ones used for the one-dimensional studies in Chapter 4.

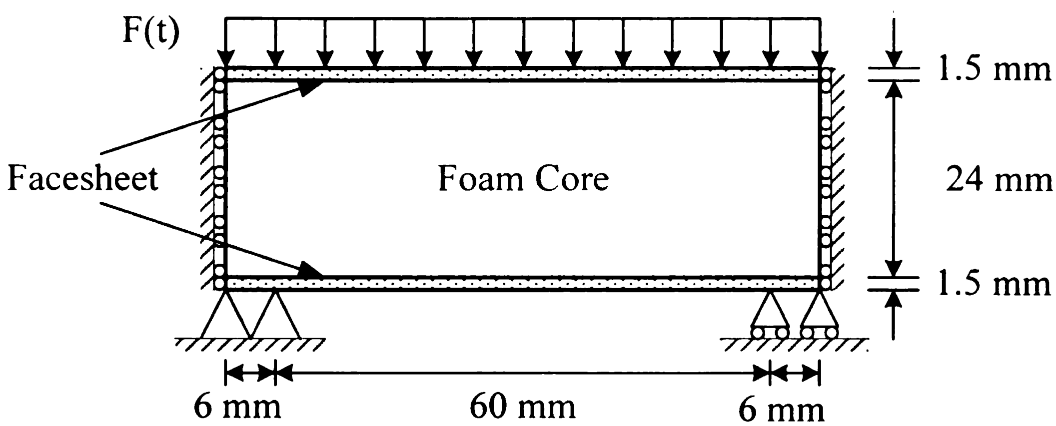

Figure 54. Model 1 with Homogeneous Foam Core

Figure 54 shows the sandwich plate geometry for Model 1. The facesheet thickness is 1.5mm, 6.25% of 24mm the foam core thickness. The length of the plate is 72 mm, and the free span is 60 mm due to the 6 mm support regions at each beam end. The foam core in Model 1 is taken as a homogeneous aluminum open-cell foam. The simply-supported boundary conditions for the beam were modeled as vertical deformation supports at the ends of the bottom facesheet. In addition, lateral deformations along the beam thickness were restrained.

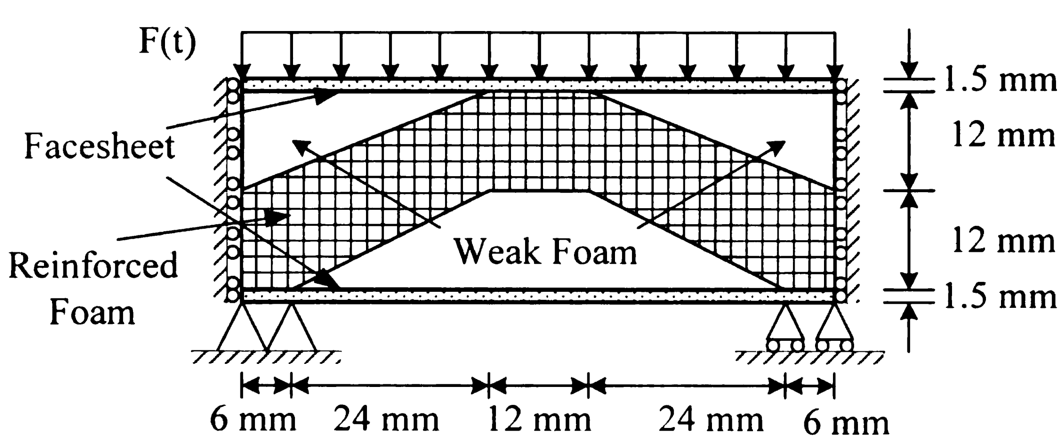

Figure 55. Model 2 with Irregularly Reinforced Foam Core

Figure 55 shows Model 2, which features a strategically reinforced foam core in which a region shaped in the form of an arch has a foam with lower relative density while the surrounding foam is a weaker (higher relative density) foam. The contact region between top facesheet and reinforced region lies in the center of top facesheet and it is 12 mm long. The contact regions between the reinforced foam and the bottom facesheet lie on the two support regions and their length is 6 mm each. The interaction among the foam regions and between the facesheets and the foam core is assumed to be one of perfect bond.

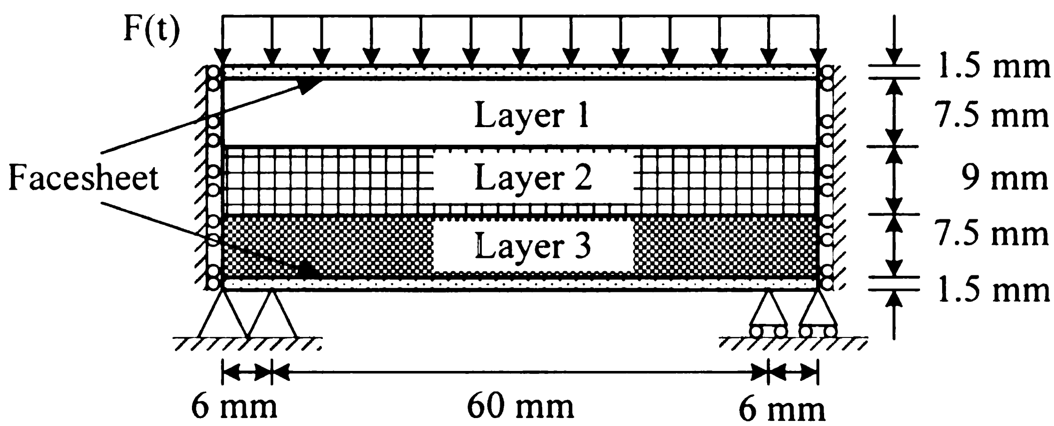

Figure 56. Model 3 with Increasing Layered Foam Core

Figure 56 shows the foam core for Model 3, which is composed by three stacked homogeneous foam layers. Due to the size of mesh element used in this study, the thickness of the first and the third layer is 7.5 mm and that of the middle layer is 9 mm. The relative densities for the foam layers increase linearly from the top to the bottom.

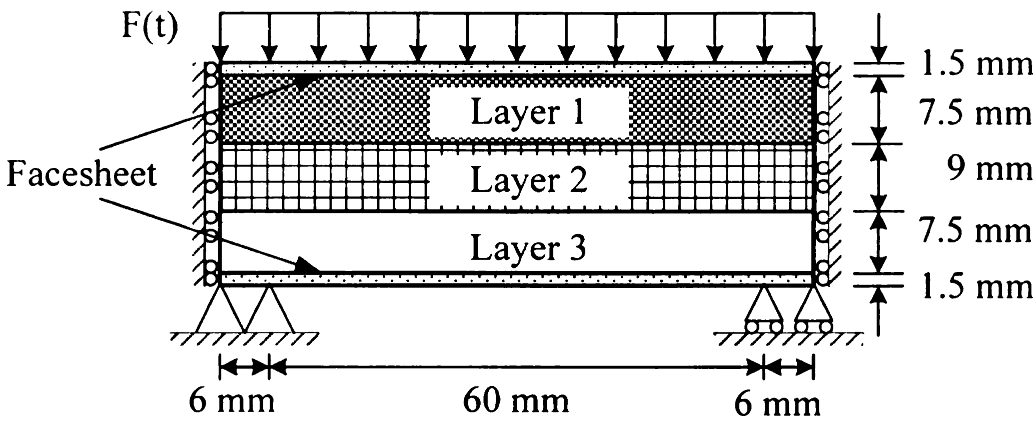

Figure 57. Model 4 with Decreasing Layered Foam Core

The foam core for Model 4 is shown Figure 57. This model also features a core with layered homogeneous foam regions. As for the previous model, the thickness of the first and the third layer is 7.5 mm and that of the middle layer is 9 mm. The relative densities for the foam layers in this model decrease linearly from top to bottom.

5.3 Material Modeling

The material used in this study is aluminum and the assumed material properties are listed in Table 8. The elastic material model MAT001 in LS-DYNA was used to model the facesheets. The properties for the open-cell foams used in this study are shown in Table 9, where the main differences between the foams (columns) is the relative density. They were computed based on the formulas presented in Section 2.3 The foam regions were modeled in LS-DYNA with the crushable foam material model MAT063.

Table 8. Properties of Aluminum Plate in 2D Sandwich Beams

E (GPa)	80
ν	0.3
ρ (kg/m^3)	2800
σ (MPa)	80

Table 9. Material Properties of Foams Used in 2D Sandwich Beams

	No.1	No. 2	No. 3	No. 4	No. 5	No. 6	No. 7
Relative density	0.06	0.08	0.10	0.24	0.26	0.28	0.30
E (GPa)	0.29	0.51	0.80	4.61	5.41	6.27	7.20
ν	0.33	0.33	0.33	0.33	0.33	0.33	0.33
ρ (kg/m^3)	168	224	280	672	728	784	840
σ (MPa)	0.35	0.54	0.76	2.82	3.18	3.56	3.94

5.4 Case Studies

All four of the previously described models were evaluated under three loading cases, namely, pressure loads of 1, 10 and 100 MPa, which define Cases 1, 2, and 3, respectively. Load intensity has a significant effect on the performance of the foam material. Thus, the relative densities for the foam materials considered in this chapter were selected based on pilot studies so that the simulations could be successfully completed and so that the results between models were comparable. Consequently, the foam properties (relative density) for Case 1 and Case 2 were identical. However, the foams used for Case 3 were stiffer so that the load of 100MPa would yield meaningful results and aid convergence of the numerical simulation.

5.4.1 Case 1

In this case a 1MPa impulse pressure load was applied on the full span of the top facesheet for all four models. The loading history is shown in Figure 38. The foam materials used in Case 1 are listed in Table 11. Please refer to Table 9 for the foam engineering properties.

Table 10. Foam Materials Used in Case 1 in 2D

	Model 1	Model 2		Model 3			Model 4		
Part	Foam Core	Weak Foam	Reinforced Foam	Layer 1	Layer 2	Layer 3	Layer 1	Layer 2	Layer 3
Foam No.	No.1	No.1	No.4	No.1	No.2	No.3	No.3	No.2	No.1

5.4.2 Case 2

In this case, a 10MPa impulse pressure load was applied on the full span of the top facesheet for all four models. The loading history is shown in Figure 58. The foam materials used in Case 2 are listed in Table 11. Please refer to Table 9 for the foam engineering properties.

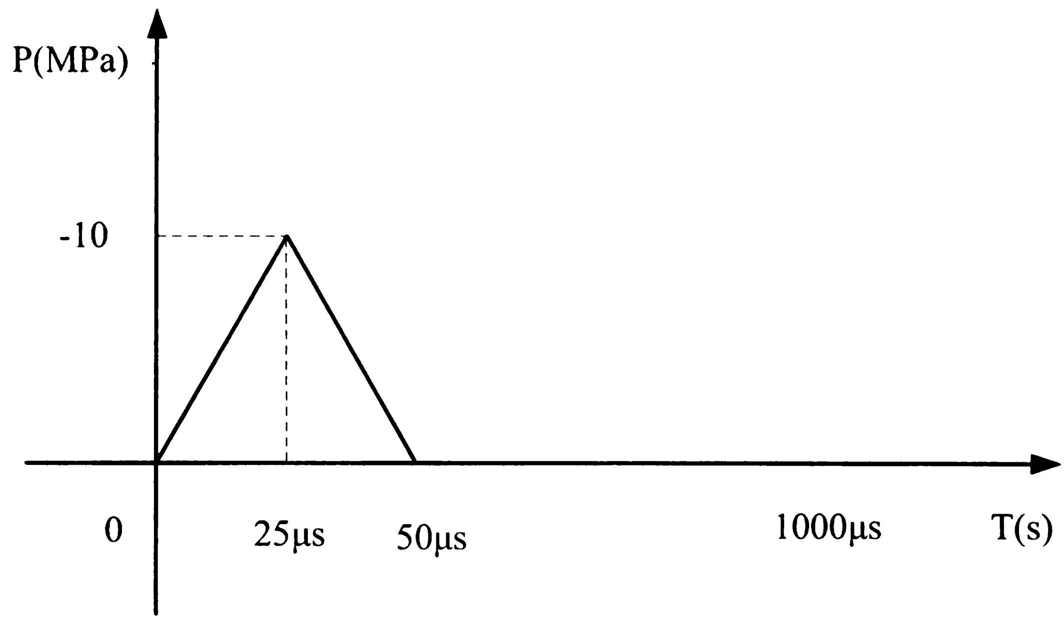

Figure 58. 10MPa Compression Pressure Load

Table 11. Foam Materials Used in Case 2 in 2D

	Model 1	Model 2		Model 3			Model 4		
Part	Foam Core	Weak Foam	Reinforced Foam	Layer 1	Layer 2	Layer 3	Layer 1	Layer 2	Layer 3
Foam No.	No.1	No.1	No.4	No.1	No.2	No.3	No.3	No.2	No.1

5.4.3 Case 3

This case featured a 10MPa impulse pressure load applied on the top facesheet for all models. The loading history is shown in Figure 25 in Section 4.4.1.3. The foam materials and their relative densities used in this case study are listed in Table 12. Table 9 provides the engineering properties for the foam materials.

Table 12. Foam Materials Used in Case 3 in 2D

	Model 1	Model 2		Model 3			Model 4		
Part	Foam Core	Weak Foam	Reinforced Foam	Layer 1	Layer 2	Layer 3	Layer 1	Layer 2	Layer 3
Foam No.	No.4	No.4	No.7	No.4	No.5	No.6	No.6	No.5	No.4

5.5 Results

This section presents the results from the mentioned study cases with emphasis on induced deformations, stress magnitudes, transferred kinetic energy and energy absorption. Because the perfect bond assumption between the foam and facesheets is not realistic, the deformations obtained from these models may not be accurate after the pressure loads are fully acting on the top facesheet of sandwich plate. The effect of delamination of the foam core from the facesheets was included in a study from Bahei-El-Din (2006). Therefore, the data up to 0.2 ms of response is considered to be more realistic and representative for evaluating and comparing the models.

5.5.1 Case 1

In this case, a 1MPa compressive pressure impulse load was applied on the full span of the top facesheet. The four models show distinct response. Figure 59 shows the kinetic energy in the top facesheet for all models. It can be seen that as the pressure load was applied on the sandwich plate the kinetic energy of the top face sheet increases gradually reaching a peak and then decaying equally fast. Model 1 and Model 3 had similar behavior with peak kinetic energy values at around 0.042 ms of 2.47×10^{-6} J for Model 1 and 2.45×10^{-6} J for Model 3. The response of Model 2 and model 4 was similar to each other with peak kinetic energy values at approximately 0.039 ms of 1.59×10^{-6} J and 1.50×10^{-6} J, respectively.

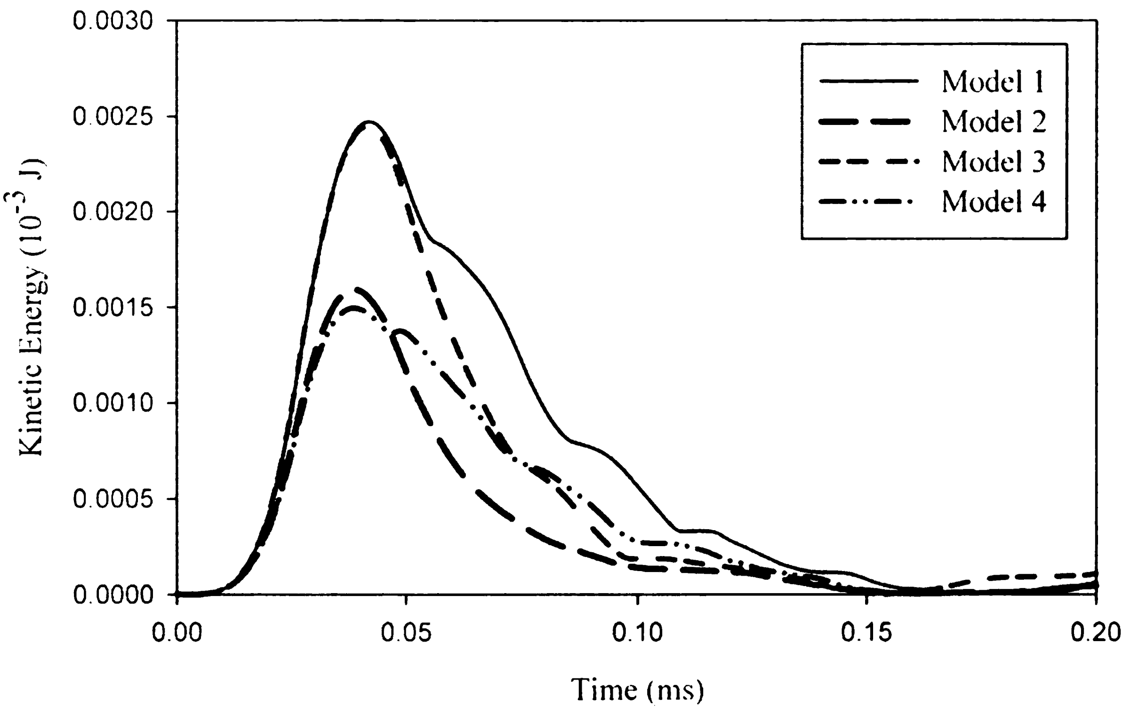

Figure 59. Kinetic Energy of the Top Facesheets in Case 1

Figure 60 shows the vertical displacement history of the top facesheet for all models. It can be seen that Model 1 had the greatest vertical displacement: -0.326 mm at a time 0.18 ms. Model 3 reached its maximum vertical displacement of -0.266 mm at 0.15 ms, and Model 4 reached its maximum vertical displacement of -0.254 mm at 0.17 ms. Model 2, with a reinforced arch foam core had the least vertical displacement: -0.198 at 0.16 ms.

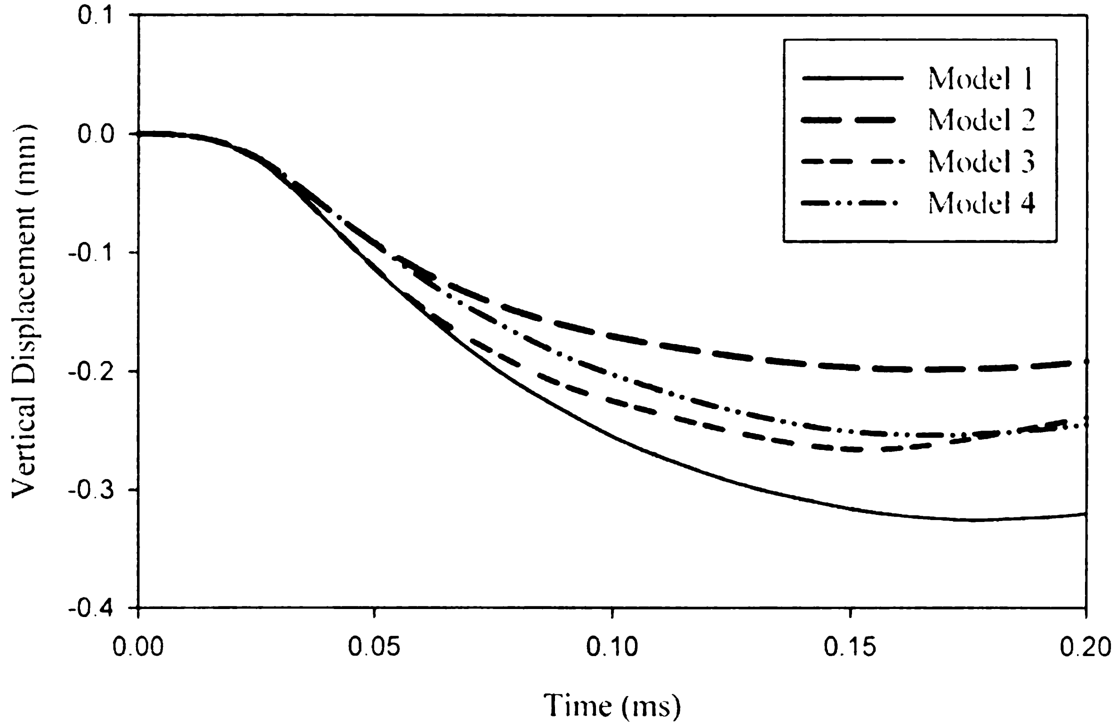

Figure 60. Displacements of the Top Facesheets in Case 1

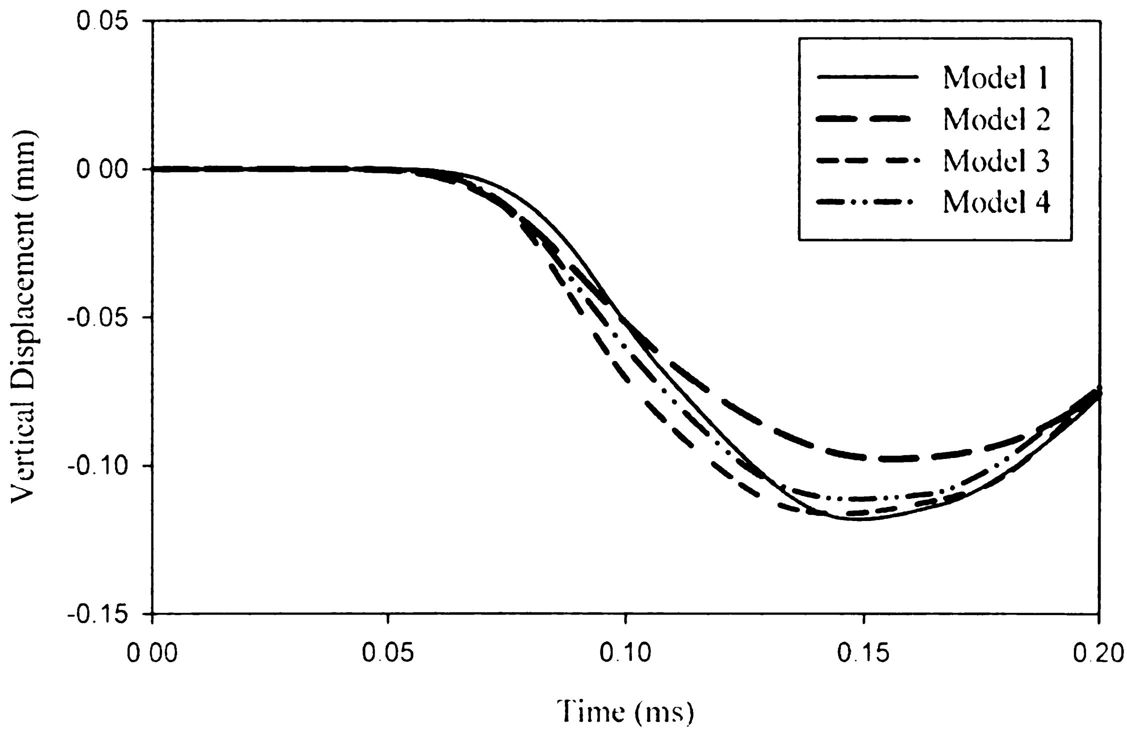

Figure 61. Displacements of the Bottom Facesheets in Case 1

Figure 61 shows the vertical deformation in the bottom face sheet for the four models. It can be seen be seen that the displacement response at bottom facesheet in the four models was similar, ranging from -0.0979 mm to 0.118 mm for Model 2 and Model 1, respectively.

Figure 62 shows the stress histories extracted from the middle of the bottom facesheet. It can be seen that the stress response for all models was very similar. The lowest stress peak values was for Model 1: -1.78×10^{-2} GPa at 0.15 ms, while the higest stress value was for Model 1: -2.34×10^{-2} GPa at 0.14 ms.

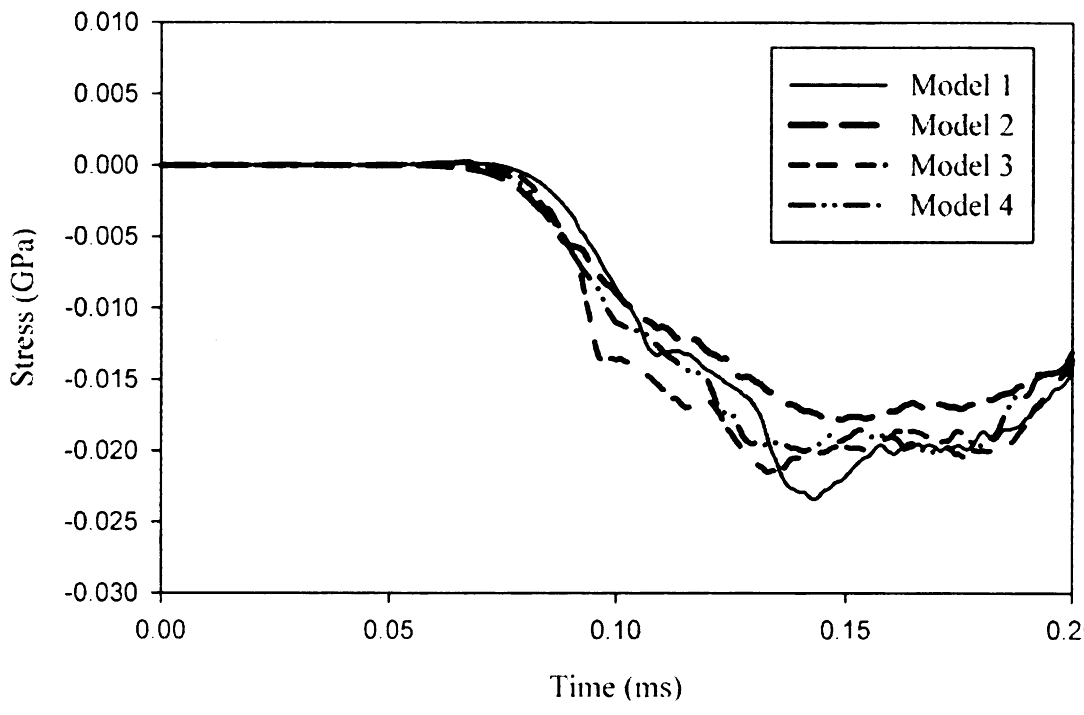

Figure 62. Stresses in the Middle of the Bottom Facesheet in Case 1

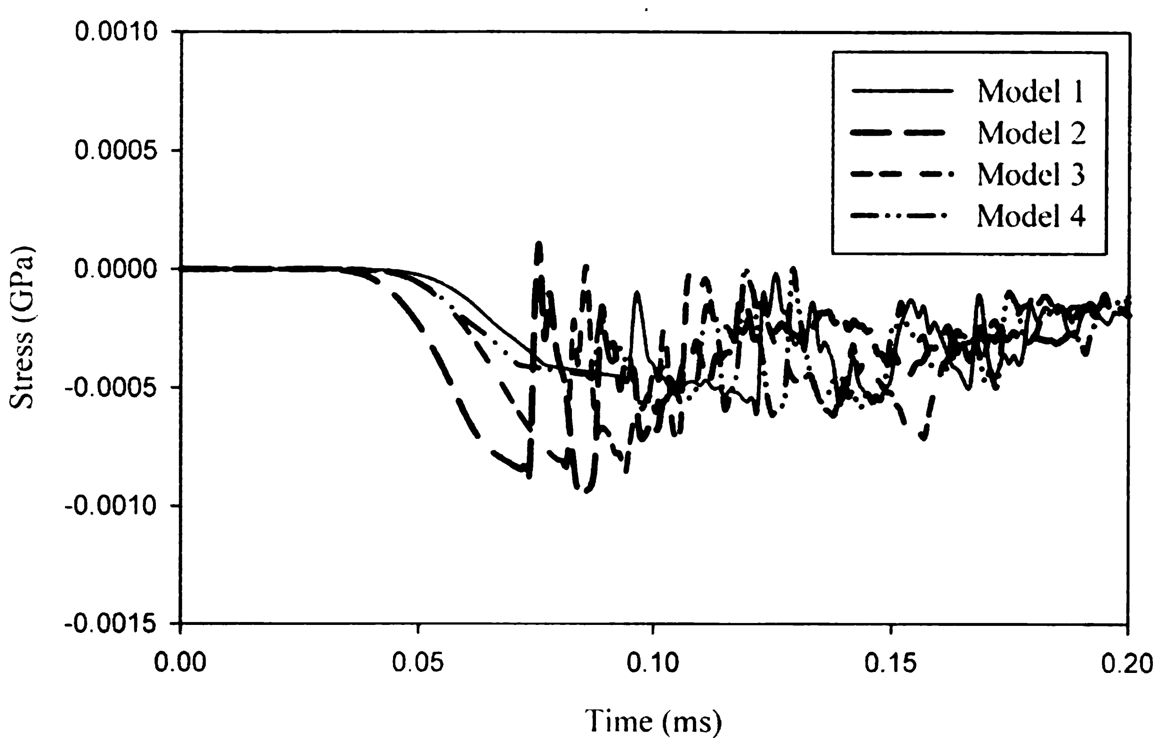

Figure 63. Redirected Stresses in the Bottom Facesheet in Case 1

The stress histories extracted from the support regions of the bottom facesheet are shown in Figure 63 It can be seen that the traces are similar in featuring an increase in the reaction stresses and then oscillations due to the reflection of waves off the supports. It is of interest to note that Model 2, which featured the arch reinforced foam had the highest reaction stress values, followed by Model 3, which used an increasingly denser foam in a layered fashion.

The history of internal strain energy stored in the foam core of Model 1 is shown in Figure 64, whereas that for Model 2 is shown in Figure 65. The results for Model 2 provide traces for the internal energy in the reinforced (arch shape) and weaker surrounding foam. It can be seen that the most of the energy absorption takes place in the weaker foam regions.

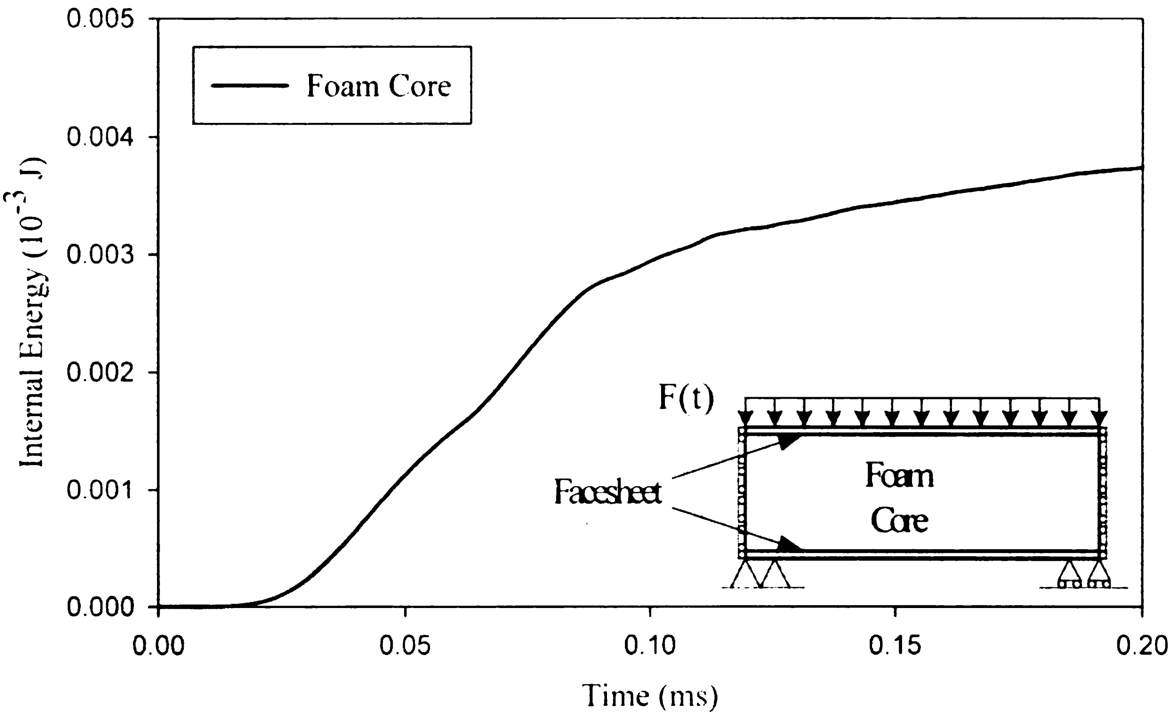

Figure 64. Internal Energy of Foam from Model 1 in Case 1

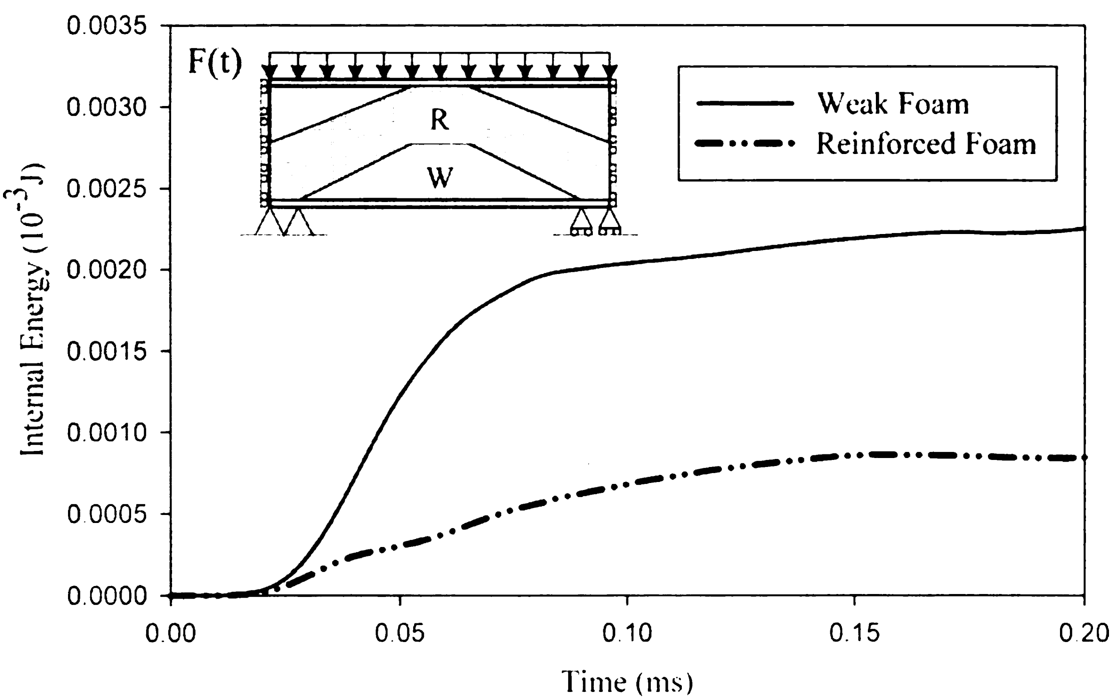

Figure 65. Internal Energy of Foams from Model 2 in Case 1

The strain energy in Model 1 stabilized at approximately 3.74 x 10^{-6} J while the total strain energy in Model 2 stabilized at a level of approximately 3.1 x 10^{-6} J. The higher strain energy in Model 1 indicates that that panel suffered more damage even though Model 2 had less total vertical deformation in the bottom and top facesheets.

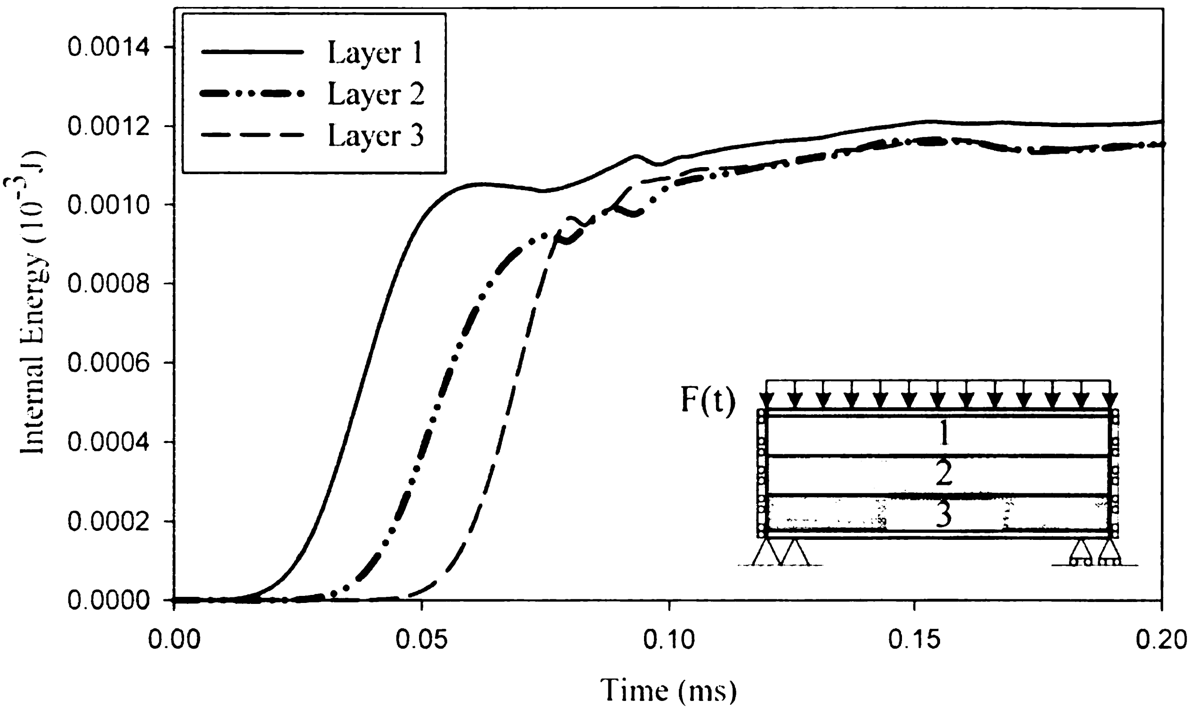

Figure 66. Internal Energy of Foams from Model 3 in Case 1

Figure 66 shows the internal energy stored in the three layers of Model 3 (model with increasing foam stiffness). It can be seen that there is a time phase lag on the increase of strain energy for each layer. However, the strain energy for all layers reaches similar magnitudes before stabilizing at a similar level. This seems to indicate that the upper layers in the foam do not impede the transmission of stress waves and the energy is transmitted to the layers below.

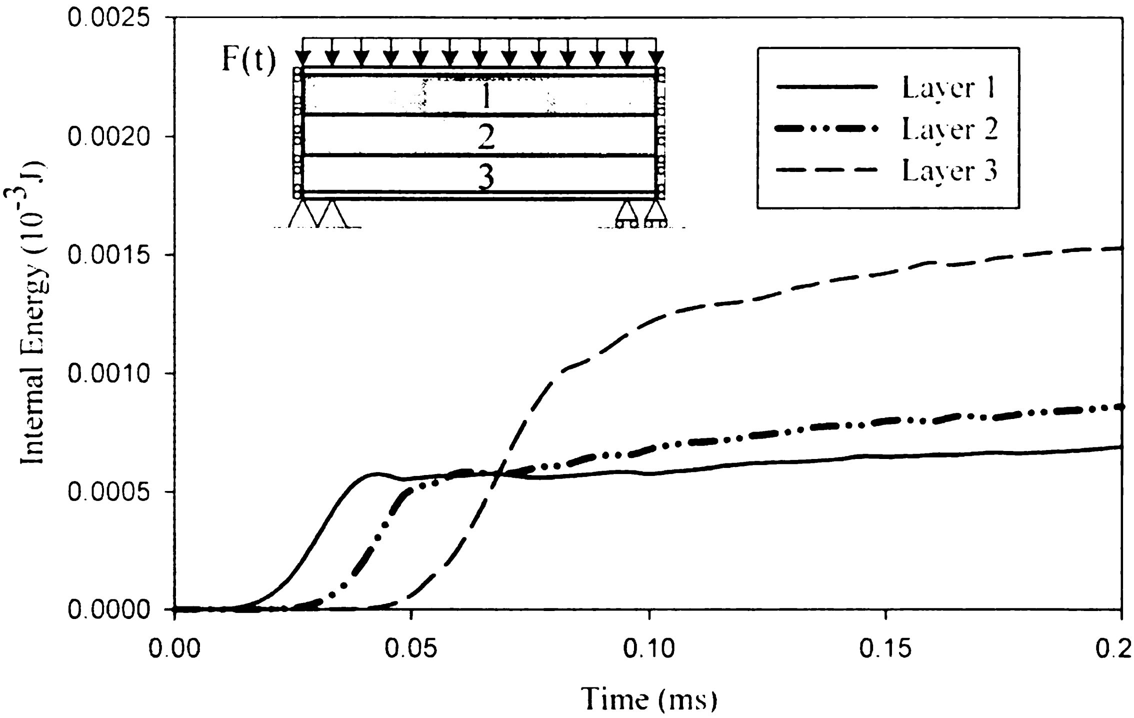

Figure 67. Internal Energy of Foams from Model 4 in Case 1

The strain energy history for Model 4 (decreasing foam stiffness) is shown in Figure 67. As for Model 3, the time lag shift on the increase of strain energy is also seen for this model. However, it can be seen that the levels of energy do not reach the same level for all layers. Rather, the inelastic deformation (and energy absorption) is concentrated in the bottom layer while the upper stiffer foam layers experience a much lower (about half) level of internal strain energy. However, the total strain energy for Model 4, which was 3.08×10^{-6} J at 0.2 ms is very similar to the total energy in Model 3 (3.52×10^{-6} J at 0.2 ms), which indicates that Model 4 was able to dissipate about the same total amount of energy but with less damage within its structure.

5.5.2 Case 2

As previously noted, Case 2 consists on the application of a 10MPa impulsive compressive pressure load applied on the full span of the top facesheet. This section provides an overview of the response of the four different sandwich foam beam models to this loading condition.

A plot of the kinetic energy history response of the top face sheet is shown in Figure 68. Model 1 (homogeneous foam) and Model 3 (increasing foam stiffness) showed a similar response transmitting the highest level of kinetic energy. Conversely, Model 2 (reinforced foam) and Model 4 (decreasing foam stiffness) transmitted less kinetic energy to the top face sheet. This indicates that Models 2 and 4 will experience less deformation in their top face sheets compared to the other designs.

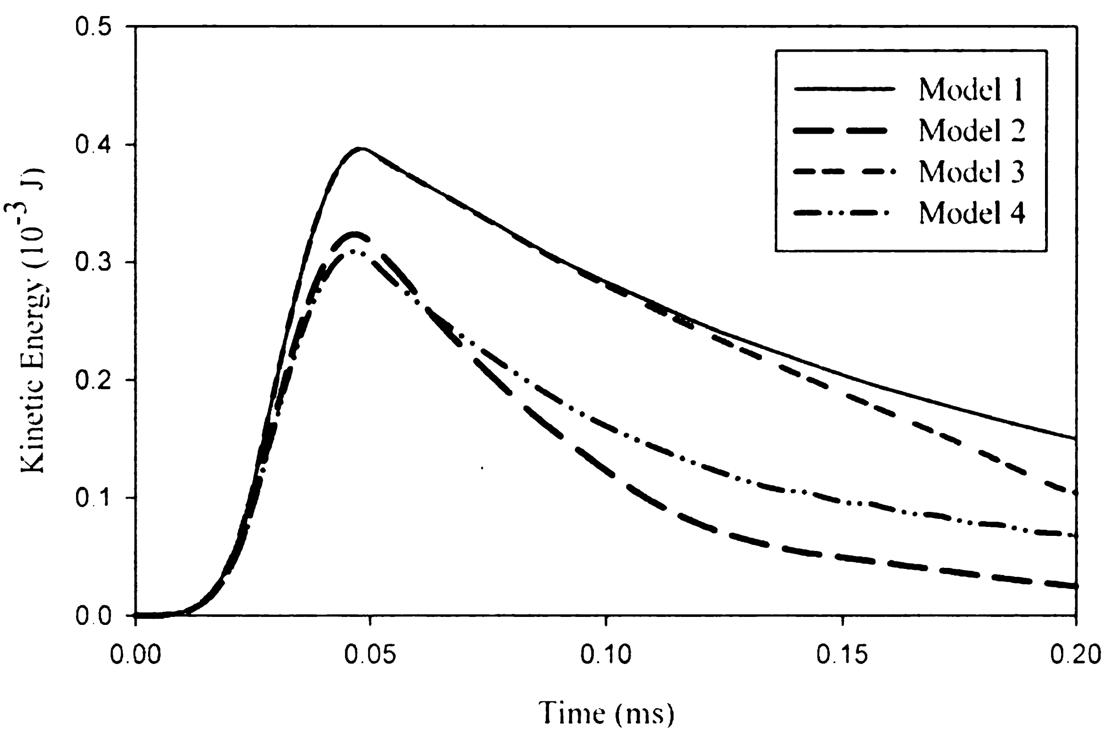

Figure 68. Kinetic Energy of the Top Facesheets in Case 2

The vertical displacements of the top and bottom facesheets are shown in Figure 69 and Figure 70, respectively. From Figure 69 it can be seen that Models 2 and 4 have the least amount of deformation on the top facesheet, which is consistent with the lower levels of kinetic energy for this part of the model. The response of Models 1 and 3 is essentially equal. Overall, Model 2 (reinforced foam) shows the least amount of deformation. Deformations of the bottom facesheet are more similar for all models, however, differences can be seen around the peak values. First, it can be seen that Models 1, 2 and 4 experience a very similar deformation history, reaching a very similar maximum value and then showing a rebound in the response. Model 3, however, experienced larger deformations and a later rebound on the response.

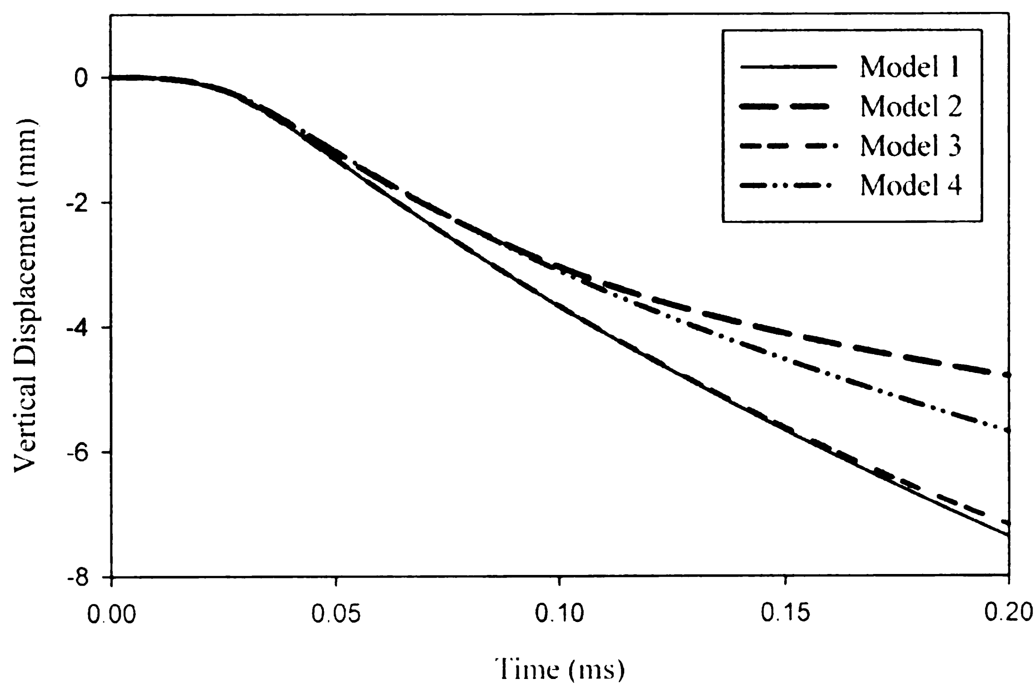

Figure 69. Displacements of the Top Facesheets in Case 2

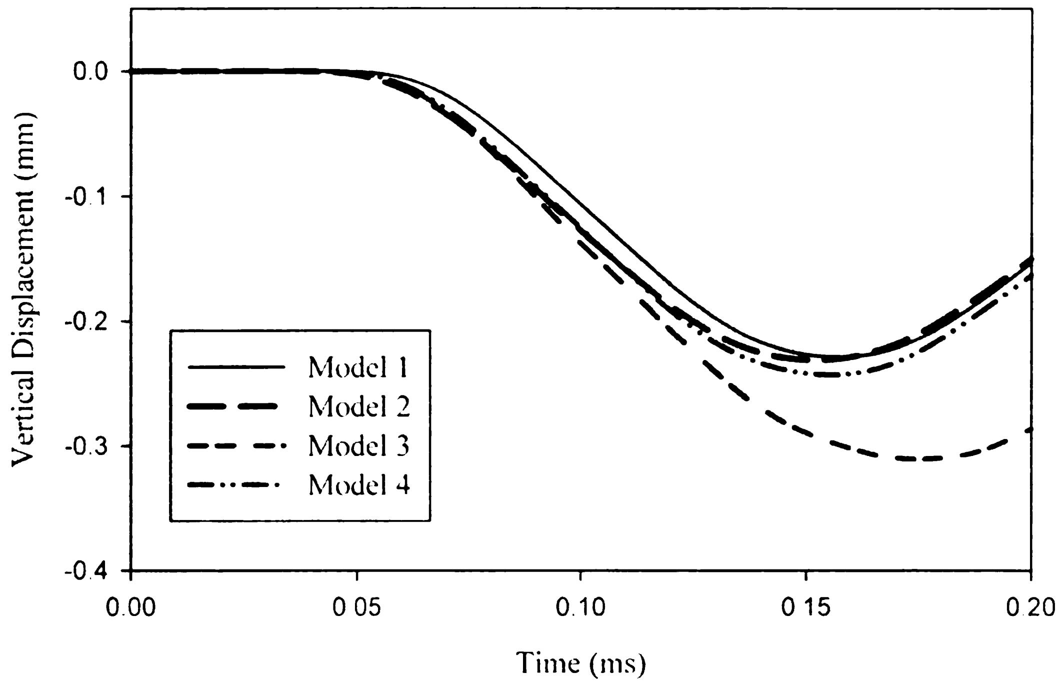

Figure 70. Displacements of the Bottom Facesheets in Case 2

Figure 71 shows that stress histories extracted from the middle of the bottom facesheet. The stress demands for Models 1, 2 and 4 was very similar, while Model 3 experienced a 40% lager peak stress. Model 3 is the one with the layered foam core with increasing stiffness. These results indicate that the use of a higher stiff material near the bottom leads to increased stresses. Thus, this design option increases the forces at the bottom of the beam rather than attenuating the loading effects.

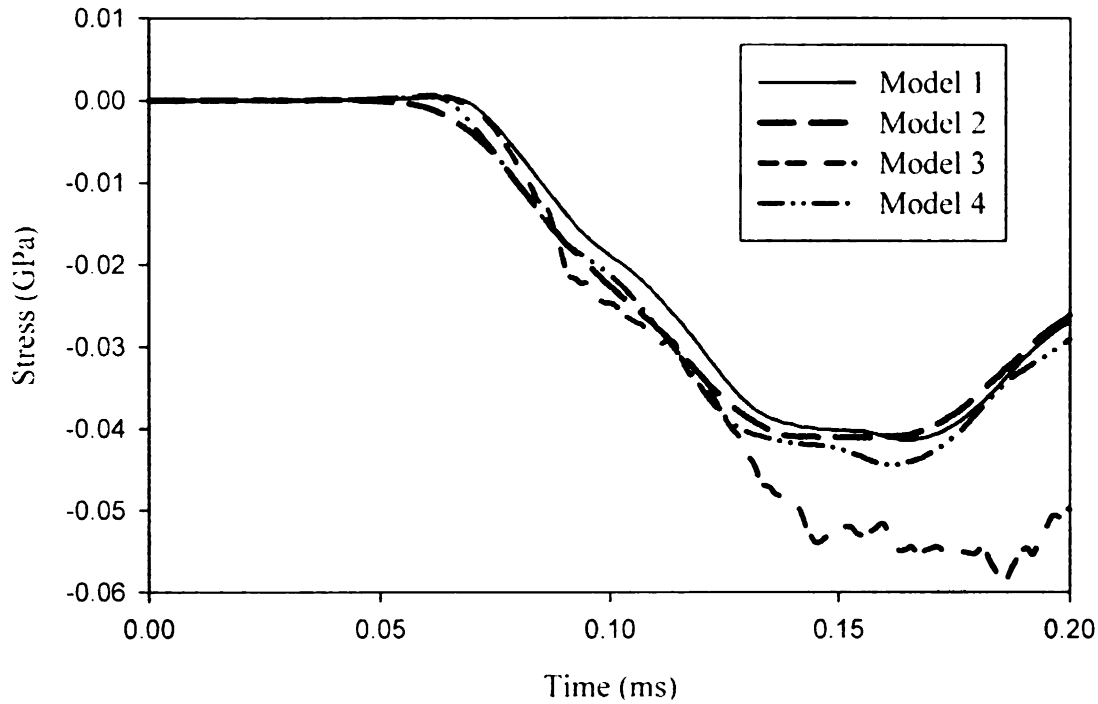

Figure 71. Stresses in the Middle of the Bottom Facesheet in Case 2

The concept of stress redirection was again explored by comparing the stress history at the support regions of the beams. As shown in Figure 72, stresses at the support region tend to increase rapidly upon arrival of the stress wave and then stabilizes with only minor oscillations due to refraction in Model 3. With the exception of Model 2, all models have a similar response, which indicates that while their individual stress, deformation, and energy levels were different, the stress wave propagated to the supports in a similar manner.

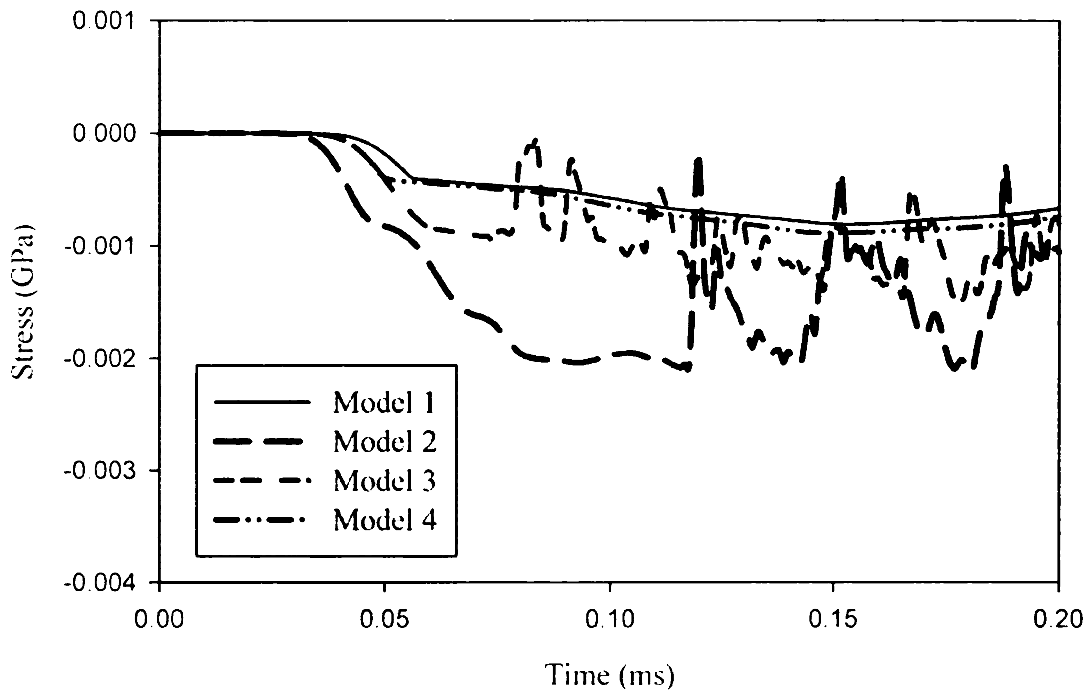

Figure 72. Redirected Stresses in the Bottom Facesheet in Case 2

However, the stresses at the support region of Model 2 not only increase more rapidly but have a higher magnitude (twice as high) and a more pronounced effect of wave refraction indicating that the stress wave is going back and forth to this same region. Such behavior indicates that, as intended, the strategic reinforced foam design of Model 2 was effective in redirecting the path of the stress wave to the supports.

The strain energy accumulated in the foam core is shown in Figure 73 to Figure 76. The internal energy in Model 1 (homogeneous foam) is shown in Figure 73. The internal energy rises rapidly and uniformly throughout the loading time span. The internal energy at 0.2 ms reaches 2.73×10^{-4} J.

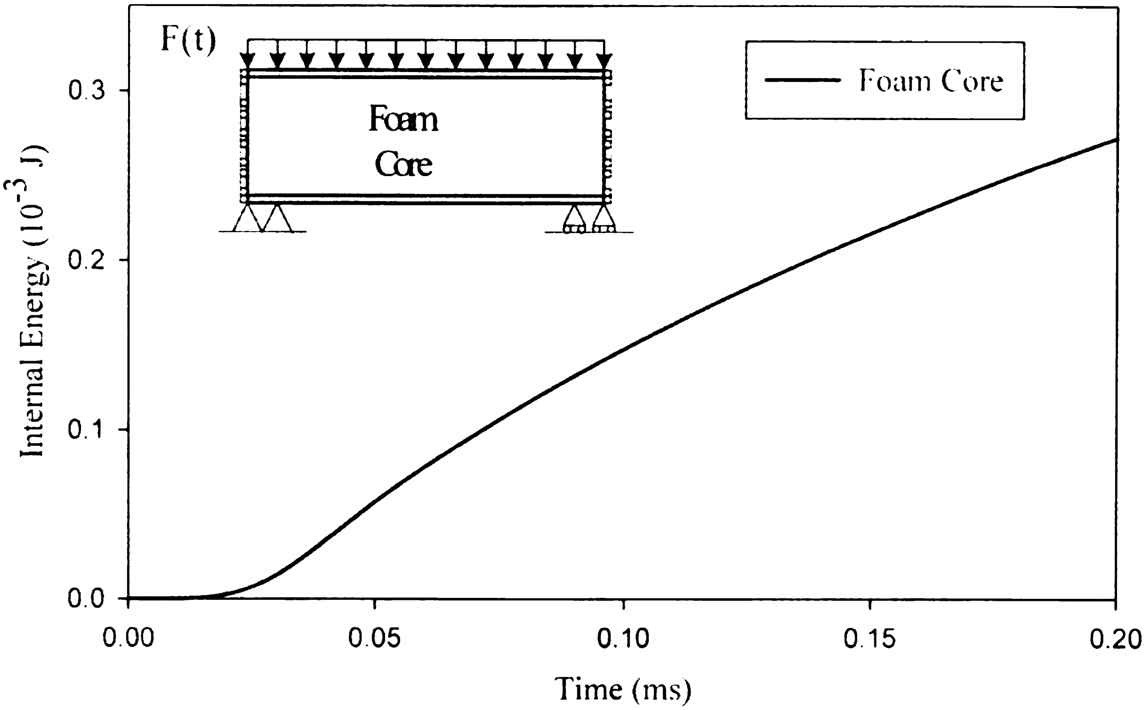

Figure 73. Internal Energy of Foam from Model 1 in Case 2

The strain energy for Model 2 (arch reinforced foam) is shown in Figure 74. It can be seen that the accumulated internal energy for the weak and stiff foam regions is similar, although slightly larger for the weak foam regions. The total internal energy for this model reached 1.79 x 10^{-4} J at 0.2 ms. This is 34% lower than that for Model 1, indicating the ability of this model to sustain less internal damage.

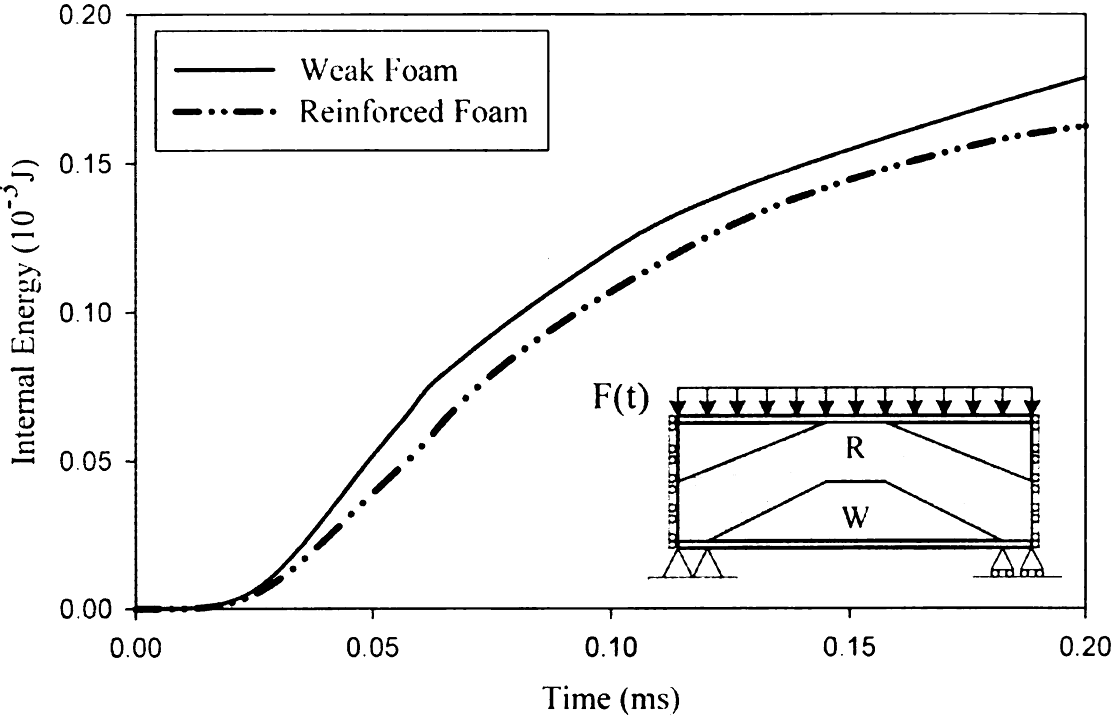

Figure 74. Internal Energy of Foams from Model 2 in Case 2

The internal energy accumulated in the foam core of Models 3 and 4 are shown in Figure 75 and Figure 76, respectively. In Model 3, most of the energy was stored in the weaker foam at the top (layer 1). In Model 4, most of the energy was again at the top layer but the bottom layers also contributed to dissipate energy, even though at a lower level. Thus damage in Model 4 was not as concentrated as that in Model 3.

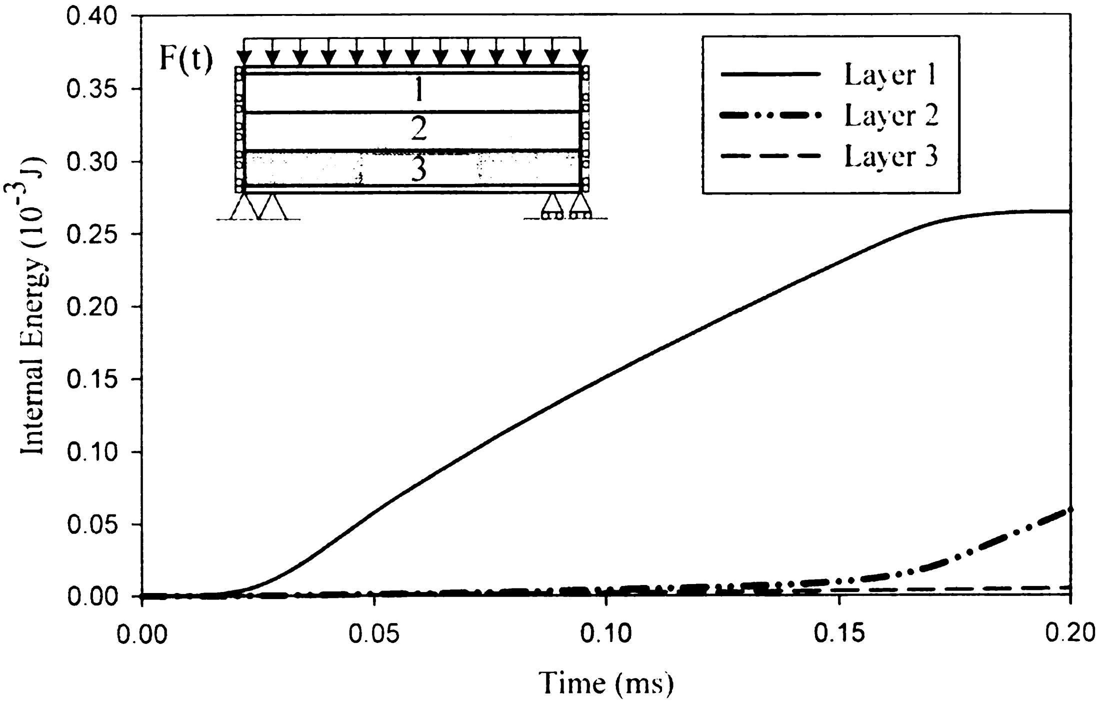

Figure 75. Internal Energy of Foams from Model 3 in Case 2

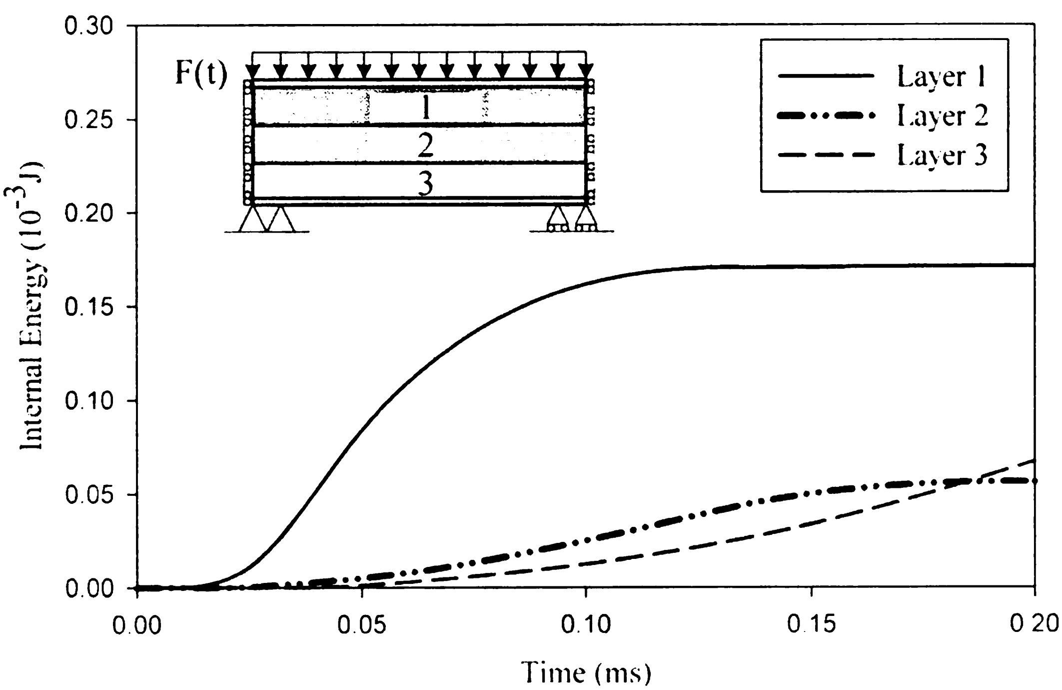

Figure 76. Internal Energy of Foams from Model 4 in Case 2

5.5.3 Case 3

The loading condition for Case 3 is a 100MPa compressive impulse pressure load applied on the full span of the sandwich beam top facesheet. As in the previous sections, results for the different beam models to this load case are presented next.

Figure 77 shows the history of kinetic energy on the top facesheet of the beam. The response for all models is similar, with slightly higher values for Models 1 and 3. Displacements for the top and bottom facesheets are shown in Figure 78 and Figure 79, respectively. In both cases, the displacement profiles are very similar, bounded by the responses of Model 1 (larger deformations) and Model 2 (smaller deformations). The difference in response is not as obvious as in previous load cases, which is thought to be due to the increased damage caused by larger load in this case.

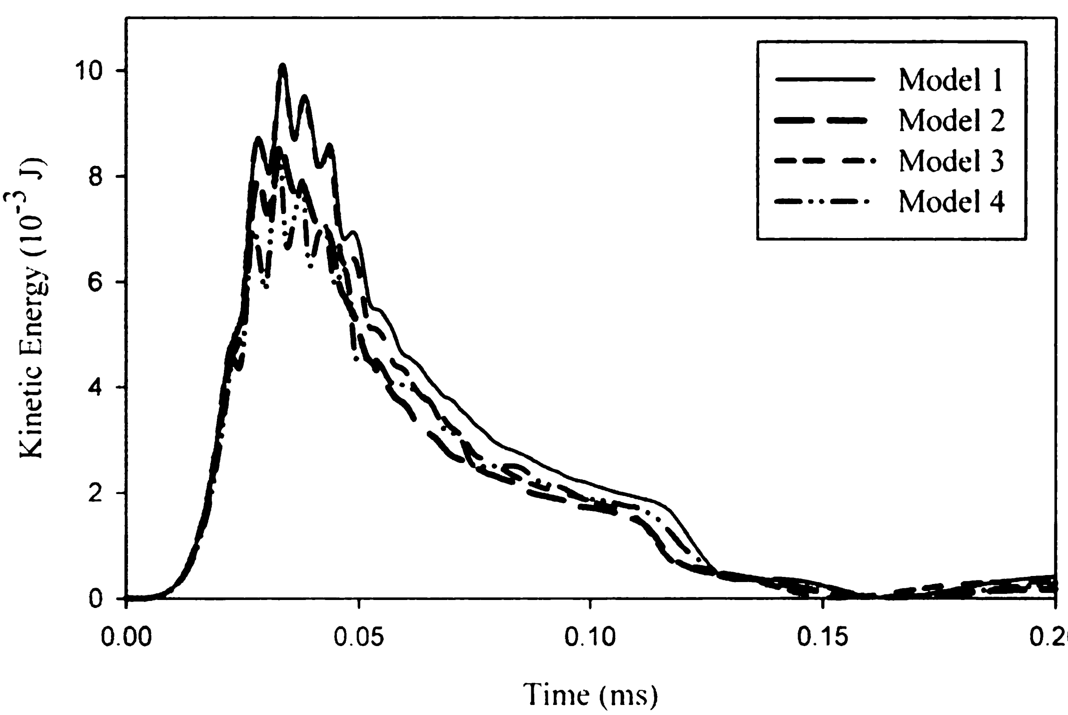

Figure 77. Kinetic Energy of the Top Facesheets in Case 3

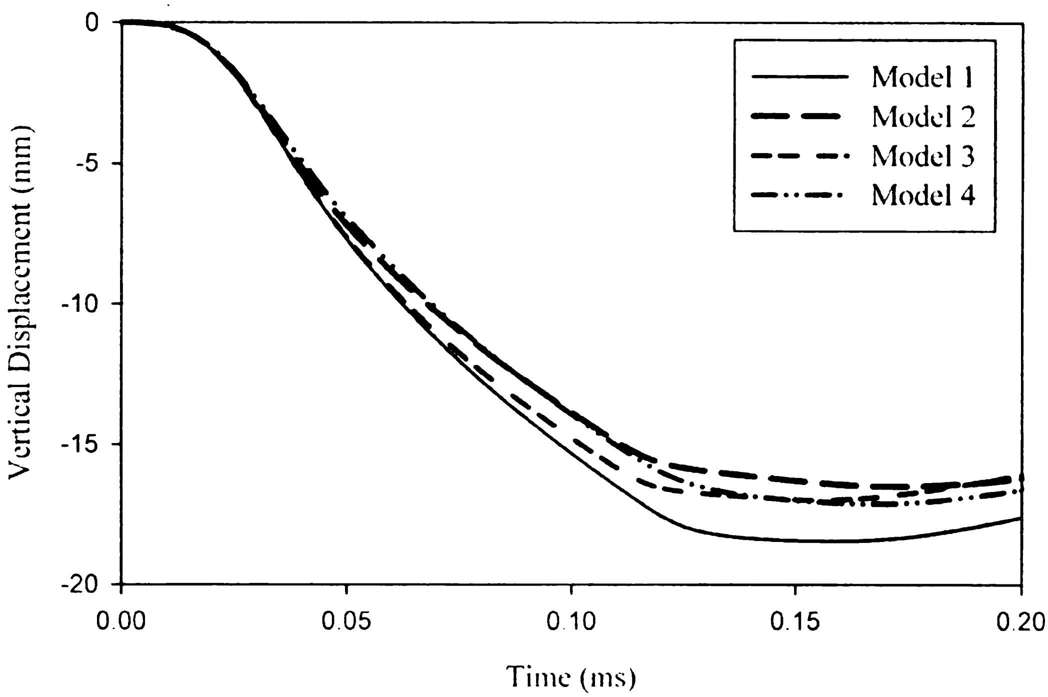

Figure 78. Displacements of the Top Facesheets in Case 3

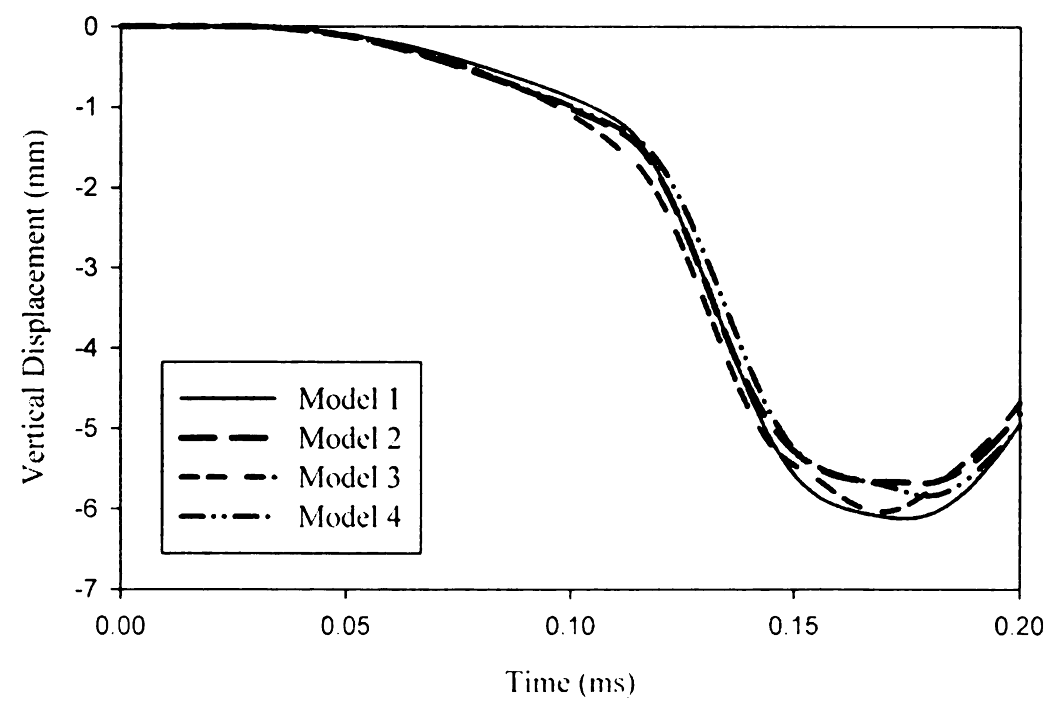

Figure 79. Displacements of the Bottom Facesheets in Case 3

Figure 80 shows the stress histories extracted from the middle of the bottom facesheet. The response for all models was very similar; indicating that the demand transferred to this bottom element was essentially the same in all cases.

The stress histories extracted from the support regions along the bottom facesheet are shown in Figure 81. The increased stress values for Model 2 indicate again that the strategically reinforced foam core is able to direct the stress waves to the support regions. However, the support stresses for the other models are now larger and closer to those of Model 2. This is due to the increased load magnitude, which indicates that as the level of damage increases the stress wave has no alternative but to increase the demands on the support regions. Thus, the differences with tailored design of Model 2 are reduced. This brings to light that the efficiency of a foam core for stress redirection and management will depend on the magnitude of the applied load.

The levels of internal stored energy in the foam cores of the beam models are shown in Figure 82 to Figure 85. The internal energy for Model 1 is shown in Figure 82, which shows a similar trend as that seen in Cases 1 and 2. The fact that the strain energy trace seems to stabilize indicates that most of the energy from the applied load has been dissipated in the form of permanent internal deformations.

The internal energy for Model 2 is shown in Figure 83, which shows that the weak and strong foams shared in the dissipation of energy almost equally. The total amount of internal energy for Model 2 was 10.9 x 10^{-3} J, which is about 43% of the energy absorbed by Model 1. Thus, Model 2 was able to sustain the load with less damage and with slightly less deformations to the top and bottom facesheets.

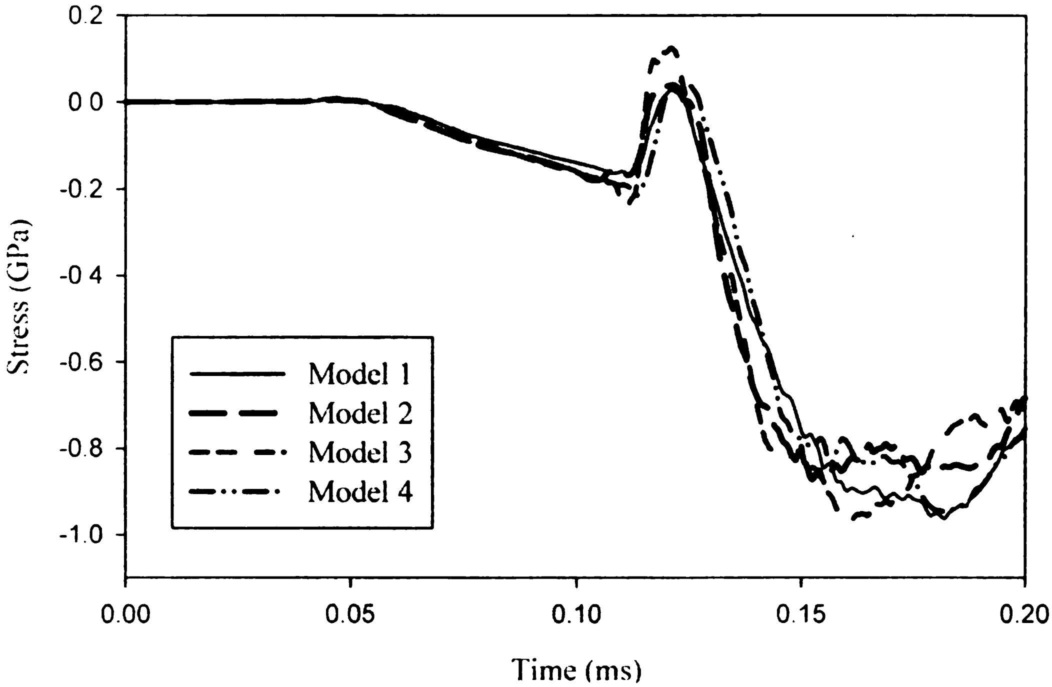

Figure 80. Stresses in the Middle of the Bottom Facesheet in Case 3

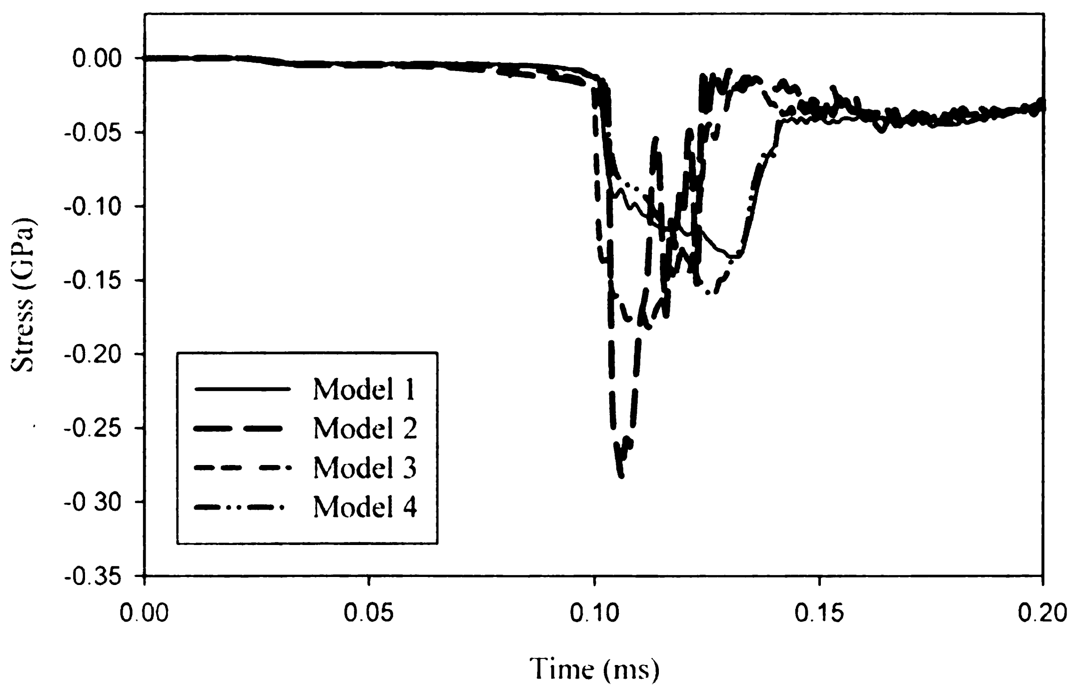

Figure 81. Redirected Stresses in the Bottom Facesheet in Case 3

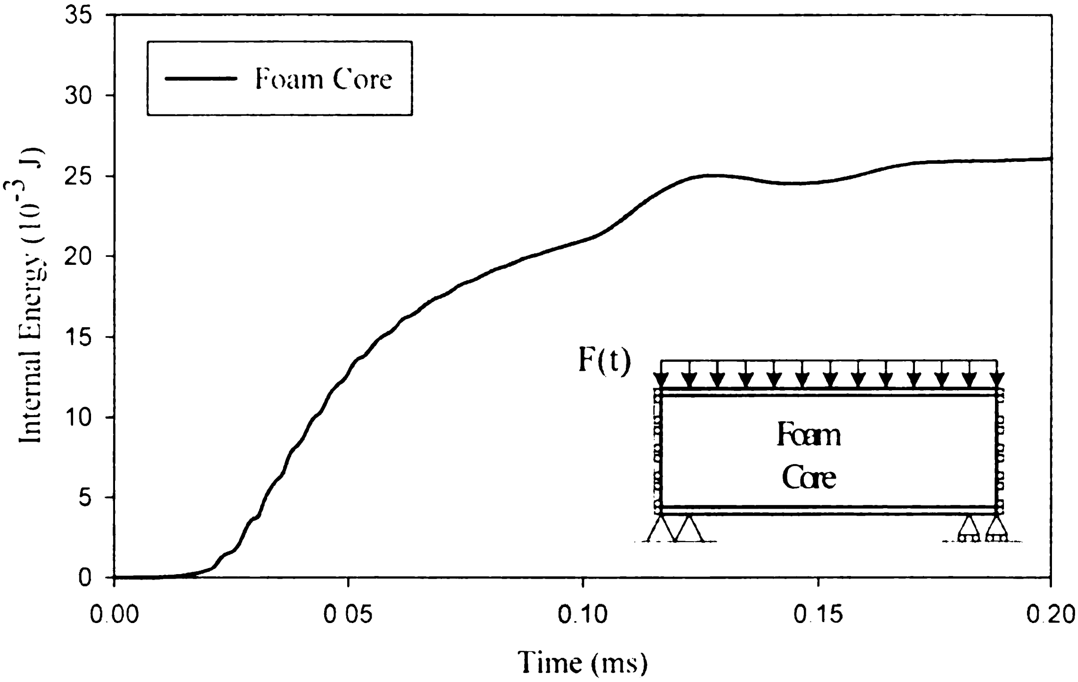

Figure 82. Internal Energy of Foam from Model 1 in Case 3

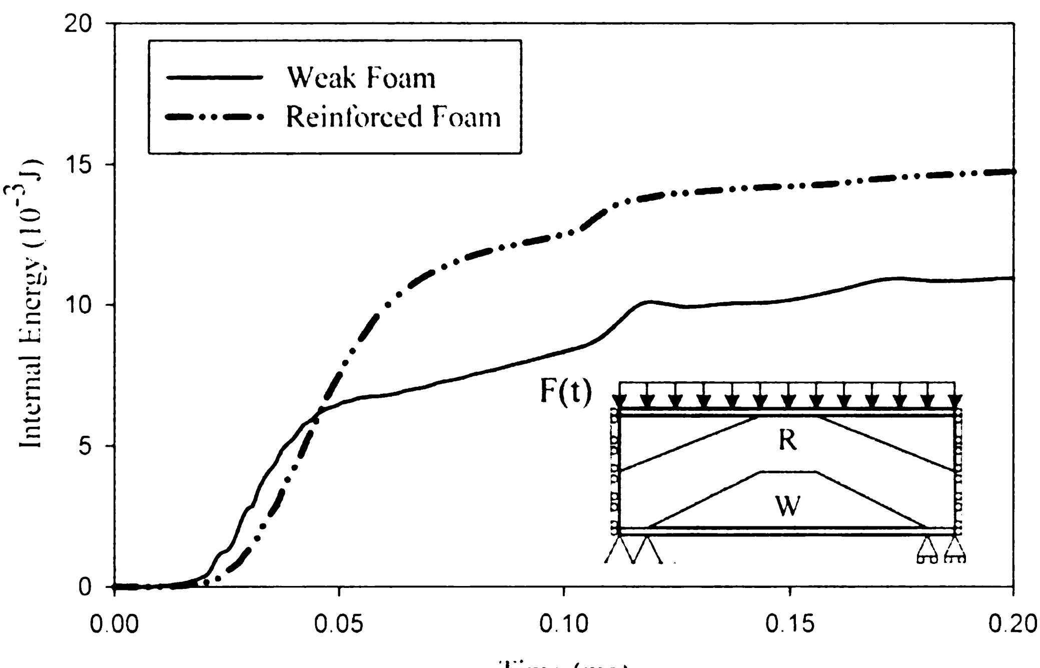

Figure 83. Internal Energy of Foams from Model 2 in Case 3

The internal strain energy for Models 3 and 4 are shown in Figure 84 and Figure 85, respectively. The results for both models indicate that the internal energy accumulated in the core was shared by the three layers, with the largest internal energy being taken by the top layer. In Model 3 the top two layers had about the same level of internal energy, indicating that the damage was extensive up to this level. In Model 4, the damage was decreasingly smaller through the layers, which signifies more distributed damage through the beam foam core. The total internal energy for the models was very similar, with Model 4 being only 10% lower than that in Model 3.

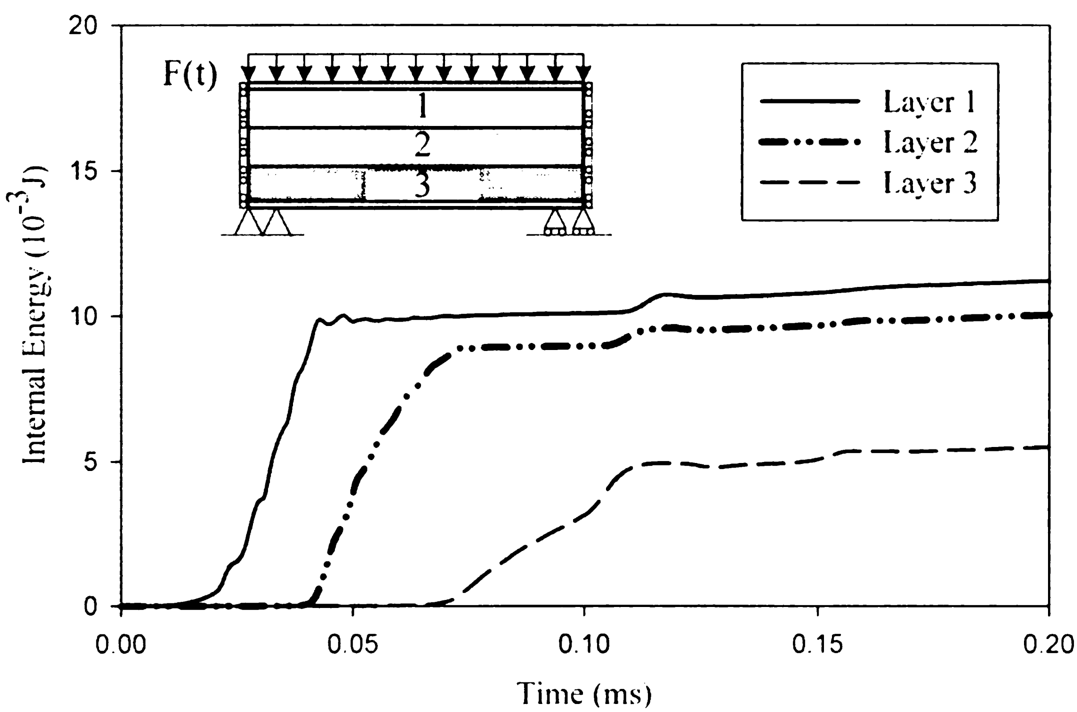

Figure 84. Internal Energy of Foams from Model 3 in Case 3

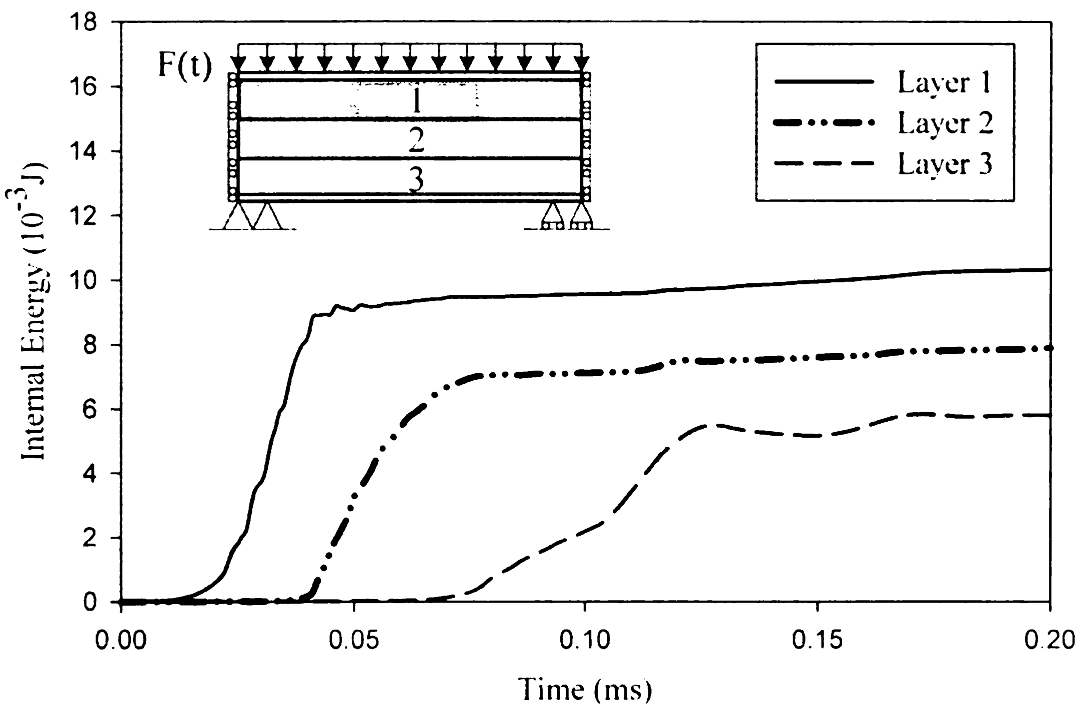

Figure 85. Internal Energy of Foams from Model 4 in Case 3

5.6 Discussion

This section provides a discussion on the results obtained from the two-dimensional stress wave simulations in sandwich foam beams. The key numerical results from the responses discussed in the previous sections are summarized in Table 13, which is used for comparisons later.

From Table 13, it can be seen that Model 2, with a reinforced foam arch had a superior performance in terms of stress mitigation, stress redirection, kinetic energy dissipation, and reduction structural deformation.

Table 13. Summary of Results for 2D Studies

		Model 1	Model 2	Model 3	Model 4
Case 1	Kinetic E., top facesheet ($\times 10^{-6}$J)	2.47	1.59	2.45	1.50
	Kinetic E.,bott. facesheet ($\times 10^{-6}$J)	0.286	0.159	0.352	0.245
	Internal E., foam ($\times 10^{-6}$ J)	3.74	3.10	3.52	3.08
	Disp., top facesheet (mm)	-0.326	-0.198	-0.266	-0.254
	Disp., bottom facesheet (mm)	-0.118	-0.098	-0.116	-0.111
	Stress, mid-bot. facesheet (MPa)	-23.4	-17.8	-21.5	-20.1
	Redirected stress (MPa)	-0.574	-0.962	-0.876	-0.617
Case 2	Kinetic E., top facesheet ($\times 10^{-4}$J)	4.0	3.2	4.0	3.1
	Kinetic E.,bott. facesheet ($\times 10^{-7}$J)	6.53	6.34	8.05	7.09
	Internal E., foam ($\times 10^{-4}$ J)	2.73	3.41	3.28	2.94
	Disp., top facesheet (mm)	-7.37	-4.80	-7.17	-5.69
	Disp., bottom facesheet (mm)	-0.228	-0.231	-0.310	-0.243
	Stress, mid-bot. facesheet (MPa)	-41.4	-41.2	-59.1	-44.4
	Redirected stress (MPa)	-0.809	-2.04	-1.47	-0.884
Case 3	Kinetic E., top facesheet ($\times 10^{-3}$J)	10.0	8.60	9.98	8.44
	Kinetic E.,bott. facesheet ($\times 10^{-3}$J)	1.12	0.94	0.95	1.02
	Internal E., foam ($\times 10^{-3}$ J)	26.1	25.7	26.7	24.0
	Disp., top facesheet (mm)	-18.4	-16.5	-17.0	-17.1
	Disp., bottom facesheet (mm)	-6.12	-5.68	-6.04	-5.84
	Stress, mid-bot. facesheet (MPa)	-963	-875	-973	-948
	Redirected stress (MPa)	-13.4	-28.3	-18.2	-16.0

For all load cases, Model 2 had the lowest kinetic energy at the top and bottom facesheets, and had the smallest deformation at the top facesheet. These two features make Model 2 a highly efficient buffer structure to prevent objects from severe damage due to impact or blast loading. This agrees with the conclusions from Bahei-El-Din (2006). The modification of the sandwich plate in Model 2 increases stiffness of the whole structure; in addition, this increment reduces vibrations of the facesheet and overall deflection of the plate and avoids severe deformations of the foam core.

The response of Model 2 also indicates that stress waves could be redirected by design. For the three load cases studied, Model 2 effectively redirected the stresses to the supported regions on the bottom facesheet. In Case 1, the support region stresses for Model 2 were 1.7 times greater than those of Model 1. For Cases 2 and 3, this ratio was 2.5 and 2.1, respectively. These results indicate that some regions in the structure would be protected since part of stresses was redirected to other regions, in this case the stiff (and typically much stronger) support regions. This explains why Model 2 had the lowest stress at the middle of the bottom facesheet for all 3 load cases.

Another finding from these studies is that the stresses in the middle of the bottom face in Model 3 were greater than those for Model 4. This also agrees with the findings from other researchers. The reason is that in Model 3, the stiffness is increasing from the top to the bottom while in Model 4 it is the opposite. Increased stiffness leads to a larger stress in the end while decreased stiffness reduces it, thus leading to a more efficient energy absorbing design.

CHAPTER 6. CONCLUSIONS AND RECOMMENDATIONS FOR FUTURE WORK

6.1 Conclusions

In this thesis, numerical studies on the stress wave propagation in solid and foam material were carried out. Theoretical principles of stress wave propagation in one dimension and the work from (Zhang and Paulino 2007) confirmed results from numerical simulations of cantilever bar in one dimension. Analyses on stress wave propagation on foam bars in one dimension and sandwich foam beams in two dimensions were conducted based on the validated numerical model. Results from these studies were in agreement with documented analytical and experimental research findings. The results show that a foam material performs very well in dissipating energy and thus mitigating transmitted of stresses. In addition, studies on sandwich beam models with reinforced foam presented characteristic of guiding stress wave propagation, a promising notion that has not been studied.

As a result, the concept of stress wave management has been fully evaluated through the presented study. The concept not only includes stress wave speed control, stress mitigation and energy dissipation, but also addresses the redirection of paths of stress wave propagation. For now, some practical principles of designing a sandwich beam model with desired capacities of stress wave management can be derived from the four sandwich beam models studied in this thesis.

The findings from this study lead to the conclusions stated below:

- By modifying the configurations of foam structures, stress waves can be directed. Among four sandwich aluminum foam beam models with dissimilar foam core configurations, the model consisting of a reinforced arch foam surrounded by relatively weaker foam showed an effective way of guiding the stress wave propagation from the middle region of the beam to its simply-supported regions. This implies the possibility that stress waves can be directed to desired regions in a specified path by using tailored foam structures.
- Adding a stiffer foam material near the location of load application can reduce deformations of the whole structures and the kinetic energy distributed to the structure. Foam bars and sandwich foam beam models with such configurations demonstrated smaller deformations and kinetic energy. This offers the possibility of optimizing foam structures to maximize their ability of escaping from severe damage as stand-alone or protect structures.
- The energy dissipation efficiency of a given configuration of tailored foam structure is dependent on the load magnitude. For instance, Model 2 of the sandwich beam studies dissipated the most energy under a 10MPa compressive impulse pressure but it dissipated the least amount of energy when the pressure load was 1MPa. This is an important consideration for the optimization of energy dissipating structures in future studies.

6.2 Recommendations for Future Work

Recommendations for future work are offered on three directions: experiments on sandwich foam beams, improved numerical simulations, and design optimization. The first and most important one is to perform experiments on sandwich foam beam model with reinforced foam regions to validate the findings from in this study. In addition, improving the numerical simulation on sandwich beam models can provide more precise results. Finally, it is necessary to develop an approach of optimizing the disposition of the reinforced foam regions for future study to offer guidance for the manufacture and design of experiments.

6.2.1 Experiments on Sandwich Foam Beams

In this study, cross section designs for the four sandwich foam beam models were as follows: a homogeneous sandwich foam beam, an arch reinforced foam sandwich beam, a decreasing layered sandwich foam beam, and an increasing layered sandwich foam beam. Of the three study cases corresponding to impulsive pressure loads of 1MPa, 10MPa and 100MPa, numerical simulations indicated that the sandwich beam with a reinforced arch foam showed the features of directing the path of the stress wave propagation. However, no experimental data or analytical solution is available for this innovative design. Therefore, experiments on reinforced sandwich foam beams are the most direct and important way of validating the conclusions derived from the numerical simulations of this thesis. In addition, experiments on homogeneous sandwich foam beams should be conducted, to obtain baseline data for comparison purposes.

Dimension for experimental samples of the homogeneous sandwich beam can be: 72 mm in length, 24 mm in width, a foam core thickness of 24 mm, and 1.5 mm thick face sheets. The width of the beam should be in the order of 24 mm. Reinforced foam designs should adopt the similar cross-section dimensions. The experimental program may include the following. Impact pressure test may be performed by drop tests. The relation between the generated pressure loads in the drop test should be well established. In addition, the sandwich beam sample should be simply-supported and constrained by a mold frame to prevent lateral displacements. Finally, measurement equipment should be provided to obtain the information of the stress, reaction forces, displacements, and kinetic and internal energy distribution.

6.2.2 Improvements on Numerical Simulation

Studies on sandwich beam models need to be modified to more realistically simulate the interaction properties between dissimilar foam materials and between foam materials and aluminum plates close. By modifying the interaction definition between at these interfaces the numerical models will be able to better assess delamination that may occur at these locations. Similar work has been done by (Bahei-El-Din et al. 2006). An additional consideration is to provide elasto-plastic constitutive properties to the face sheets in sandwich beam models in order to better capture localized failure and input load to the foam core. These improvements will increase the fidelity of the numerical simulations and offer better guidance to further experiment studies.

6.2.3 Design Optimization

The studies conducted in this thesis assumed materials properties based on existing analytical and experimental information, and the configurations for the sandwich foam beam models were arbitrarily designed based on engineering judgments. Therefore, in order to maximize the potential of stress wave management, further research on design optimization should be conducted in three directions: the material's properties, combinations of dissimilar materials and configurations of of reinforced foam in sandwich structures.

In the presented work, the material used to simulate foam behavior was aluminum. Other materials such as steel and ceramic can also be used to build reinforced foam because they have relatively high yield stress and could be stiffer. In addition, other foam materials such as functionally graded metal materials (FGM) and functionally graded foam material (FGF) can be introduced in the future because FGM and FGF can be designed and manufactured to meet the desired demands. Variations in material properties are possible based on specified functions (linear or non-linear) on mass density, Young's modulus, and relative density for FGF. The vast variation on material properties offers many possibilities for optimization.

Optimization can also be conducted on combinations between dissimilar materials. The combination of solid materials, foam materials, FGM and FGF, offer many combination possibilities that can be obviously optimized for improved behavior. Promising combinations should be investigated through optimization algorithms and experiments.

BIBLIOGRAPHY

ABAQUS ABAQUS Analysis User's Manual, Version 6.7, ABAQUS, Inc, 2007.

Achenbach, J. D. (1973). Wave Propagation in Elastic Solids. New York, American Elsevier Publishing Company, Inc.

Ashby, M. F., A. Evans, et al. (2000). Metal Foams: A Design Guide, Elsevier Science.

Bahei-El-Din, Y. A., G. J. Dvorak, et al. (2006). "A blast-tolerant sandwich plate design with a polyurea interlayer." International Journal of Solids and Strcutures 43: 7644-7658.

Berezovski, A., M. Berezovski, et al. (2006). "Numerical simulation of nonlinear elastic wave propagation in piecewise homogeneous media." Materials Science and Engineering A 418: 364-369.

Berezovski, A., J. Engelbrecht, et al. (2003). "Numerical simulation of two-dimensional wave propagation in functionally graded materials." European Journal of Mechanics A/Solids 22: 257-265.

Chen, X., N. Chandra, et al. (2004). "Analytical solution to the plate impact problem of layered heterogeneous material systems." International Journal for Solids and Structures 41: 4635-4659.

Chiu, T. C. and F. Erdogan (1999). "One Dimensional Wave Propagation in A Functionally Graded Elastic Medium." Journal of Sound and Vibration 222(3): 453-487.

Cui, L., S. Kiernan, et al. (2009). "Designing the energy absorption capacity of functionally graded foam materials." Materials Science and Engineering A 507: 215-225.

Davis, J. L. (2000). Mathematics of Wave Propagation, Princeton University Press.

Dizaji, A. F. and A. Jafari (2009). "Three-dimensional fundamental solution of wave propagation and transient heat transfer in non-homogeneous media." Engineering Analysis with Boundary Elements 33: 1193-1200.

Donnell, L. H. (1930). "Longitudinal wave transmission and impact." Trans. ASME 52: 153-167.

Erdogan, F. (1995). "Fracture mechanics of functionally graded materials." Composites Engineering 5(7): 753-770.

G.Vaughn, D., J. M. Canning, et al. (2005). "Coupled Plastic Wave Propagation and Column Buckling." Journal of Applied Mechanics Vol.72: 1-8.

Gibson, L. J. and M. F. Ashby (1988). Cellular solids: structure and properties, Pergamon Press Ltd.

Hanssen, A. G., M. Langseth, et al. (2001). "Crash behaviour of foam-based components: validation of numerical simulations." Cellular Methal and Metal Foaming Technology: 329-338.

Kiernan, S., L. Cui, et al. (2009). "Propagation of a stress wave through a virtual functionally graded foam." International Journal of Non-linear Mechanics 44: 456-468.

Kolsky, H. (1963). Stress waves in solids. New York, Dover Publications.

Lamb, H. (1904). "On the Propagation of Tremors over the surface of an Elastic Solid." Philosophical Transactions of the Royal Society of London 203: 1-42.

Li, Y., K. T. Ramesh, et al. (2001). "Dynamic characterization of layered and graded structures under implusive loading." International Journal of Solids and Strcutures 38: 6045-6061.

LS-DYNA LS-DYNA Keyword User's Manual. Livermore, California, Livermore Software Technology Corporation (LSTC), 2007.

Meirovitch (1967). Analytical Methods in Vibration. New York, The Macmillan Company.

Pattofatto, S., I. Nasri, et al. (2009). "Shock Enhancement due to Shock Front Propagation in Cellular Materials." Mechanical Properties of Cellular Materials: 159-167.

Paulino, G. H. and Z. J. Zhang (2005). "Cohesive zone modeling of dynamic failure in homogeneous and functionally graded materials." International Journal of Plasticity: 1195–1254.

Paulino, G. H. and Z. J. Zhang (2007). "Wave propagation and dynamic analysis of smoothly graded heterogeneous continua using graded finite elements." International Journal of Solids and Structures: 3601–3626.

Santare, M. H., P. Thamburaj, et al. (2003). "The use of graded finite elements in the study of elastic wave propagation in continuously nonhomogeneous materials." International Journal of Solids and Structures 40: 5621-5634.

Shim, V. P. W., Y. B. Guo, et al. (2008). "Eastic stress transmission in cellular systems-Analysisi of wave propagation." International Journal of Impact Engineering 35: 845-869.

Smith, P. D. and J. G. Hetherington (1994). Blast and Ballistic Loading of Structures, Laxton's

Smith, P. D. and J. G. Hetherington (1994). Blast and Ballistic Loading of Structures, Laxton's.

Tasdemirci, A. and I. W. Hall (2009). "Development of novel multilayer materials for impact applications: A combined numerical and experimental approach." Materials and Design 30: 1533-1541.

Wang, B., D. He, et al. (2001). "Compressive properties and energy absorption of foamed Al alloy." Cellular Methal and Metal Foaming Technology: 351-354.

Zhang, Z. J. and G. H. Paulino (2007). "Wave propagation and dynamic analysis of smoothly graded heterogeneous continua using graded finite elements." International Journal of Solids and Strcutures 44: 3601-3626.

Zhao, H. (2001). "Impact Testing of Metallic Honeycombs and Foams." Cellular Methal and Metal Foaming Technology: 339-344.

Zhao, H., H. Tsitsiris, et al. (2007). "Shock enhancement of cellular structures under impact loading: Part I Experiments." Journal of the Mechanics and Physics of Solids: 2652–2671.

Zhuang, S., G. Ravichandran, et al. (2003). "An experimental investigation of shock wave propagation in periodically layered composites." Journal of the Mechanics and Physics of Solids 51: 245-265.